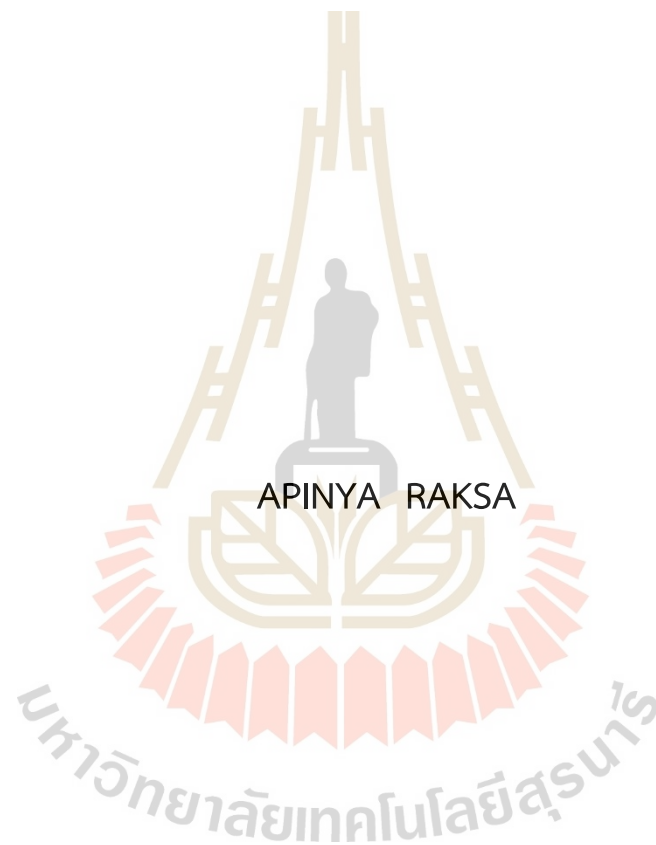


NANOFIBROUS SCAFFOLD OF ELECTROSPUN  
SILK FIBROIN/POLY(VINYL ALCOHOL) BLENDS  
FOR MENISCUS TISSUE ENGINEERING APPLICATION



A Thesis Submitted in Partial Fulfillment of the Requirements for the  
Degree of Doctor of Philosophy in Chemistry  
Suranaree University of Technology  
Academic Year 2023

โครงร่างเลี้ยงเซลล์เส้นใยนาโนอิเล็กทรอนิกส์ปั่นจากไหมไฟโบรอินผสม  
พอลิไวนิลแอลกอฮอล์สำหรับการประยุกต์ใช้ใน  
วิศวกรรมเนื้อเยื่อหมอนรองเข่า



วิทยานิพนธ์นี้เป็นส่วนหนึ่งของการศึกษาตามหลักสูตรปริญญาวิทยาศาสตรดุษฎีบัณฑิต  
สาขาวิชาเคมี  
มหาวิทยาลัยเทคโนโลยีสุรนารี  
ปีการศึกษา 2566

NANOFIBROUS SCAFFOLD OF ELECTROSPUN SILK FIBROIN/POLY(VINYL ALCOHOL) BLENDS FOR MENISCUS TISSUE ENGINEERING APPLICATION

Suranaree University of Technology has approved this thesis submitted in partial fulfillment of the requirements for the Degree of Doctor of Philosophy.

Thesis Examining Committee



(Assoc. Prof. Dr. Anyanee Kamkaew)

Chairperson



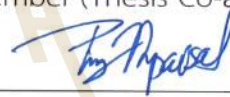
(Assoc. Prof. Dr. Rapee Utke)

Member (Thesis advisor)



(Assoc. Prof. Dr. Yupaporn Ruksakulpiwat)

Member (Thesis Co-advisor)



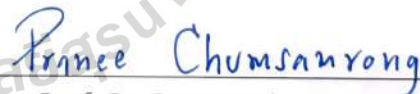
(Asst. Prof. Dr. Piya-on Numpaisal)

Member (Thesis Co-advisor)



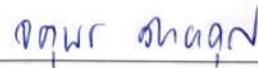
(Assoc. Prof. Dr. Ittipol Jangchud)

Member



(Assoc. Prof. Dr. Pranee Chumsamrong)

Member



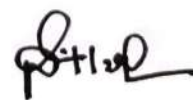
(Prof. Dr. Jatuporn Wittayakun)

Member



(Assoc. Prof. Dr. Chatchai Jothityangkoon)

Vice Rector for Academic Affairs  
and Quality Assurance



(Prof. Dr. Santi Maensiri)

Dean of Institute of Science

อภิญา รักษา : โครงร่างเลี้ยงเซลล์เส้นใยนาโนอิเล็กโทรสปินจากไหมไฟโบรอินผสม  
พอลิไวนิลแอลกอฮอล์สำหรับการประยุกต์ใช้ในวิศวกรรมเนื้อเยื่อหมอนรองเข่า  
(NANOFIBROUS SCAFFOLD OF ELECTROSPUN SILK FIBROIN/POLY(VINYL  
ALCOHOL) BLENDS FOR MENISCUS TISSUE ENGINEERING APPLICATION)  
อาจารย์ที่ปรึกษา : รองศาสตราจารย์ ดร.ระพี อุทเคอ, 120 หน้า

คำสำคัญ: ไหมไฟโบรอิน, พอลิไวนิลแอลกอฮอล์, โครงร่างเลี้ยงเซลล์, คอลลาเจน, อะกรีแคน, หมอนรองเข่า

วิทยานิพนธ์นี้ได้นำวิธีการในสาขาวิศวกรรมเนื้อเยื่อมาใช้โดยมุ่งเน้นไปที่การประดิษฐ์โครง  
ร่างเลี้ยงเซลล์เส้นใยนาโนเพื่อจัดการกับอาการบาดเจ็บและการเสื่อมสภาพของหมอนรองเข่า  
งานวิจัยนี้จะใช้กระบวนการผลิตโครงร่างเลี้ยงเซลล์เส้นใยนาโนโดยใช้เทคนิคอิเล็กโทรสปินนิ่งโดยใช้  
ส่วนผสมที่แตกต่างกันของไหมไฟโบรอิน และพอลิไวนิลแอลกอฮอล์ การสกัดไหมไฟโบรอินจะใช้ตัว  
ทำละลายสองชนิดคือ แคลเซียมคลอไรด์ และ ลิเทียมโบรไมด์ โดยที่ไหมไฟโบรอินที่สกัดด้วยตัวทำ  
ละลายลิเทียมโบรไมด์นั้นให้ผลผลิตสูง นอกจากนี้การศึกษายังตรวจสอบเปอร์เซ็นต์ความเป็นผลึกและ  
น้ำหนักโมเลกุลสำหรับไหมไฟโบรอินจะมีค่าที่ใกล้เคียงกัน รูปแบบการเลี้ยวเบนของรังสีเอ็กซ์และฟู  
เรียร์ทรานส์ฟอร์มสเปกตรัมยืนยันการมีอยู่ของผลึกแบบเบต้าซีต แบบขดลวดสุ่ม และแบบโครงสร้าง  
เกลียวแอลฟา อย่างไรก็ตามการตรวจสอบพารามิเตอร์ของอิเล็กโทรสปินนิ่งพบว่าสภาวะที่เหมาะสม  
โดยความเข้มข้นของพอลิไวนิลแอลกอฮอล์ 10 เปอร์เซ็นต์โดยน้ำหนักต่อปริมาตร ความชื้นสัมพัทธ์  
50 เปอร์เซ็นต์ และการใช้กระแสไฟฟ้าแรงสูงที่ 20 กิโลโวลต์ เงื่อนไขเหล่านี้ส่งผลให้เส้นผ่าน  
ศูนย์กลางเส้นใยเฉลี่ยและคุณสมบัติแรงดึงนั้นเหมาะสมสำหรับโครงร่างเลี้ยงเซลล์เส้นใยนาโน การ  
สร้างโครงร่างเลี้ยงเซลล์เส้นใยนาโนโดยใช้ส่วนผสม SF(CaCl<sub>2</sub>)/PVA และ SF(LiBr)/PVA ที่อัตราส่วน  
ต่าง ๆ (100:0, 75:25, 50:50, 25:75, 0:100) แสดงให้เห็นว่าการเพิ่มขึ้นของไหมไฟโบรอินช่วยเพิ่ม  
ความสามารถในการเปียกน้ำของพื้นผิว คุณสมบัติทางความร้อน ความต้านทานแรงดึง และการยึดตัว  
เมื่อขาด ในทางกลับกันไหมไฟโบรอินจะลดความหนืดและเส้นผ่านศูนย์กลางเส้นใยเฉลี่ย การสกัดไหม  
ไฟโบรอินโดยใช้ตัวทำละลายแคลเซียมคลอไรด์และลิเทียมโบรไมด์ ให้คุณสมบัติต่างกันเพียงเล็กน้อย  
โครงร่างเลี้ยงเซลล์เส้นใยนาโน SF/PVA ถูกเลือกสำหรับการทดสอบความเข้ากันได้ทางชีวภาพ ใน  
บรรดาอัตราส่วนต่าง ๆ ของโครงสร้างเส้นใยนาโนอิเล็กโทรสปินพบว่า SF(LiBr)/PVA 50:50 ถือเป็น  
สภาวะที่เหมาะสมที่สุดสำหรับวิศวกรรมเนื้อเยื่อหมอนรองเข่า ซึ่งส่งเสริมความมีชีวิตของเซลล์และ  
แสดงคุณสมบัติที่ไม่เป็นพิษ นอกจากนี้ยังช่วยเพิ่มการแสดงออกของยีนคอนโทรลไซโตโดยเฉพาะอย่าง  
ยิ่งคอลลาเจนประเภทหนึ่ง และอะกรีแคนซึ่งมีประสิทธิภาพสูงกว่าโครงร่าง SF(CaCl<sub>2</sub>)/PVA จากการ

ค้นพบเหล่านี้ทำให้โครงร่างเลี้ยงเซลล์เส้นใยนาโนอิเล็กโทรสปินของ SF(LiBr)/PVA (50:50) ประสบความสำเร็จในการผลิตและมีศักยภาพในการใช้เป็นโครงสร้างเลียนแบบทางชีวภาพสำหรับเย็บเสริมเพื่อใช้เป็นโครงร่างเลี้ยงเซลล์ในหมอนรองเข่า ด้วยลักษณะทางสัณฐานวิทยา คุณสมบัติเชิงกล ความมีชีวิตของเซลล์ และลักษณะการแสดงออกของยีนที่ดี ซึ่งโครงร่างเลี้ยงเซลล์เส้นใยนาโน SF(LiBr)/PVA (50:50) แสดงให้เห็นว่ามีแนวโน้มที่เหมาะสมเป็นโครงสร้างวิศวกรรมเนื้อเยื่อหมอนรองเข่า โดยสามารถเป็นตัวเลือกที่มีศักยภาพสำหรับการฟื้นฟูหมอนรองเข่าในเนื้อเยื่อและการทำงานด้านวิศวกรรมเนื้อเยื่อ



สาขาวิชาเคมี

ปีการศึกษา 2566

ลายมือชื่อนักศึกษา \_\_\_\_\_

ลายมือชื่ออาจารย์ที่ปรึกษา \_\_\_\_\_

ลายมือชื่ออาจารย์ที่ปรึกษาร่วม \_\_\_\_\_

ลายมือชื่ออาจารย์ที่ปรึกษาร่วม \_\_\_\_\_

*[Signature]*

*[Signature]*

*[Signature]*

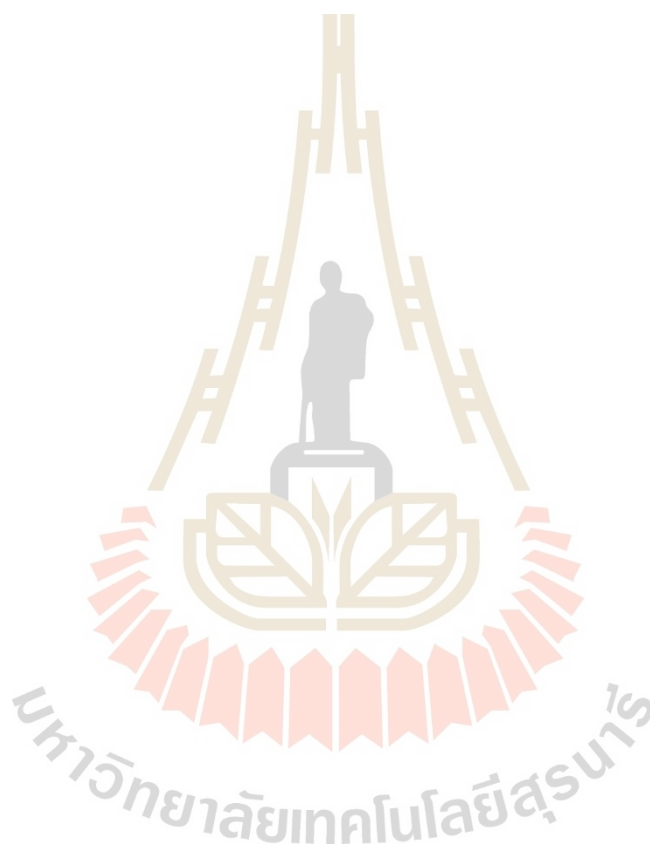
*[Signature]*

APINYA RAKSA : NANOFIBROUS SCAFFOLD OF ELECTROSPUN SILK FIBROIN/POLY(VINYL ALCOHOL) BLENDS FOR MENISCUS TISSUE ENGINEERING APPLICATION. THESIS ADVISOR : ASSOC. PROF. RAPEE UTKE, Ph.D. 120 PP.

Keyword: silk fibroin, poly(vinyl alcohol), scaffold, collagen, aggrecan, meniscus

This thesis introduces a novel methodology in the field of tissue engineering, focusing on the fabrication of nanofibrous scaffolds for addressing meniscus injuries and degeneration. The research explores the manufacturing process of nanofibrous scaffolds using the electrospinning technique, employing a distinct blend of silk fibroin (SF) and poly(vinyl alcohol) (PVA). SF extraction is conducted using  $\text{CaCl}_2$  and LiBr solvents, with LiBr-extracted SF exhibiting a high yield. Furthermore, the study examines %crystallinity and molecular weight for similarity values. XRD patterns and FTIR spectra confirm the presence of  $\beta$ -sheet crystalline, random coil, and  $\alpha$ -helix structures. However, investigations into electrospinning parameters reveal that optimal conditions include PVA at 10% w/v, a relative humidity of 50%, and a high voltage of 20 kV. These conditions yield an average fiber diameter and tensile properties suitable for the resulting electrospun scaffold. Fabrication of nanofibrous scaffolds using SF( $\text{CaCl}_2$ )/PVA and SF(LiBr)/PVA blends at different ratios (100:0, 75:25, 50:50, 25:75, 0:100) demonstrates that the addition of SF enhances surface wettability, thermal properties, tensile strength, and elongation at break. Conversely, SF reduces viscosity and average fiber diameter. SF extraction using  $\text{CaCl}_2$  and LiBr solvents yields slightly different properties. Both SF/PVA nanofibrous scaffolds are selected for biocompatibility testing. Among these, the electrospun SF(LiBr)/PVA 50:50 nanofibrous scaffold emerges as the optimal condition for meniscus tissue engineering, promoting cell viability and exhibiting non-toxic properties. Additionally, it enhances chondrogenic gene expression, particularly collagen types I and aggrecan, outperforming the SF( $\text{CaCl}_2$ )/PVA scaffold. Based on these findings, the electrospun nanofibrous scaffold of SF(LiBr)/PVA (50:50) is successfully manufactured and holds potential for use as biomimetic meniscus scaffolds for scaffold-augmented sutures. With its favorable morphology, mechanical properties, cell viability, and gene expression characteristics,

the SF(LiBr)/PVA (50:50) nanofibrous scaffold shows promise as a meniscus tissue engineering scaffold, positioning it as a viable candidate for meniscus regeneration in tissue engineering applications.



School of Chemistry  
Academic Year 2023

Student's Signature \_\_\_\_\_  
Advisor's Signature \_\_\_\_\_  
Co-Advisor's Signature \_\_\_\_\_  
Co-Advisor's Signature \_\_\_\_\_

## ACKNOWLEDGEMENT

First and foremost, I would like to sincerely thank my advisors, Assoc. Prof. Dr. Rapee Utke, Assoc. Prof. Dr. Yupaporn Ruksakulpiwat, and Asst. Prof. Dr. Piya-on Numpaisal, for support, suggestions, encouragement, and discussion throughout my graduate studies. I would like to acknowledge Assoc. Prof. Dr. Ittipol Jangchud, Prof. Dr. Jatuporn Wittayakun, Assoc. Prof. Dr. Pranee Chumsamrong, and Assoc. Prof. Dr. Anyanee Kamkaew for contributing to the thesis-examining committees. Importantly, I would like to thank Rajamangala University of Technology Isan, Nakhon Ratchasima, Thailand, and Research Center for Biocomposite Materials for Medical Industry and Agricultural and Food Industry, Nakhon Ratchasima, Thailand for the financial support. I wish to thank all the lecturers in the School of Chemistry and the lecturers in the School of Polymer Engineering for their good attitudes and useful advice. Additionally, I would like to also thank all staff at the Center for Scientific and Technological Equipment for their assistance and suggestions for the use of instruments. Thank you to all of my good friends in Research Center for Biocomposite Materials for Medical Industry and Agricultural and Food Industry and other friends for their friendship and all their help. Last and foremost, I would like to thank my family for their love, understanding, support, and encouragement during my studies.

Apinya Raksa

# CONTENTS

	Page
ABSTRACT IN THAI.....	I
ABSTRACT IN ENGLISH.....	III
ACKNOWLEDGEMENTS.....	V
CONTENTS.....	VI
LIST OF TABLES.....	IX
LIST OF FIGURES.....	X
<b>CHAPTER</b>	
<b>I INTRODUCTION.....</b>	<b>1</b>
1.1 Significance of the study.....	1
1.2 Background.....	1
1.2.1 Structure, composition, and function of the meniscus.....	1
1.2.2 Meniscal injury and treatment.....	4
1.2.3 Meniscus scaffold for tissue engineering.....	5
1.2.4 Biomaterials for meniscus tissue engineering.....	7
1.2.5 Electrospinning process for tissue engineering.....	11
1.3 Objective.....	13
1.4 Scope and limitations of the study.....	14
<b>II LITERATURE REVIEW.....</b>	<b>15</b>
2.1 Silk fibroin-based for tissue engineering applications.....	15
2.1.1 Silk fibroin extraction.....	15
2.1.2 Silk fibroin-based scaffold for tissue engineering applications.....	17
2.2 Poly(vinyl alcohol) based for tissue engineering applications.....	21
2.2.1 Effect of PVA concentration on mechanical properties.....	21
2.2.2 Poly(vinyl alcohol)-based scaffold for tissue engineering applications.....	22
2.3 Electrospinning for tissue engineering applications.....	28
2.3.1 Parameters affecting the electrospinning efficacy.....	28
2.3.2 Electrospun nanofibrous scaffolds for tissue engineering applications.....	34
2.4 Meniscus scaffolds for tissue engineering applications.....	35

## CONTENTS (Continued)

		Page
<b>III</b>	<b>RESEARCH METHODOLOGY.....</b>	<b>40</b>
	3.1 Preparation of <i>Bombyx mori</i> cocoons and degumming process.....	40
	3.1.1 Weight loss.....	40
	3.1.2 Residual sericin.....	40
	3.2 Preparation of silk fibroin extraction by CaCl <sub>2</sub> and LiBr solvent.....	41
	3.2.1 Measurement of molecular weight.....	41
	3.2.2 Characterization of Silk fibroin.....	42
	3.3 Preparation of electrospun PVA nanofiber and electrospun SF/PVA nanofiber.....	43
	3.3.1 Polymer solution preparation.....	43
	3.3.2 Preparation of blend SF/PVA.....	43
	3.3.3 Electrospinning of 5% w/v, 10% w/v PVA and blended SF/PVA nanofiber.....	43
	3.3.4 Characterization of blended electrospun nanofiber.....	44
	3.4 Fabrication of electrospun SF/PVA nanofibrous scaffold.....	44
	3.4.1 Materials.....	44
	3.4.2 Electrospinning of SF/PVA solution.....	45
	3.4.3 Characterization of blended electrospun nanofiber.....	45
<b>IV</b>	<b>RESULTS AND DISCUSSION.....</b>	<b>48</b>
	4.1 The effect of solvent for silk fibroin extraction on physical properties and biological properties of electrospun nanofibrous scaffold.....	48
	4.1.1 Time on degumming silk.....	48
	4.1.2 Effect of silk fibroin extraction by CaCl <sub>2</sub> and LiBr solvent.....	50
	4.2 The effect of electrospinning parameters on the morphology and mechanical properties of electrospun nanofibrous scaffold.....	55
	4.2.1 The effect of PVA concentration.....	55
	4.2.2 The effect of humidity.....	58
	4.2.3 The effect of voltage.....	61
	4.3 The effect of silk fibroin content on physical properties and mechanical properties of electrospun SF/PVA nanofibrous scaffold.....	65
	4.3.1 Measurements of Viscosity.....	65

## CONTENTS (Continued)

	Page
4.3.2 Effect of CaCl <sub>2</sub> solvent for extraction silk fibroin on SF(CaCl <sub>2</sub> )/PVA nanofibrous scaffold.....	66
4.3.3 Effect of LiBr solvent for extraction silk fibroin on SF/PVA nanofibrous scaffold.....	74
4.4 The development of electrospun SF/PVA for biomimetic scaffold for potential meniscus tissue engineering application.....	81
4.4.1 In vitro cell viability and toxicity of SF(CaCl <sub>2</sub> )/PVA nanofibrous scaffold.....	81
4.4.2 Gene expression of SF(CaCl <sub>2</sub> )/PVA nanofibrous scaffold.....	82
4.4.3 In vitro cell viability and toxicity of SF(LiBr)/PVA nanofibrous scaffold.....	83
4.4.2 Gene expression of SF(LiBr)/PVA nanofibrous scaffold.....	85
<b>V CONCLUSION AND RECOMMENDATION.....</b>	<b>87</b>
REFERENCES.....	89
APPENDIX.....	112
CURRICULUM VITAE.....	120

## LIST OF TABLES

Table		Page
2.1	Mechanical properties of electrospun PVA nanofibers.....	22
2.2	Mechanical Properties of Native and Repaired Menisci Pulled to Failure.....	35
3.1	Composition of SF blend with PVA (SF/PVA).....	45
3.2	Sequences of primer sets for qRT-PCR.....	47
4.1	Time of degumming silk.....	49
4.2	Silk fibroin yields of different extraction method.....	51
4.3	Molecular weight of silk fibroin dissolved following different methodologies.....	53
4.4	Some Properties of the electrospun PVA nanofiber.....	58
4.5	Mechanical properties and Fiber diameter size of SF/PVA blended nanofiber at different relative humidity.....	61
4.6	Mechanical properties and Fiber diameter size of SF/PVA blended nanofiber at different applied voltage.....	65
4.7	Contact angle and Tensile properties of SF(CaCl <sub>2</sub> )/PVA nanofibrous scaffold various ratio.....	71
4.8	Tensile properties of SF(LiBr)/PVA nanofiber various ratio.....	78

## LIST OF FIGURES

Figure	Page
1.1 Anatomic location of the meniscus (Chamber et al., 2015). Copyright 2015 Musculoskeletal Regeneration.....	2
1.2 Schematic diagram a) Schematic diagram of the ultrastructure of collagen fibres within the meniscus b) Schematic diagram of meniscus internal ultrastructure.....	3
1.3 Illustrations showing appearances orientations of different meniscal tears a) longitudinal tear, b) radial tear (Wadhwa et al., 2016). Copyright 2016 European Journal of Radiology.....	5
1.4 Schematic Tissue Engineering (Sun et al., 2016). Copyright 2016 Operative Techniques in Orthopaedics.....	6
1.5 Chemical structure of Poly(vinyl) alcohol (Lamminmeaki et al., 2011).....	8
1.6 Structures of silk fibroin. (A) Popular silk sources (B) Bombyx. mori silkworm (C) Composition of silk fibroin (D) Hydrogen bonds between primary amino acid sequence of silk fibroin (E) Semi-crystal network consists of sheet crystallites and amorphous matrix.....	9
1.7 Primary structure of fibroin, showing the [Gly-Ser-Gly-Ala-Gly-Ala] sequence....	10
1.8 beta-pleated structure of silk fibroin macromolecules.....	10
1.9 Schematic of a Basic Electrospinning process.....	12
1.10 Schematic presentation of the meniscal composite structure.....	12
2.1 Mechanical properties and SEM image of electrospun mats produced with 17 wt.% dissolutions of SF in HFIP.....	17
2.2 Cell adhesion and Cell proliferation.....	19
2.3 a) MTT assay and b) DNA estimation of meniscus cells seeded on scaffolds....	19
2.4 SEM images of the methanol-treated electrospun fibers.....	20
2.5 Hoechst-stained images of osteoblast cells (MG63) control (A), cells attached to film (B), electrospun nanofibrous scaffold (C), and lyophilized sponge (D).....	21
2.6 NIH 3T3 fibroblast cell morphology on PVA nanofiber and PVA/Chitosan nanofiber.....	24

## LIST OF FIGURES (Continued)

Figure	Page
2.7	Representation of the interactions established between PVA and gellan, after crosslinking.....24
2.8	MTT optical microscopy images of L-929 cells growth after 48 hr. culturing in presence of the nanofibrous mats (l) Cell viability of fibroblast (L-929) cell cultured for 24 and 48 hr. in presence of nanofibrous mats.....25
2.9	SEM images of MC3T3-E1 cells cultured on TCD, pure PVA hydrogel (molar ratio of GA and PVA ~ 10.3:1.0), and PVA/HA hydrogel (molar ratio of GA and PVA ~24.8:1.0) nanofibers as a function of cell-culture time.....26
2.10	Growth of ATDC5 cells on Chitosan/PVA, Chitosan/PVA-CaCO <sub>3</sub> (4 wt%), Chitosan/PVA-apatite fibers after 1, 4, 7 and 14 days of culture and morphology of ATDC5 cells growing on chitosan/PVA-CaCO <sub>3</sub> (4 wt%) matrix on (a) day 1, (b) day 4, (c) day 14, (d) enlarged image of day 1 and (e) enlarged image of day 4.....27
2.11	Fluorescence merged image of 3T3 fibroblast cells cultivated on random and aligned PVA and PVA-gelatin meshes for 1, 3, and 5 days.....27
2.12	SEM micrographs and mechanical properties of electrospun CA nanofibers.....28
2.13	SEM morphologies at 10,000x of electrospun PVA and PVA/TE blend (60:40) fibers at different concentrations and molecular weights.....29
2.14	Adhesion of osteoblastic cells to PCL fiber meshes after 7 days in culture: a) flat copper plate, b) screw collector and c) wire net collector.....31
2.15	FE-SEM images of hMSCs cultured on the chitosan/PEO/BG scaffolds after 1 (a), 3 (b), 5 (c) and 7 (d) days.....32
2.16	Histological analysis of NFS MSC cultures maintained in a chondrogenic medium supplemented with TGF-b1 for 21 days. H&E staining showed flat fibroblast-like cells on the top zone (bracket, *), round chondrocyte-like cells embedded in lacunae (arrows) in the middle zone (bracket, **), and small, flat cells at the bottom zone (bracket, ***). Alcian blue staining showed the presence of sulfated proteoglycan-rich ECM in the construct.....33
2.17	Suture repair of meniscal tears and mechanical testing set-up. A) Suture repair of fully transected meniscus. Inset shows dimension of suture placement. B) Scaffold-augmented repair. C) Suture repaired meniscus clamped in materials testing machine prior to tensile loading protocol).....34

## LIST OF FIGURES (Continued)

Figure	Page
2.18 Twenty-four weeks after implantation of PLDLA/PCL-T scaffold.....	36
2.19 Immunohistochemical staining for collagen type II of inner zone of (A) normal meniscus and tissue engineered meniscus at (B) 6 and (C) 10 weeks.....	37
2.20 Picrosirius red staining.....	38
2.21 Meniscus-derived matrix (MDM) was prepared from porcine medial meniscus.....	38
2.22 Compressive modulus of individual silk meniscus scaffold layers.....	39
3.1 The preparation process of degumming silk.....	41
3.2 The preparation process of silk fibroin extraction by CaCl <sub>2</sub> and LiBr solvent....	42
3.3 The preparation process of electrospun PVA nanofiber and electrospun SF/PVA nanofiber.....	44
3.4 The fabrication process of electrospun SF/PVA nanofibrous scaffold.....	45
3.5 Representative clonally derived human chondrogenic progenitor cells (HCPCs) on day 1, day 3, and day 7.....	47
4.1 FE-SEM image of cocoon a) outer fiber of cocoon and b) silk fiber showing the two filaments of fibroin and sericin coating.....	49
4.2 FE-SEM image of degumming silk a) degumming time 10 min, b) degumming time 20 min, c) degumming time 30 min, and d) degumming time 40 min.....	50
4.3 FTIR spectra of a) raw cocoon, b) degumming time 10 min, c) degumming time 20 min, d) degumming time 30 min, e) degumming time 40 min.....	50
4.4 FE-SEM image of silk fibroin a) and b) silk fibroin extracted by LiBr solvent using magnification 250x and 1000x and c) and d) silk fibroin extracted by CaCl <sub>2</sub> solvent using magnification 250x and 1000x.....	51
4.5 SDS-PAGE analysis of silk fibroin dissolved following different methodologies. 46% w/v CaCl <sub>2</sub> (lane a) and 9.3 M LiBr (lane b).....	53
4.6 FT-IR spectra of silk fibroin extracted by a) CaCl <sub>2</sub> solvent and b) LiBr solvent.....	54
4.7 XRD pattern of silk fibroin extracted by a) CaCl <sub>2</sub> solvent and b) LiBr solvent.....	55

## LIST OF FIGURES (Continued)

Figure	Page
4.8 FE-SEM images and histograms of electrospun of PVA nanofiber at different concentration; (a-i, a-ii, a-iii) = 5% w/v, (b-i, b-ii, b-iii) = 10% w/v (Magnification 2500x and 20000x).....	56
4.9 The stress-strain curve of nanofiber prepared using different concentration of PVA solutions.....	57
4.10 FE-SEM images and histograms of electrospun SF/PVA blended nanofiber at different relative humidity; (a-I, a-II, a-III) = 50%, (b-I, b-II, b-III) = 60%, (c-I, c-II, c-III) = 70%, (d-I, d-II, d-III) = 80%.....	60
4.11 Stress–strain curves of electrospun SF/PVA nanofiber at different relative humidity.....	61
4.12 FE-SEM images and histograms of electrospun SF/PVA blended nanofiber at different applied voltage; (a-i, a-ii, a-iii) = 10 kV, (b-i, b-ii, b-iii) = 15 kV, (c-i, c-ii, c-iii) = 20 kV, (d-i, d-ii, d-iii) = 25 kV.....	64
4.13 Stress–strain curves of electrospun SF/PVA nanofiber at different applied voltage.....	65
4.14 Viscosity of SF/PVA solution at different ratio (the green line represent the viscosity value of SF(CaCl <sub>2</sub> )/PVA and the yellow line represent the viscosity value of SF(LiBr)/PVA).....	66
4.15 FE-SEM image of SF/PVA nanofibrous scaffold various ratio and different magnification; a) SF/PVA 100:0, b) and c) SF/PVA 75:25, d) and e) SF/PVA 50:50, f) and g) SF/PVA 25:75, h) and i) SF/PVA 0:100.....	68
4.16 Contact angle of SF(CaCl <sub>2</sub> )/PVA nanofibrous scaffold.....	70
4.17 Stress-Strain curve of SF(CaCl <sub>2</sub> )/PVA nanofibrous scaffold at different ratio.....	72
4.18 FT-IR spectra of SF(CaCl <sub>2</sub> )/PVA nanofibrous scaffold at different ratio.....	73
4.19 TGA thermogram of SF(CaCl <sub>2</sub> )/PVA nanofibrous at various ratio; a) SF(CaCl <sub>2</sub> )/PVA 100:0, b) SF(CaCl <sub>2</sub> )/PVA 75:25, c) SF(CaCl <sub>2</sub> )/PVA 50:50, d) SF(CaCl <sub>2</sub> )/PVA 25:75, and e) SF(CaCl <sub>2</sub> )/PVA 0:100.....	73
4.20 FE-SEM image of SF(LiBr)/PVA nanofiber different ratio at magnification 10000x (a) SF(LiBr)/PVA 100:0, (b) SF(LiBr)/PVA 75:25, (c) SF(LiBr)/PVA 50:50, (d) SF(LiBr)/PVA 25:75, and (e) SF(LiBr)/PVA 0:100.....	75
4.21 Contact angle of SF(LiBr)/PVA electrospun nanofibrous scaffold different ratio.....	76

## LIST OF FIGURES (Continued)

Figure	Page
4.22 Stress-strain curve of SF(LiBr)/PVA nanofiber.....	78
4.23 FTIR spectra of SF(LiBr)/PVA nanofiber various ratio.....	80
4.24 TGA thermogram of SF(LiBr)/PVA nanofiber various ratio.....	81
4.25 Relative cell viability of SF(CaCl <sub>2</sub> )/PVA nanofibrous scaffold.....	82
4.26 The gene expression of COL1A1, COL2A1, and aggrecan at days 7, 14, and 28 were demonstrated in (a, b, and c), respectively.....	83
4.27 Cell viability of SF(LiBr)/PVA nanofiber various ratio.....	84
4.28 The gene expression of COL1A1, COL2A1, and ACAN at days 7, 14, and 28 were demonstrated in (a, b, and c), respectively.....	86



# CHAPTER I

## INTRODUCTION

### 1.1 Significance of the study

Tissue engineering has been developed as a response to the problems associated with the replacement of tissues lost to disease or trauma. Currently, tissue replacements must overcome important challenges such as rejection, severe organ donor shortages, and chronic inflammation (Godbey et al., 2002). Actually, thousands of patients die every year in waiting donor for organ transplantation (Lanza et al., 2000). The development of tissue engineering is the desire to avoid these problems by creating biological substitutes capable of replacing the damaged tissue. Biomolecules, viable cells, and scaffolds are generally mentioned to as the tissue engineering. Scaffolds, typically made of polymeric biomaterials, which provide the structural support for cell attachment, cell proliferation, and subsequent tissue development (Chan et al., 2008). Therefore, it is the motivation in this study was to design the nanofibrous scaffold from silk fibroin that would best mimic the structure and function of the natural tissue.

### 1.2 Background

This thesis focuses on the investigation of design nanofibrous scaffold from silk fibroin-based for meniscus tissue engineering. Understanding the relationship between structure, composition and the obtained properties is a key point of the study. Therefore, this part presents basic knowledge of structure, composition, and function of the meniscus, meniscal injury and treatment, meniscus scaffold for tissue engineering, biomaterials for meniscus tissue engineering, and electrospinning for tissue engineering, which an important to this work

#### 1.2.1 Structure, composition, and function of the meniscus

##### 1.2.1.1 Anatomy and extracellular matrix of the meniscus

The meniscus is a semilunar disc-shaped fibrocartilaginous tissues located on the tibial plateau within the medial and lateral compartments of the knee (Figure 1.1 Anatomic location of the meniscus (Chamber et al., 2015). The major functions of this tissue include transmission of load and contribution to joint lubrication (Ghosh et al.,

1987). The meniscus can be divided into outer and inner regions containing cells that are responsible for maintaining tissue homeostasis under the high shear and compressive forces experienced in the knee joint. The wedge shape semilunar sections of the meniscus and its horn attachment contribute to altering the perpendicular compressive tibiofemoral forces to horizontal hoop stresses (Makris et al., 2011). Meanwhile, shear forces are developed between the collagen fibers within the meniscus while the meniscus is contorted outward (Mcdevitt et al., 2002).

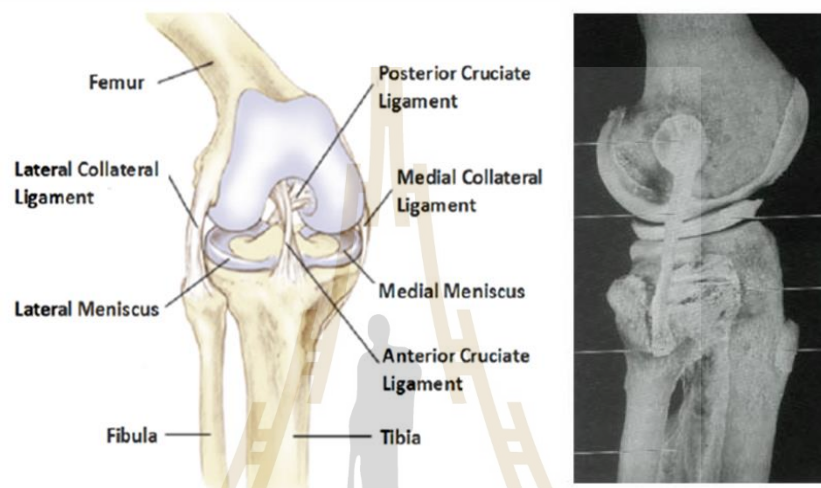


**Figure 1.1** Anatomic location of the meniscus (Chamber et al., 2015). Copyright 2015 Musculoskeletal Regeneration.

The meniscus is described as fibrocartilaginous as it shares characteristics of both fibrous tissues (tendon and ligament) as well as cartilaginous tissues (articular cartilage). In bulk, the meniscus extracellular matrix (ECM) contains 85-95% dry weight collagen, of which greater than 90% is type I (Eyre et al., 1983), with the remainder consisting mostly of types II, III, V, and VI (Mcdevitt et al., 1990). Proteoglycans makes up less than 2-3% of the dry weight, eight times less than is seen in articular cartilage (Figure 1.2) (Fithian et al., 1990; Mcdevitt et al., 1990). The meniscus, like articular cartilage, is highly hydrated, with 72-77% of the wet weight comprised of water (Mow et al., 1992). Furthermore, the tissue ranges from being heavily vascularized in the outer periphery to completely lacking blood supply in the inner region (Arnoczky et al., 1982). In the adult meniscus, the inner avascular region is more hyaline-like, while the outer vascular region is more fibrous in appearance (Figure 1.2).

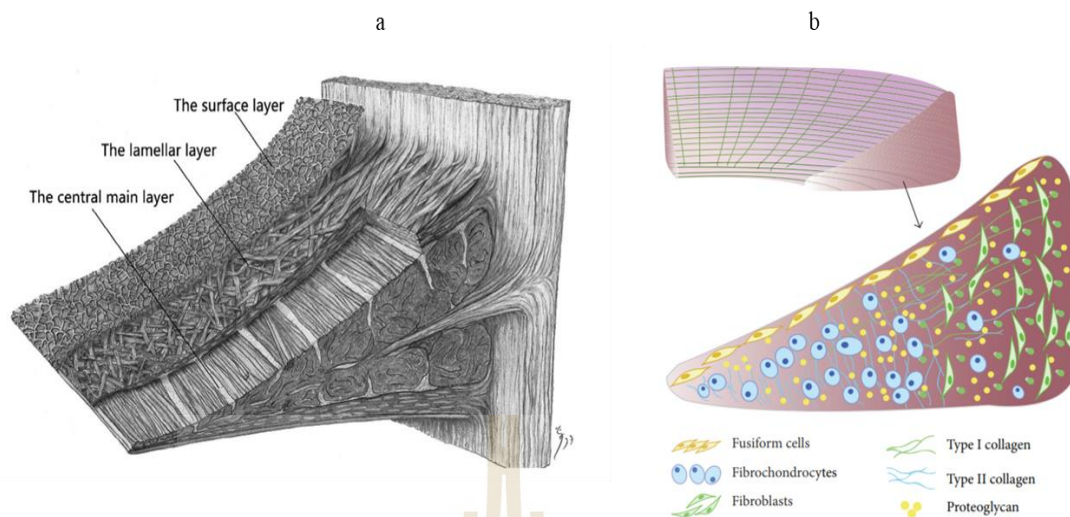


**Figure 1.2** Schematic diagram a) Schematic diagram of the ultrastructure of collagen fibres within the meniscus (Chen et al., 2018). b) Schematic diagram of meniscus internal ultrastructure (Nui et al., 2016). Copyright 2016 Stem Cells International.

#### 1.2.1.2 Mechanical Properties of the Meniscus

Given its central position in the knee, there has been significant interest in elucidating the mechanical properties of the meniscus. Paramount to its mechanical function, the unique architecture of the meniscus consists of circumferentially oriented collagen fibers interspersed with radial collagen “tie” fibers (Fithian et al., 1990). Proteoglycans are present at low levels in general and are highest in the inner avascular zone (Petersen et al., 1998; Buma et al., 2004). As may be expected for such a fiber-reinforced matrix, the mechanical properties of this tissue are highly anisotropic (different in opposing directions), and strongly dependent on the prevailing fiber direction (Setton et al., 1999). This can be seen in the tensile stress-strain response of samples oriented in the circumferential direction as compared to those oriented in the radial direction. Circumferential samples show a pronounced “toe” region common to fiber reinforced tissues, and a higher linear modulus thereafter. Radial samples are relatively linear in their stress-strain response, with a much lower modulus. The tensile properties of the meniscus range from 48-259 MPa in the circumferential direction and 3-70 MPa in the radial direction, depending on anatomic location and species (Fithian et al., 1990; Setton et al., 1999). The compressive properties of the meniscus are low relative to articular cartilage (50-400 kPa, about one-half) (Sweigart et al., 2004; Bursac et al., 2009). The meniscus, while less stiff in compression, is also much less permeable than articular cartilage (Fithian et al., 1990), suggesting that the tissue is optimized to

enhance congruency, load distribution, and shock absorption across the joint (Setton et al., 1999).

## **1.2.2 Meniscal injury and treatment**

### **1.2.2.1 Meniscus damage and healing**

As the meniscus continually operates in a rigorous mechanical environment, damage is common with most patients over the age of 45 displaying some evidence of meniscal scarring. The annual incidence of meniscal injuries is estimated at 60 to 70 per 100,000 per year with the peak in male patients occurring between ages 21 to 30 and between 11 and 20 years of age in female patients (Hede et al., 1990; Nielsen et al., 1991). The cause of meniscal tears in young people is commonly traumatic due to sports injuries. Conversely, in people older than 40 years of age, tears are more often degenerative in nature (Greis et al., 2002). Meniscal injury occurs more frequently in the medial meniscus than the lateral, at a ratio of approximately 2:1 (Campbell et al., 2001), possibly due to the more stable fixation of the medial meniscus. Meniscal damage can manifest in a variety of forms (Figure 1.3) including circumferential or longitudinal tears (where fracture occurs between collagen bundles), or radial tears (where collagen bundles are disrupted). Different tears commonly arise from different origins; trauma leads to bucket handle circumferential tears, while degeneration often results in horizontal and radial tears. Degeneration-associated tears occurring in older patients tend to be complex, involving a combination of the above and displaying largely in the posterior horn. Depending on the tear modality, symptoms manifest differently; for example, bucket handle tears frequently lead to mechanical locking of the knee (Figure 1.3).

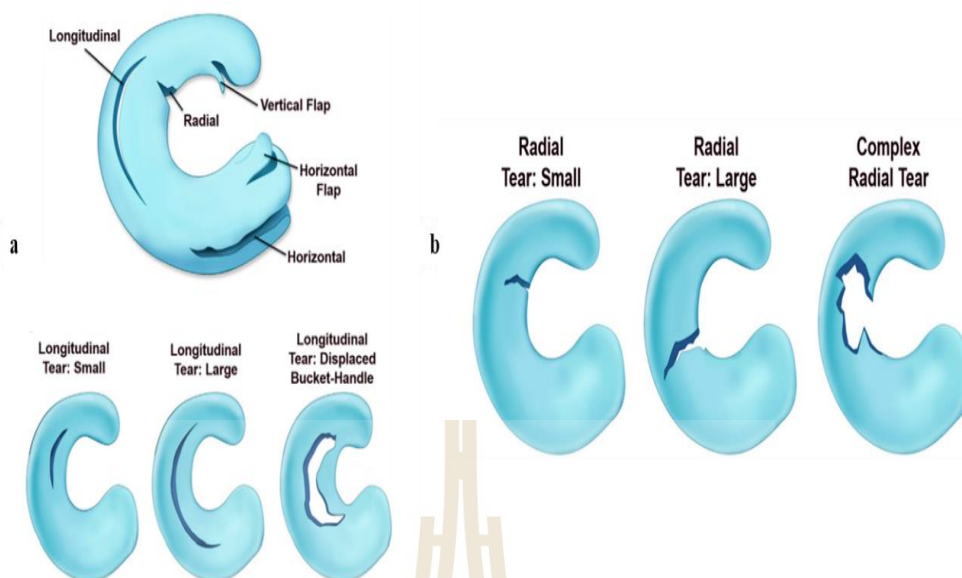


**Figure 1.3** Illustrations showing appearances orientations of different meniscal tears a) longitudinal tear, b) radial tear (Wadhwa et al., 2016). Copyright 2016 European Journal of Radiology.

#### 1.2.2.2 Meniscus repair

The most common and successful repair technique is suturing and stabilizing the meniscal tears, bringing the torn portions back into apposition, whether open repair or arthroscopic surgery (Venkatachalam et al., 2001). These suturing techniques consist of “inside-out” (inside the joint capsule to the meniscus periphery) or “outside-in” (from the periphery to the internal space) approaches (Rodeo et al., 2000). Moreover, there was growing interest in the use of devices which apply inside arthroscopic technique for meniscal repair. These include commercially available biodegradable fixation devices such as screws, darts, and arrows. That provide for reduced surgical times, easier approaches for implantation and make less surgical risk.

#### 1.2.3 Meniscus scaffold for tissue engineering

Disease, and injury can lead to damage and degeneration of tissues in the human body, which necessitates treatments to support their repair, replacement or regeneration. Treatment typically focuses on transplanting tissue from one site to another in the same patient or from one individual to another. Although these treatments have been lifesaving, but they have problems contain with both techniques. Therefore, tissue engineering purpose to regenerate damaged tissues replacing original organ by developing biological substitutes that restore, maintain or improve tissue function. Generally, the term of tissue engineering was mean ‘the

application of principles and methods of engineering and life sciences toward the fundamental understanding of structure-function relationships in normal and pathological mammalian tissues and the development of biological substitutes to restore, maintain or improve tissue function (Chamber et al., 2015) (Figure 1.4).

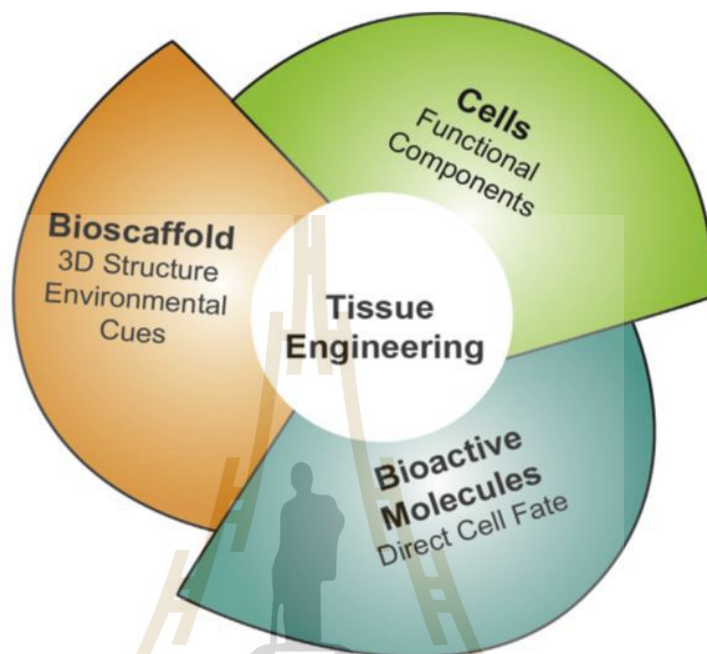


**Figure 1.4** Schematic Tissue Engineering (Sun et al., 2016). Copyright 2016 Operative Techniques in Orthopaedics.

Meniscus damages remain a significant challenge due to the poor for healing potential of the inner avascular zone. Even though advances in surgical techniques and fixation devices, there remains a clinical demand for new strategies for effecting repair of the meniscus. Tissue engineering is considered a hopeful for meniscus repair and regeneration. In meniscus tissue engineering, a scaffold is the basis for regenerating a new structure. The important factor for scaffold is biodegradability, biocompatibility, and mechanical strength. Mechanism of scaffold for tissue engineering is cell seeding into the scaffold, or host cell infiltration into scaffold, which cell will enable the production and homeostatic maintenance of biologic tissue (Makriss et al., 2011). Then, the scaffold was implant into tissue. Scaffold materials are typically selected from polymeric synthetic materials, such as poly-L-lactic acid (PLA), polycaprolactone (PCL), and polyglycolic acid (PGA) and natural material, such as silk fibroin, collagen type I, chitosan, fibrin, and proteoglycans.

### 1.2.4 Biomaterials for meniscus tissue engineering

The basis of important tissue engineering is search material for replace load-bearing structures, which is a suitable scaffold material. Importantly, this structure should be biocompatible with tissue, must support cells, provide the formation of tissue that approximates the model, and function of the native tissue. Normally, biomaterials for meniscus scaffold are synthetic polymers are advantageous in a few characteristics such as tunable properties, endless forms, established structures over natural polymers, and natural polymers as primary bioactive materials used in the applications of biomedical materials. The polymer properties depend on their composition, macromolecules structure, and arrangement. Because of their specific characteristics, such as biocompatible with cell, biodegradation rates, high porosity, high surface-to-volume ratio, and mechanical property (Sun et al., 2016).

#### 1.2.4.1 Synthetic polymers

Many synthetic polymers have been applied for scaffolds development including poly-lactic acid (PLLA), polycaprolactone (PCL), polyglycolic acid (PGA) and their copolymer poly-*dl*-lactic-co-glycolic acid (PLGA), Poly(vinyl alcohol) (PVA) (Figure 1.5). These materials have been much successful towards bone, cartilage, skin, bladder, and liver tissue engineering. Due to architecture and degradation can be well controlled by varying individual polymer composition. The advantages of the synthetic material scaffold are easily controlled physicochemical properties and quality, ability to be processed with various techniques, good biocompatibility, and biodegradation rate. However, limitations of these polymers include the risk of implant rejection due to less bioactivity and the degradation byproduct (CO<sub>2</sub> gas) that lowers the local pH finally effect to cell and tissue (Donnalaja et al., 2020), poor cell adhesion, proliferation and chondrogenic differentiation. In this research, we chosen poly(vinyl alcohol) (PVA) for preparation electrospun nanofiber. PVA is semi-crystalline, hydrophilic, non-toxic, good biocompatibility and good mechanical properties. PVA scaffolds are known to provide mechanical stability for example high tensile strength and elongation at break, flexibility and slow degradation kinetics compared to scaffolds made of natural polymers. These properties have offered PVA scaffolds with the ability to absorb more strain during muscles and bone mechanical loading. Which support more easily the strain changes caused by cardiac contractions. In neural tissues, the PVA scaffold aligned fibers is as important for biological properties. Although several materials and techniques have been employed to this purpose, PVA-based electrospun nanofibers have been shown to meet all the requirements as they can be tuned to fit specific

alignments, porosity, while maintaining their flexibility and biological characters (Teixeira et al., 2019).

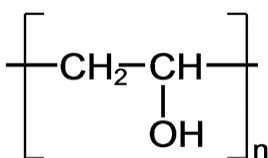


**Figure 1.5** Chemical structure of Poly(vinyl) alcohol (Lamminmeaki et al., 2011).

#### 1.2.4.2 Natural polymers

The use of natural polymers as scaffold materials is most promising for tissue engineering and biomedical applications due to their good biodegradability and biocompatibility. The structure of natural polymers is categorized into three classes as follows

1. Polypeptide and protein-based: fibrin, fibrinogen, gelatin, silk fibroin, collagen, elastin, and keratin.
2. Polysaccharide-based: alginate, chitin, chitosan, hyaluronic acid, glycosaminoglycans. and cellulose.
3. Polynucleotide-based: DNA, linear plasmid DNA, and RNA.

These consist of long chains, including monosaccharides, nucleotides, or amino acids. Which it is repeating unit of covalent bond. Bifunctional molecules which ensure biomimetic nature, bioactivity, and natural restructuring are typically found in natural polymers. The scaffolds made up of natural polymers are biologically active and promote cell proliferation and adhesion. Moreover, they are biodegradable and replaced by biological extracellular matrix over time. Conversely, the limitations are microbial contamination, immunogenic reaction, decreased tunability, uncontrollable rate of degradation, and poor mechanical strength restrict their application for difficult tissue regeneration. Naturally derived polymers including chitin, chitosan, gelatin, silk fibroin, collagen, soybean, fibrin, elastin, and hyaluronan have showed great potential in the tissue engineering application (Figure 1.6). In this research we chosen silk fibroin (SF) for preparation electrospun nanofiber (Chen et al., 2018; Donnalaja et al., 2020).

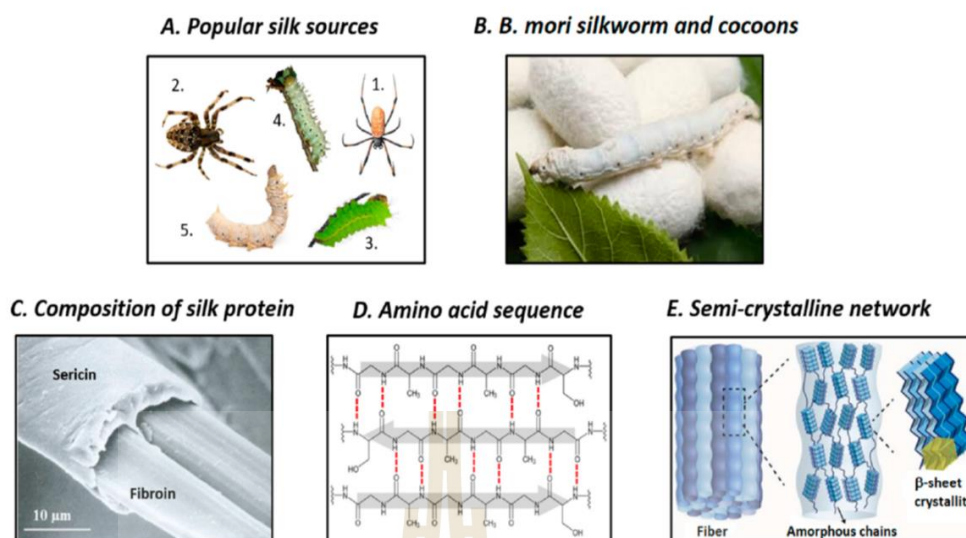


**Figure 1.6** Structures of silk fibroin. (A) Popular silk sources (B) *Bombyx mori* silkworm (C) Composition of silk fibroin (D) Hydrogen bonds between primary amino acid sequence of silk fibroin (E) Semi-crystal network consists of sheet crystallites and amorphous matrix (Nguyen et al., 2019). Copyright 2019 Polymers.

Silk Fibroin (SF) from *Bombyx mori* cocoon is a natural polymer. SF contains with sericin and silk fibroin. The sericin protein present on the outer surface of fiber creates problem in regeneration process, therefore, it should be removed prior to regeneration process. The presence of sericin affects the solubility of fibroin in various solvents. In addition to that sericin is detected as antigenic factor by T cells and has reported to cause immunogenic reactions *In vivo* (Panilaitis et al., 2003). The gummy sericin is easily removed by boiling the cocoons in water with salts (Perez-Rigueiro et al., 2001). The structure of silk fibroin is generally  $\beta$ -sheet due to the dominance of hydrophobic domains of short side chain amino acids in the primary sequence and the spun. The  $\beta$ -sheets are arranged in such a way that the methyl groups and hydrogen groups of opposing sheets interact to form the inter-sheet stacking in the crystals. Strong hydrogen bonds and van der waals forces generate a structure that is thermodynamically stable. The inter and intra-chain hydrogen bonds form between amino acids perpendicular to the axis of the chains and the fiber. Silk fibroin fibers are about 10 – 25  $\mu\text{m}$  in diameter and consist of two proteins: heavy chain (~390 kDa) and light chain (~26 kDa) linked by a single disulfide bond. This structure permits tight packing of stacked sheets of hydrogen bonded anti-parallel chains of the protein. Large hydrophobic domains interspaced with smaller hydrophilic domains foster the assembly of silk and the strength and resiliency of silk fiber. For silk fibroin, in crystalline areas, can be found three structures: silk I ( $\alpha$ -helix), silk II ( $\beta$ -sheet), and silk III. Silk I is

the natural raw form of fibroin found in the *Bombyx mori* silk glands. While Silk II has the arrangement of fibroin molecules in silk with greater strength often applied commercially and silk III is a newly recognized structure of the silk fibroin consist of the [Gly-Ser-Gly-Ala-Gly-Ala] sequence (Figure 1.7) (Valluzzi et al., 1999).

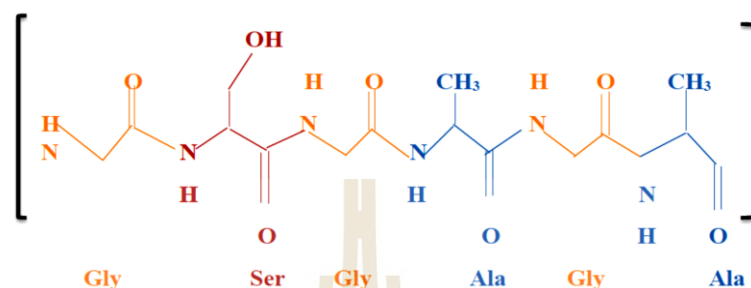


**Figure 1.7** Primary structure of fibroin, showing the [Gly-Ser-Gly-Ala-Gly-Ala] sequence (Valluzzi et al., 1999).

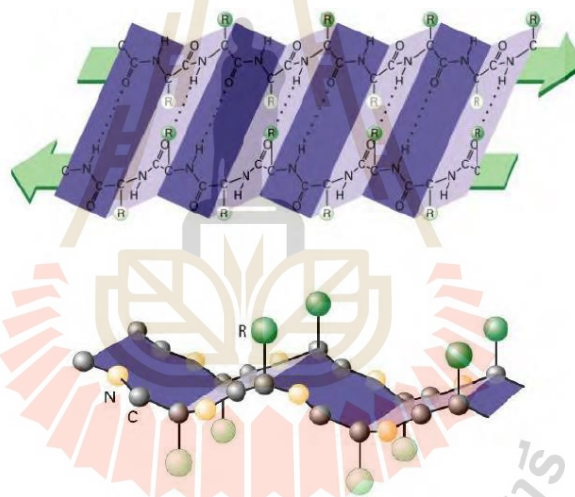


**Figure 1.8** beta-pleated structure of silk fibroin macromolecules (Kudug et al., 2004).

These structures depend on several conditions such as the pH, temperature, solvents, and concentrations of solutions. The sequence of amino acids influences the structural properties of fibroin. In silk II, alanine and serine affect the rigidity of  $\beta$ -sheets (Figure 1.8). Alanine provides stability to the sheets, whereas serine is responsible for hydrophobicity. Several study research of the differences in the structural characteristics and properties of cocoons produced by varieties of *Bombyx mori* summarized that the molecular weight of regenerated silk fibroin, viscosity in solution, and mechanical properties depended on the type of the silkworm. Although the structural characteristics and polymer properties depend on the specific variety of silkworm. The silkworm species is rarely considered in biomedical applications. Even though the variety in the composition of silks, these biomaterials tend to have similar

functionality (Moncada- Saucedo et al., 2019). Silk-based materials manufactured processed from silk fibroin solution is weak as well brittle. The strength of regenerated silk fibroin can be improved from the native silk fiber. There are several studies reported which demonstrated that regenerated silk fibers can keep their initial tensile integrity for 21 days within the *In vitro* conditions (Jin and Kaplan, 2003). Solvents used for electrospinning have an effect on the  $\beta$ -sheet formation of the scaffold structure that can induce modification mechanical properties. Solvents such as formic acid, hexafluoro isopropanol, and water have used to dissolve silk fibroin for electrospun silk fibroin scaffolds. Studies of formic acid and water to improve the mechanical properties of scaffolds (Jeong and Park, 2007; Wang et al., 2004). More recently, SF has been used for medical and tissue engineering applications due to it is non-toxic, good biodegradable and biocompatibility. Silk fibroin can be used as an electrospun scaffold. It can be applied to vascular, bone, cartilage, meniscus, or ligament engineering with its many options.

#### 1.2.5 Electrospinning process for tissue engineering

Electrospinning, also known as electrostatic spinning, is a polymer fiber fabrication process which is typically referred to as a random type of production method due to the nonwoven fiber substrates it typically produces (Thompson et al., 2007). The electrospinning processing method utilized a strong electric field generated by a high voltage power supply between a polymer containing fluid and a grounded conducting collector. The high voltage creates an electrically charged jet which ejects from a needle and undergoes very large stretching. During inject and at the arrival on the conducting collector the solvent evaporates and the polymer solution, creating polymeric fibers. The creating scaffold from electrospinning due to be able to produce a porous, ideally fibers structure and good mechanical properties. In consequence, the electrospinning had the best selection. It is apparent that in order to create a more complex tissue, one has to be able to manipulate the scaffolds at these length scales (Figure 1.9). A nanofibers scaffold has a much closer similarity to the extracellular matrix and offers a much larger surface area on which the cells can attach (Platt et al., 2005). The electrospun nanofibers have mechanical strength and biocompatible qualities and provide an advantage over other 3-dimensional (3-D) scaffolds formed with techniques such as gas-foamed, salt-leached, freeform fabrication, topography library, and hydrogels (Annabi et al., 2010; Hong et al., 2012; Kumar et al., 2011). The high surface to volume ratio and porosity generated by electrospun nanofibers facilitate cell attachment and cell proliferation scaffold (Kumbar et al., 2008).

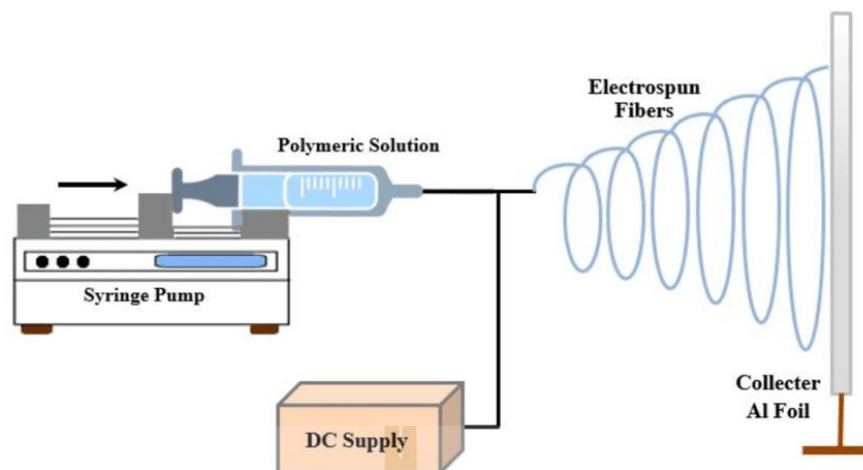


**Figure 1.9** Schematic of a Basic Electrospinning process (Annabi et al., 2010).

Specifically, for meniscus tissue engineering, a scaffold that provides the necessary mechanical properties of the meniscus may be useful to enhance repair of meniscal tear defects and may permit early rehabilitation. Active joint motion during the early phase of repair also helps prevent restrictive adhesions and scar tissue formation that affect a range of motion and limit recovery of function (Figure 1.10) (Platt et al., 2005). Electrospinning has been used for the fabrication of extracellular matrix mimicking fibrous scaffolds. Electrospun nanofibrous scaffolds provide nanoscale fibrous structures with an interconnected pore similar to a natural extracellular matrix in tissues.

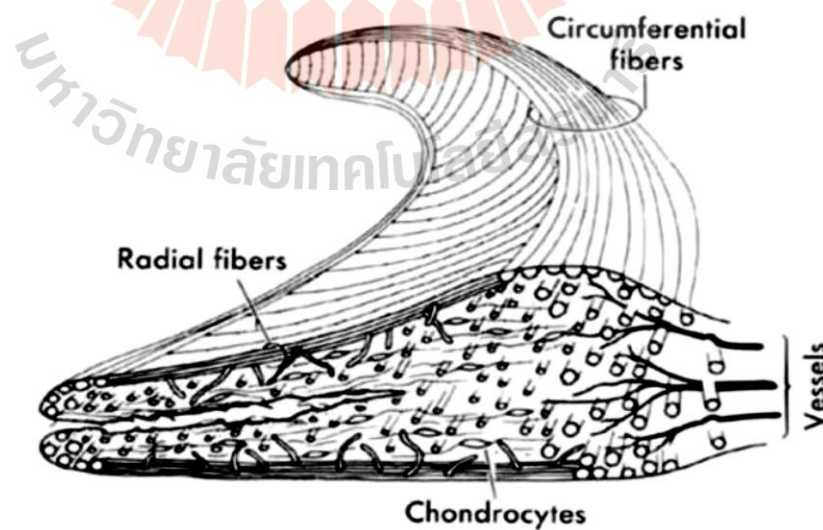


**Figure 1.10** Schematic presentation of the meniscal composite structure (Dasic et al., 2015).

The parameters have been affected to nanofiber morphology in electrospinning can be separated into three groups such as process, solution, and ambient parameters. Although process and solution parameters have been considered by most of the studies, ambient parameters such as temperature and relative humidity (RH) are low investigated.

#### 1.2.5.1 Parameters of electrospinning process

##### 1.2.5.1.1 Processing parameters

There are three important processing parameters that can influence fiber morphology. These parameters that can control the production of bead defects during electrospinning are applied voltage, flow rate, and distance between tip to collector (Sill TJ et al., 2008).

##### 1.2.5.2 Solution parameters

A number of solution parameters also take part in a critical role in fiber production and morphology. Listed in order of relative importance to the electrospinning process, the variables include polymer concentration, solvent volatility, and solvent conductivity (Sill TJ et al., 2008).

##### 1.2.5.3 Ambient parameters

The limited number of studies on effect of ambient parameters on morphology of electrospun nanofibers has been performed. Which it is ambient relative humidity and ambient temperature (Deitzelet al., 2001; Kirecci et al., 2011).

### 1.3 Objectives

1. To study the effect of solvent for silk fibroin extraction on physical properties and biological properties of electrospun nanofibrous scaffold.
2. To study the effect of electrospinning parameters on morphology and mechanical properties of electrospun nanofibrous scaffold.
3. To study the effect of SF/PVA blend ratio on physical properties and mechanical properties of electrospun nanofibrous scaffold.
4. To study the development of electrospun SF/PVA for biomimetic scaffold for potential meniscus tissue engineering application.

## 1.4 Scope and limitations of the study

The scope and limitations of the study are listed:

1.4.1 Silk fibroin extraction by  $\text{CaCl}_2$  and LiBr solvents to fabricate the scaffold.

1.4.2 Silk fibroin powder was characterized by Field emission scanning electron microscopy (FE-SEM), Fourier transform infrared spectroscopy (FT-IR), X-ray diffraction (XRD), and Sodium dodecyl sulfate polyacrylamide gel electrophoresis (SDS-PAGE).

1.4.3 The parameters of electrospinning were studied: humidity, voltage, PVA concentration and nanofibers were characterized by Field emission scanning electron microscopy (FE-SEM) and mechanical properties.

1.4.4 Silk fibroin and Poly(vinyl) alcohol was used to prepare SF( $\text{CaCl}_2$ )/PVA and SF(LiBr)/PVA nanofibrous scaffold at different ratios with electrospinning.

1.4.5 SF/PVA nanofibrous scaffolds were characterized by Field emission scanning electron microscopy (FE-SEM), Fourier transform infrared spectroscopy (FT-IR), thermal gravimetric analysis (TGA), contact angle, mechanical properties, and biocompatibility.

1.4.6 The suitable ratio of SF/PVA was chosen to study gene expression.

1.4.7 The material future research direction. The subsequent step involves testing it with an explant model, and upon successful outcomes, it could undergo testing in animal models, culminating in eventual evaluation through a clinical study.

## CHAPTER II

### LITERATURE REVIEW

#### 2.1 Silk fibroin-based for tissue engineering applications

##### 2.1.1 Silk fibroin extraction

The most common sources to obtain silk fibroin (SF) are *Nephila clavipes* web and *Bombyx mori* cocoon. SF was reported to have much interest in biomedical and tissue engineering applications. A solution of SF protein that is very difficult to extract provides a high molecular weight approximate of 325 kDa and its high crystallinity. Many methods were proposed to dissolve SF which related the use of strong acids solvent or ionic concentrated salt solutions. Researchers used strong acids such as hydrochloric, sulphuric, or nitric acids to dissolve the fibers. Other solvents for example LiBr, CaCl<sub>2</sub>, or Ajisawa's reagent (Abdel-Fattah et al., 2015). Liu et al., (2003) studied silk fibroin by boiling the cocoons by peeling the glue-like sericin with 0.05 wt% sodium carbonate solution. Boiling at  $98 \pm 2^\circ\text{C}$  for 30 minutes, rinsing with warm water and then drying at room temperature. After that, prepared CaCl<sub>2</sub>: ethanol: water (1: 2: 8) 500 mL. boil at  $78 \pm 2^\circ\text{C}$  and stirred, freeze dryer for 48 hours. Wang et al. (2021) studied silk fibroin were prepared from degumming processes by boiling the cocoons in an alkaline solution to eliminate sericin. After that, SF was extracted by salt, such as CaCl<sub>2</sub> or Ca(NO<sub>3</sub>)<sub>2</sub>, then dissolved the salt was removed by dialysis. Which SF can dissolve in the solvent, such as 98% formic acid or 1,1, 1,3,3,3-hexafluoro-2-propanol (HFIP). Bhattacharjee et al. (2014) prepared silk fibroin from posterior silk glands by used aqueous solution of 1% w/v sodium dodecyl sulfate with 10 mM Tris and 5 mM EDTA. After that, the silk fibroin was submitted to extended dialysis to remove surfactant. Luetchford et al. (2020) prepared silk cocoons to extract silk fibroin. The chopped cocoons were degummed by boiling in 0.02 M sodium carbonate for 1 hour and washed 5 times in distilled water. Degummed silk was dried at room temperature. The dried degummed silk was dissolved at 15% w/v in 9 M LiBr at 60°C for 4 h. After that, it was filtered and dialyzed 2-3 days. The SF solution was freeze dried and kept at 4°C.

Pillai et al. (2016) extracted SF from cocoons. SF threads were degummed using 0.5 M  $\text{Na}_2\text{CO}_3$  solution at 100°C for 1 h and washed 3 times with distilled water. The degummed silk was dissolved in  $\text{CaCl}_2$ /ethanol/water (1:2:8) at 60°C until solution was clear. This solution was dialyzed 2 days in distilled water followed by dialysis with polyethylene glycol for 1 day. Li et al. (2015) prepared silk fibroin by dissolving SF with  $\text{CaCl}_2$ /ethanol/water (1:2.5:8) and dialysis with distilled water 3 days. The SF solution was lyophilized at -55°C for 24 h and stored at 4°C. Liu et al. (2013) prepared waste cocoons were, which cut and boiled in 1% sodium carbonate solution for degumming. Degummed silk was put into 10 g.  $\text{CaCl}_2$  solution of different concentration and stirred for 1 h at 98±2°C, cooled and filtered. Dialysis SF solution with deionized water and the regenerated SF solution after dialysis was stored at 4°C. Garcia et al., (2009) prepared silk fibroin with cocoons and purified its sericin content. The degummed SF was dissolved at 10% w/v in 9 M LiBr solution at 55°C until a clear solution was obtained. This solution was dialyzed with ultrapure water for 48 h and 5 changes of water phase. The aqueous silk fibroin solutions could be stored at 4°C. Wang et al., (2019) extracted silk proteins, which were dried and dissolved in 9.3 M LiBr solution at 60°C for 4-6 h at 20% concentration. The silk solution was dialyzed against Milli-Q water for at least 2 days in a dialysis cassette. SF solution was frozen at -20°C for 24 h and freeze dried. Aznar-Cervantes et al. (2013) also compared different silk fibroin extraction methods. The SF extraction methods used 9.3 M LiBr, 50 wt%  $\text{CaCl}_2 \cdot 2\text{H}_2\text{O}$ , and Ajisawa's reagent composed of  $\text{CaCl}_2$ :EtOH:H<sub>2</sub>O (1:2:8 in molar ratio). The molecular weight of silk fibroin polypeptides was found to play an important role in the nanofiber sizes of the electrospun fiber creating thinner fibers. Which SF was extracted with LiBr 9.3 M generate high molecular weight than Ajisawa's reagent or  $\text{CaCl}_2$ . The mechanical properties of silk fibroin nanofiber were found that ultimate tensile strength and young modulus of  $\text{CaCl}_2$  higher than LiBr and Ajisawa's reagent shown in Figure 2.1.

Protocol	Young's modulus (MPa)	Elongation (%)	Ultimate strength (MPa)
<i>LiBr</i>	270 ± 44	2.78 ± 0.78	5.92 ± 1.08
<i>CaCl<sub>2</sub>:EtOH:H<sub>2</sub>O</i>	252 ± 41	3.90 ± 0.67	7.45 ± 1.34
<i>CaCl<sub>2</sub></i>	252 ± 75	5.03 ± 1.32	9.33 ± 2.62

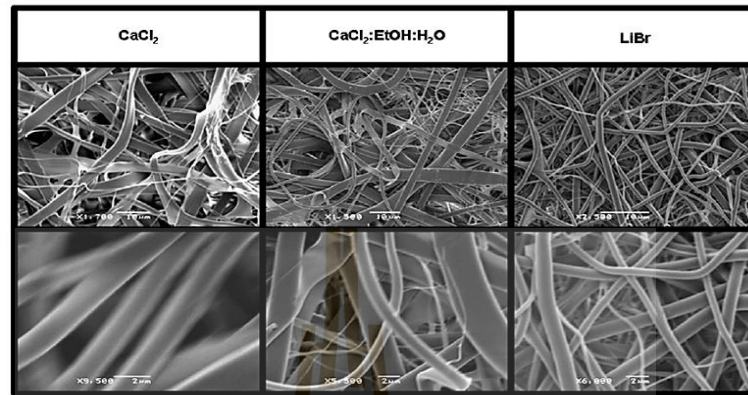


**Figure 2.1** Mechanical properties and SEM image of electrospun mats produced with 17 wt.% dissolutions of SF in HFIP (Aznar-Cervantes et al., 2013). Copyright 2013 Materials Science and Engineering: C.

Cao et al. (2009) extracted silk fibroin with 9.3 M LiBr solution at 60°C. The solution was dialyzed with distilled water for 3 days using a cellulose membrane with a molecular weight cut-off of 8000-14000. They compared silk fibroin dissolving with 98% formic acid and hexafluoroisopropanol (HFIP). After that, the silk fibroin solution was fabricated with the electrospinning method. The electrospun nanofiber dissolving with formic acid was found to be  $\beta$ -sheet more than silk fibroin dissolving with HFIP.

### 2.1.2 Silk fibroin-based scaffold for tissue engineering applications

The utilization of silk fibroin (SF), which is the main protein of silkworms, has not been limited to the textile industry but has been further extended to many high technology applications including biomaterials for biomedical and tissue engineering. Several researchers applied SF to developing research due to the properties of SF composed of its facile processability, good biocompatibility, biodegradation, and versatile functionalization. Therefore, SF was accepted for its use in innovative applications. Farokhi et al. (2018) studied silk fibroin (SF) with strong potential for many biomedical applications. Especially, SF has attracted interest in the work of bone tissue engineering due to its special characteristics in terms of biocompatibility, biodegradability, elasticity, and flexibility. In this research, they used SF blend with hydroxyapatite for bioceramic with good biocompatibility and it is suitable for constructing orthopedic and dental substitutes. Yan et al. (2012) showed the result of the mechanical properties of the silk fibroin scaffold at different concentrations as follows

silk-8%, silk-10%, silk-12%, and silk-16% was found to increase tensile strength with an increase of silk fibroin concentration. The SF scaffold was presented a more swelling capability that increased with increasing porosity. Therefore, the silk fibroin scaffolds are good candidates for use in tissue engineering applications for cartilage and meniscus regeneration. Min et al. (2004) studied the silk fibroin nanofiber was produced by the electrospinning method is introduced for the application of wound dressing. The SF nanofiber was characterized by pore size distribution, high porosity, and high surface areas. Which are suitable parameters for cell attachment, cell growth, and cell proliferation. Kim et al. (2005) studied biocompatibility of the silk fibroin nanofiber, and to examine its effect on bone regeneration in a rabbit. The result was shown to possess good biocompatibility with enhanced bone regeneration and no evidence of any inflammatory reaction. Therefore, the silk fibroin nanofiber was suitable useful as a tool for guided bone regeneration. Lee et al. (2017) developed auricular cartilage using silk fibroin and polyvinyl alcohol hydrogel. They prepared different hydrogels with various ratios of SF and PVA using freeze-thawing, salt leaching, and silicone mold casting methods. The cell viability results found a blended hydrogel at a ratio of 50% PVA and 50% SF to be the optimal hydrogel among the fabricated hydrogels. Bhattacharjee et al. (2014) used silk fibroin from non-mulberry tropical tasar of *Antheraea mylitta* for the bioactive polymer is blended with polyvinyl alcohol. Which blended polymer was fabricated with the electrospinning method. The nanofiber scaffold of 2 wt% SF presented higher cell attachment and cell growth when compared to PVA as control and the other blend ratio (Figure 2.2). Cell adhesion of SF/PVA by MG-63 cells showed that MG 63 cells were attached to 2SF/PVA and 4SF/PVA within initial 1 h and the percentage increased after 6 h. When compared to pure PVA, Pure PVA has a lower percentage of attached cells than PVA with silk fibroin. Cell proliferation showed result proliferation of the cells during cell culture for 21 days indicated superior cell response on the blended matrix compared to PVA alone. The mechanical properties of constructs similar to the native bone tissue exhibited to possible for polymer blend in bone regeneration and reconstruction.

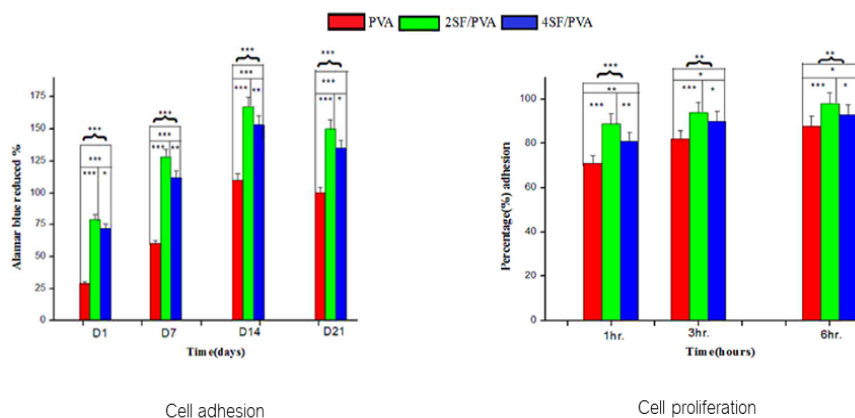


**Figure 2.2** Cell adhesion and Cell proliferation (Bhattacharjee et al., 2014).

Pillai et al. (2016) developed silk fibroin nanofibrous scaffolds to examine cell attachment and cell proliferation of primary human meniscal cells. SF:PVA electrospun nanofibrous scaffolds with various blend ratios 2:1, 3:1, and 4:1 were fabricated with electrospinning. Meniscus cell attachment studies confirmed that ratio 3:1 SF:PVA nanofibrous scaffolds promoted better cell attachment and cell growth. The DNA and collagen content increased highly with ratio 3:1 SF:PVA. These results showed in Figure 2.3 and the nanofiber of SF:PVA at 3:1 ratio is proper for meniscus cell proliferation when compared to pure SF:PVA nanofibers.

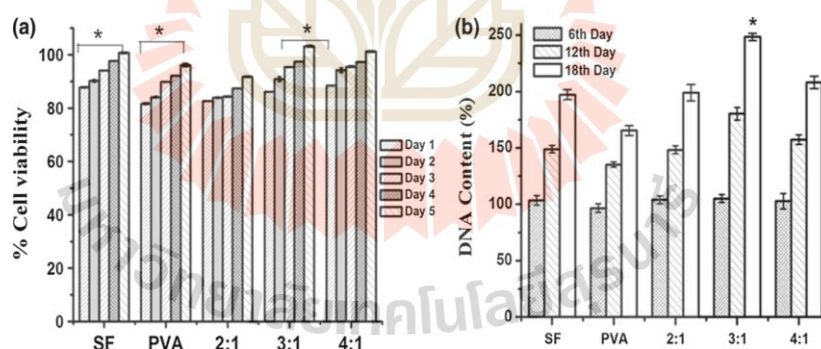


**Figure 2.3** a) MTT assay and b) DNA estimation of meniscus cells seeded on scaffolds (Pillai et al., 2016).

Zhou et al. (2013) studied composite nanofibrous membranes of N-carboxyethyl chitosan/poly(vinyl alcohol)/silk fibroin nanoparticles that were prepared by electrospinning. The cytotoxicity evaluation of the nanofibers was studied. The result indicated the nanofibers had good biocompatibility. This electrospun nanofiber would be used as a developing wound dressing for skin regeneration. Mohammadzadehmoghadam et al. (2019) studied *Bombyx mori* silk fibroin (SF) /gelatin nanofiber with various blend ratios of 100:0, 90:10, and 70:30 was fabricated by

electrospinning and crosslinked with glutaraldehyde. The tensile properties of nanofiber depending on the gelatin content. The blending of 10% and 30 wt% gelatin into SF affected higher tensile strength and Young's modulus of SF/Gelatin nanofiber. However, the blend ratio of 70:30 demonstrated the lowest 3T3 fibroblast cell responses for proliferation rates. Dehghan-Manshadi et al. (2019) have prepared scaffold composing of silk fibroin (SF) and elastomer polyurethane (EPU) 2 medical grad and various mass ratios were fabricated by electrospinning method. The nanofibrous scaffolds have been already, demonstrated that both the mechanical properties and the structural features of electrospun scaffolds are an important role in cell proliferation. The biocompatibility of all nanofiber scaffolds in contact with Fibroblast cells from human neonatal foreskin for 1, 5, and 7 days was confirmed. When SF has increased, the cell attachment and cell proliferation rates were increased (Figure 2.4 ).

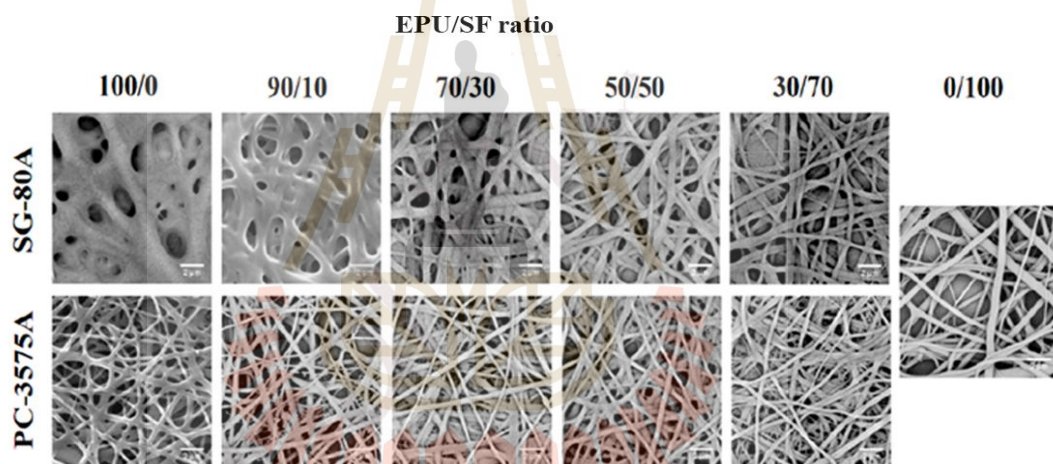


**Figure 2.4** SEM images of the methanol-treated electrospun fibers (Dehghan-Manshadi et al., 2019).

Selvakumar et al. (2015) prepared silk fibroin from *Bombyx mori* cocoon after degumming. SF solution was used to fabricate scaffolds such as nanofibers, sponge and porous film. They studied cell culture of the cytocompatibility of scaffold in vitro by seeding osteoblast-like cell onto the methanol treated scaffold in Dulbecco's Modified Eagle's Medium (DMEM). The result showed that the cells started extending their cytoplasm over the surface of the scaffold after five days of cells seeding. The number of cells on the scaffold surface was found to increase with increasing in incubation time. This image showed stained nuclei indicated the attachment of cells on the scaffold surface. SF film and SF nanofibers supported more cells attachment on the surface (Figure 2.5).

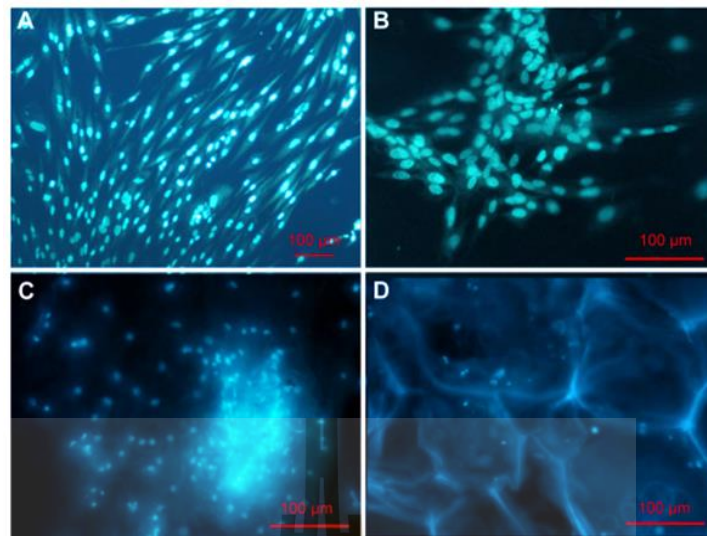


**Figure 2.5** Hoechst-stained images of osteoblast cells (MG63) control (A), cells attached to film (B), electrospun nanofibrous scaffold (C), and lyophilized sponge (D) (Selvakumar et al., 2015).

## 2.2 Poly(vinyl alcohol) based for tissue engineering applications

Poly (vinyl alcohol) (PVA) is a synthetic polymer with hydrophilicity (-OH groups), it had properties of biodegradability and good biocompatibility. Baum et al. (1924) prepared PVA by using vinyl acetate and since then the biomaterial has been used widely range in industrial and biomedical applications. They used PVA due to its unique properties such as water solubility, excellent biocompatibility, promising biodegradability, low toxicity, and adhesive properties. PVA has attracted much attention in the biomedical field and especially in tissue engineering applications.

### 2.2.1 Effect of PVA concentration on mechanical properties

Various research has shown the influence of molecular weight on the properties of the PVA polymer. Whereas Hajij et al. (2016) studied high molecular weight PVA films with higher tensile strength and elongation at break and that high degree of hydrolysis provides great rigidity to the blended films. Ngadiman et al. (2015) used PVA solution with 5% w/v and 10% w/v and dissolved in deionized water 80°C with constant stirring for at least 4 h. PVA solution was formed with electrospinning machine. The parameter used high voltage 35 kV, flow rate was used 1.0 ml/h and distance from the tips to collector was 8.0 cm. The result of mechanical properties shows that the higher solution concentration 10% w/v has higher mechanical properties compared to the lower solution concentration 5% w/v. Lower concentration of PVA tend to produce smaller diameter nanofibers. The mechanical properties of

electrospun nanofibers of PVA were lowered. Which is show mechanical properties in Table 2.1.

**Table 2.1** Mechanical Properties of electrospun PVA nanofibers (Ngadiman et al., 2015).

Molecular Weight (k Da)	Tensile Strength (MPa)		Young's Modulus (MPa)		Contact Angle (°)	
	5% w/v	10% w/v	5% w/v	10% w/v	5% w/v	10% w/v
60	16.8±0.4	20.5±0.9	54.0±0.6	55.5±0.3	34.62±0.51	35.37±0.69
124	23.6±0.7	26.2±1.3	60.1±0.7	69.6±0.9	35.81±0.73	35.60±0.84
145	25.1±0.5	28.5±0.3	65.7±1.1	76.0±0.4	36.72±0.98	34.82±0.57
200	27.0±0.2	29.8±0.3	68.0±0.4	77.9±0.8	34.69±0.52	35.73±0.48

Sharifi et al. (2016) prepared poly(vinyl alcohol) (PVA) (Mw: 61000 g/mol) concentration 6% w/v and 12% w/v and dissolved in DMSO was heated to 120°C within 20 min, and then PVA solution was vigorous stirring. After stirring for 2 hours, the mixture was cooled to room temperature. The results of tensile test showed that a wide range of mechanical properties can be achieved by changing the PVA concentration. When the PVA concentration increases from 6% to 12%, the tensile stress at break and Young's modulus are enhanced by 390% and 102%, respectively. Ou et al. (2017) prepared PVA with distilled water and heated at 90°C with vigorous stirring to obtain homogeneous PVA solution. Then added AM monomer into PVA solution. The mixture of PVA content was 2.5 wt%, 5.0 wt%, 7.5 wt% and 10 wt%. The result of mechanical properties shows increased tensile strength for higher PVA content. The tensile strength of Freeze Thawed gels increases from 0.15 MPa to 1.62 MPa. Lee et al. (2004) also concluded that high molecular weight PVA displays a highly crystalline structure, improved thermal stability and superior mechanical properties than low molecular weight PVA. Teixeira et al. (2020) summarized that polymer crystallinity is also influenced by the degree of hydrolysis. As acetate groups are larger than -OH groups. Hence PVA with a low degree of hydrolysis exhibits lower crystallinity. As such, a highly hydrolyzed PVA is more crystalline than partially hydrolyzed PVA and presents higher glass transition and melting temperatures.

### 2.2.2 Poly(vinyl alcohol)-based scaffold for tissue engineering applications

Liang et al. (2009) studied PVA and chitosan for many tissue engineering applications. They fabricated PVA nanofiber and PVA/Chitosan nanofiber with

electrospinning. NIH 3T3 fibroblast cells were seeded onto scaffolds for different time points. The result showed that the number of living cells both on the PVA/Chitosan and empty well were significantly higher than PVA nanofiber. The nanofiber indicated good cell viability and gene expression on the PVA/Chitosan nanofiber scaffold. Thus, PVA/Chitosan nanofiber scaffold could be the better choice for further tissue engineering applications (Figure 2.6).

Gholipourmalekabadi et al. (2014) studied a PVA/PCL/chitosan nanofiber for applications in burns and wound healing. Scaffolds were tested with and without seeded hMSCs, which the target was to recruit other host cells and induce the secretion of growth factors. Nanofibrous scaffolds were implanted in vivo on the dorsum of rats, and the healing process was monitored. Seed cells onto scaffolds were found successful in promoting wound healing than the acellular scaffolds. While, the chitosan antioxidant, anti-inflammatory, and antibacterial capacities reduced the number of inflammatory cells in the wounded area. The physical and mechanical properties of the PVA and PCL maintained the integrity of the fibers while in contact with fibrin and blood. PVA-based scaffolds have been applied for skin healing and renewal purposes. Vashisth et al. (2016) developed a scaffold based on the PVA and gellan (PVA/gellan) for skin repair. Gellan, as a natural polymer, shows excellent properties to this objective including biocompatibility, biodegradability, and water adsorption properties. In polymer blending, PVA reduced the polymer repulsive forces, leading to the formation of uniform nanofibers. PVA/gellan nanofibers were physically crosslinked by heat treatment at 150°C for 30 min. The interactions between the PVA and gellan showed in Figure 2.7. Cell culture studies using human dermal fibroblast (3T3 L1) for scaffolds as promoters of cell adhesion and cell proliferation compared to gellan dry films and hydrogel showed in Figure 2.6.

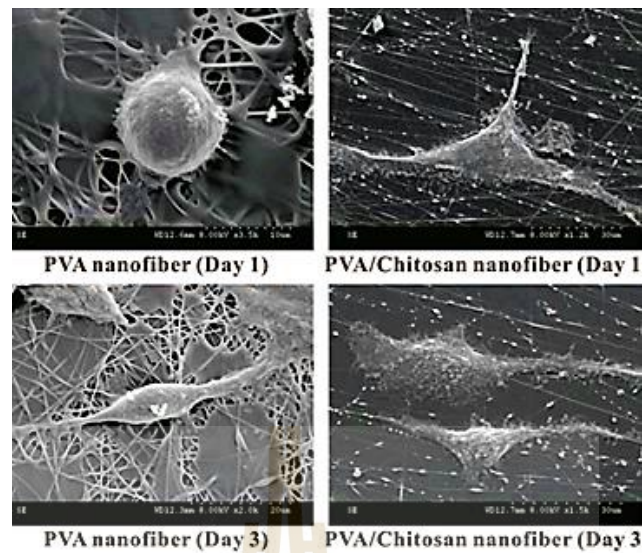


**Figure 2.6** NIH 3T3 fibroblast cell morphology on PVA nanofiber and PVA/Chitosan nanofiber (Liang et al., 2009).

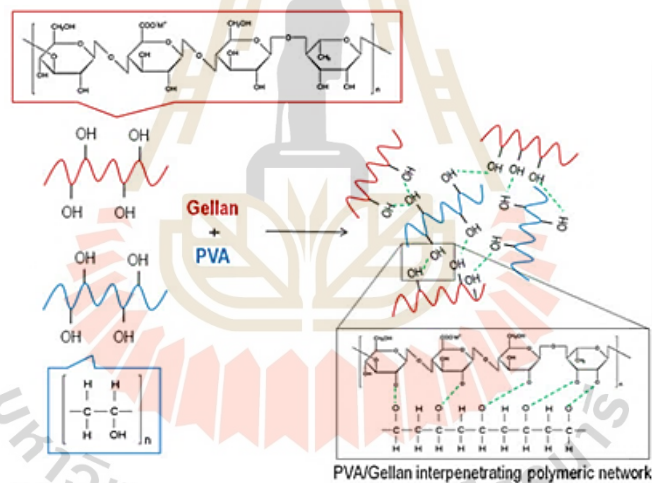


**Figure 2.7** Representation of the interactions established between PVA and gellan, after crosslinking (Vashisth et al., 2016).

Adeli et al. (2019) designed a blend of PVA, chitosan, and starch nanofibrous scaffold for wound dressings which used starch for additive. The hybrid formulation indicated great capacity to support a moist environment for wound regeneration, with balanced water absorption and water vapor transmission rates. They protect the wounded area against external forces during the healing process. The scaffold has good antibacterial activity against both *Escherichia coli* and *Staphylococcus aureus*. Moreover, cell culture studies fibroblast (L-929) and in vitro cytotoxicity assays showed appropriate cytocompatibility and cell viability showed in Figure 2.8, which was also confirming the potential of a hybrid polymer combination for wound healing.

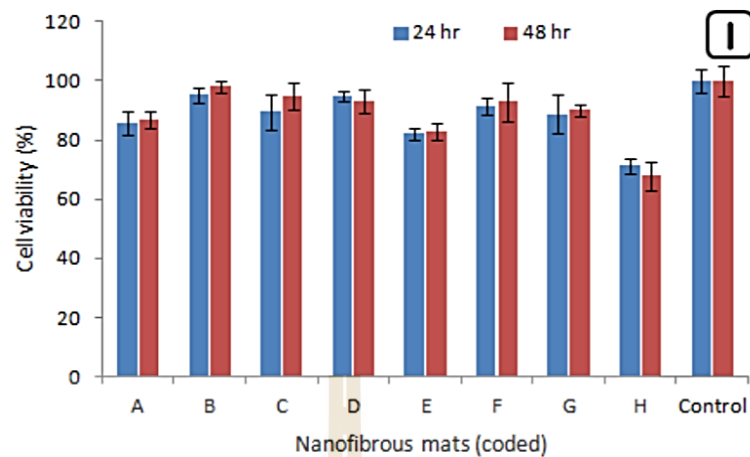


**Figure 2.8** MTT optical microscopy images of L-929 cells growth after 48 hr. culturing in presence of the nanofibrous mats (I) Cell viability of fibroblast (L-929) cell cultured for 24 and 48 hr. in presence of nanofibrous mats (Adeli et al., 2019).

Kim et al. (2011) prepared and cell affinity studies of the pure PVA and PVA/hyaluronic acid (HA) crosslinked nanofibers with hydrochloric vapor and post crosslink with the electrospinning method. Cell culture studies MC3T3-E1 osteoblast-like cells found that SEM images in Figure 2.9 of MC3T3-E1 showed growth onto Total cell density (TCD), pure PVA, and PVA/HA hydrogel nanofibers with different cell culture times. Which it appeared that MC3T3-E1 cells have well adhered to the PVA/HA hydrogel nanofibers different pure PVA hydrogel nanofibers. After the cell culture for 24 hr. The MC3T3-E1 cells grown onto PVA/HA hydrogel nanofibers became large cells with cell-to-cell interactions, suggesting an enhanced cell migration for cell organization (Figure 2.9).

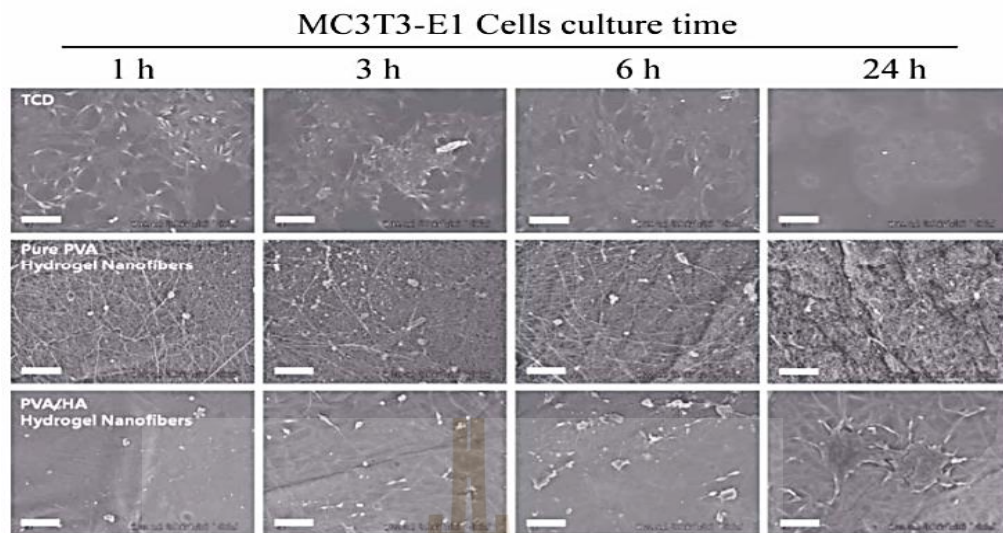


**Figure 2.9** SEM images of MC3T3-E1 cells cultured on TCD, pure PVA hydrogel (molar ratio of GA and PVA  $\sim 10.3:1.0$ ), and PVA/HA hydrogel (molar ratio of GA and PVA  $\sim 24.8:1.0$ ) nanofibers as a function of cell-culture time (Kim et al., 2011).

Mozafari et al. (2012) have fabricated electrospun PVA/chitosan nanofibrous scaffolds that have been synthesized with large pore sizes as potential matrices for nervous tissue engineering. The result of PVA blend with chitosan at different weight ratios showed chitosan scaffold was used for in vitro cell culture in contact with PC12 nerve cells. They were found to present the most suitable properties to meet the basic required specifications for nerve cells. The addition of chitosan to the PVA scaffolds increases the cell viability and cell proliferation of nerve cells, which increases the biocompatibility of the scaffolds. Sambudi et al. (2015) have developed electrospun Chitosan/PVA nanofibrous scaffolds, which adding  $\text{CaCO}_3$  nanoparticles for reinforcing agents in increasing mechanical properties, biocompatibility for cartilage tissue engineering. The tensile test gave the highest Young's modulus of Chitosan/PVA- $\text{CaCO}_3$  (4 wt%). Cell culture studies ATCD5 cells showed in Figure 2.10, The cell proliferation assay indicated Chitosan/PVA- $\text{CaCO}_3$  (4 wt%) provides the most suitable for cell growth (Figure 2.10)

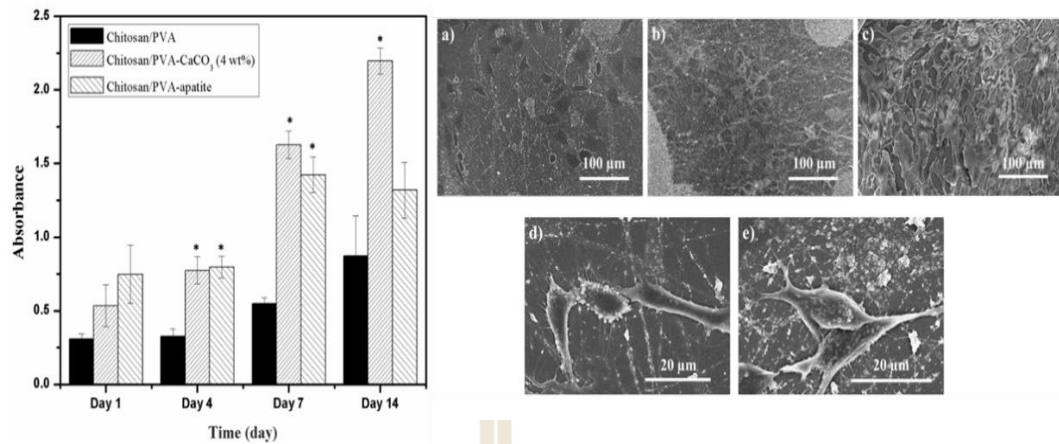


**Figure 2.10** Growth of ATDC5 cells on Chitosan/PVA, Chitosan/PVA-CaCO<sub>3</sub> (4 wt%), Chitosan/PVA-apatite fibers after 1, 4, 7 and 14 days of culture and morphology of ATDC5 cells growing on chitosan/PVA-CaCO<sub>3</sub> (4 wt%) matrix on (a) day 1, (b) day 4, (c) day 14, (d) enlarged image of day 1 and (e) enlarged image of day 4 (Sambudi et al., 2015).

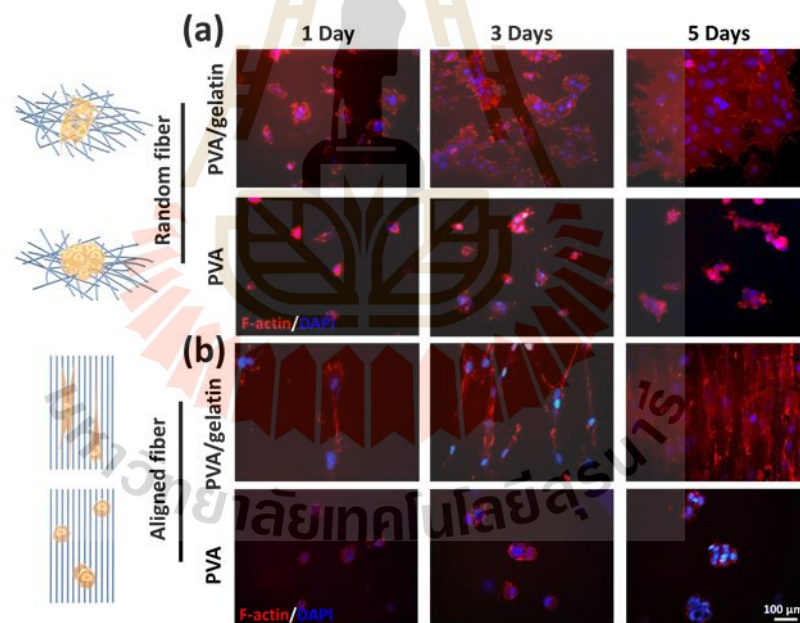


**Figure 2.11** Fluorescence merged image of 3T3 fibroblast cells cultivated on random and aligned PVA and PVA-gelatin meshes for 1, 3, and 5 days (Huang et al., 2016).

Huang et al. (2016) studied cell behavior of randomly oriented or aligned PVA nanofiber and PVA-gelatin nanofiber. The result showed fibroblasts cells growing on PVA-gelatin fibers indicate a larger area as compared with PVA nanofiber. They found the limit of colonies on PVA nanofibers. The initial survival of cell culture showed that the low protein affinities with PVA limit the absorption of extracellular matrix to support cell attachment showed in Figure 2.11.

## 2.3 Electrospinning for tissue engineering applications

Tissue engineering uses for biology, medicine, and engineering with the design of biological substitutes to repair, restore, and maintain for improving the functions of the tissue. To fabricate a function of tissue, the engineered structures have to be able to mimic the extracellular matrix. Electrospinning has been accepted and is one of the most useful methods based on the similarity between electrospun nanofibers and the native tissues.

### 2.3.1 Parameters affecting the electrospinning efficacy

For electrospinning, process parameters have affected the surface morphology, fiber diameter, and texture of the fibers. These parameters consist of the polymer solution such as concentration, viscosity, surface tension, and electrical conductivity. The operational settings such as electrical field, the distance between the tip to the collector, flow rate, and rotating speed of the collector. The last condition is the environment such as humidity and temperature. The concentration of the polymer solution is a key factor controlling the electrospinning process. Tarus et al. (2016) studied cellulose acetate (CA) and poly (vinyl chloride) (PVC) nanofiber that were electrospun nanofibers. The morphology of nanofiber showed a beaded fibrous structure could be electrospun at 10% CA in both Acetone/DMAc and Acetone/DMF solvent systems. For PVC, beaded fibers were formed at 12% PVC. Tensile tests showed that the non-aligned nanofiber was influenced by solution concentration. When increasing solution concentration, the tensile strengths, strains at break and initial modulus of the CA nanofiber was increased. Thus, the solution concentration was increased, the nanofiber diameter, tensile strength and the rupture increased (Figure 2.12).

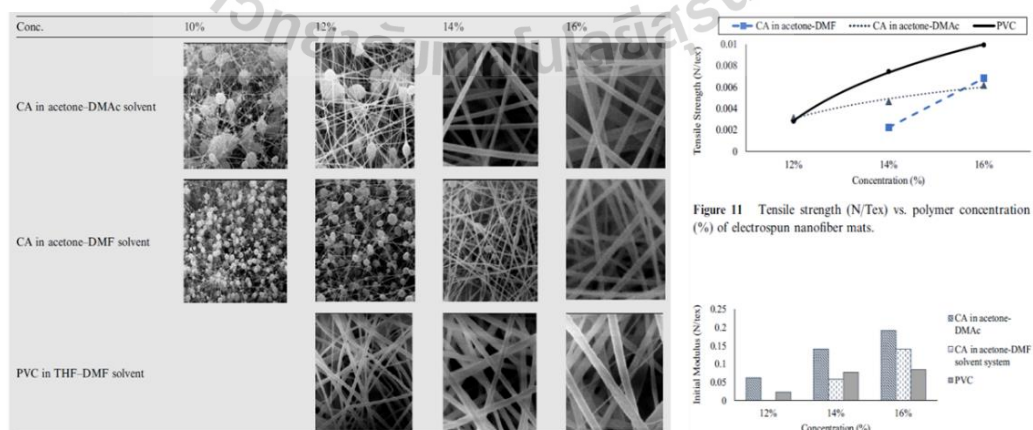


**Figure 2.12** SEM micrographs and mechanical properties of electrospun CA nanofibers (Tarus et al., 2016).

Mwiiri et al. (2020) studied PVA-based electrospun fibers with a colloidal dispersion of a birch bark extract as the active agent for increased wound healing. The concentration and molecular weight of the PVA as the important parameters have affected on the rheological properties of the polymer solution and affect directly the resulting fiber properties. Therefore, the viscosity of polymer solutions increased when the concentration and molecular weight was increased (Figure 2.13). The colloidal triterpene dry extract (TE) dispersions resulted in electrospun fibers of thinner diameters. The thickness of the electrospun nanofibers which can be adjusted with the polymer concentration and molecular weight. Uniform and smooth nanofibers constructs can be obtained by selects polymers with suitable molecular weights. At low molecular weight polymer solutions, beads may appear instead of fibers, while high molecular weight polymer solutions effect to fibers with relatively increased average diameter. Furthermore, suitable of surface tension which is a function of solvent can impact the electrospinning process and fiber fabrication. In a solution with high surface tension, the formation of fibers can be limited because of an unstable jet and dispersion of droplets. Lower surface tension can facilitate the electrospinning process at lower electric fields (Rahmati et al. 2020). Fiber diameter first increases and then decreases slightly when the electrical conductivity of the polymer solution was increased. Yang et al. (2008) demonstrated that the electrical field distribution of PEO solution. Force of the electric field increases with an increasing voltage at the nozzle, which causes decreasing the fiber diameter because of the elongated jet path and increased bending frequency. A uniform electric field provides a proper electric field distribution. The formation of thinner fibers as a result of higher bending speed, which

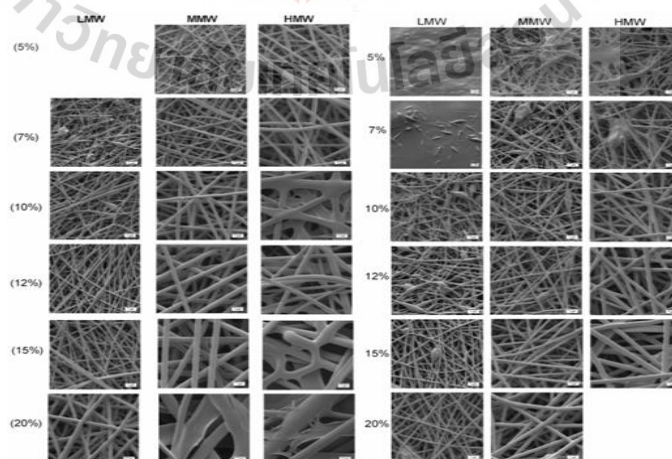


**Figure 2.13** SEM morphologies at 10,000 $\times$  of electrospun PVA and PVA/TE blend (60:40) fibers at different concentrations and molecular weights (Mwiiri et al., 2020).

stretches the fibers. Electrospinning can be generated nanofibrous scaffolds whereas there overcomes the threshold voltage that causes various charge differences in solution during the process. Beachley et al. (2008) showed that continuous PCL nanofibers with diameters in the range of 350 nm to 1  $\mu\text{m}$ , and high voltage, polymer concentration, and plate size had effects on maximum fiber diameter, fiber length, and fiber uniformity. This result indicates that shown that all of these parameters can be controlled by changing the electrospinning conditions. It was shown that fiber length could be increased by increasing the PCL concentration in the solution. When increasing the voltage and the charge value, the formation of droplets and beads in the fibers can be changed. The other important factor in this consider is the flow rate of the polymer solution. While the feed rate of the solution was decreased the time required for solvent evaporation was increased. For electrospinning, a lower flow rate is normally applied to ensure the complete evaporation of solvents from fibers (Greiner et al., 2007; Fridrikh et al., 2003; Sukigara et al., 2003). Moreover, the distance between the tip of the needle to the collector is a key factor that controls the fiber diameter and morphology. When the distance is short, the fibers do not have enough time to solidify before reaching the collector, and a larger average of fiber diameters. After that, the distance is large, thinner fibers may be formed (Yuan et al., 2004). The ambient parameters for instance humidity and temperature of the environment while fabricating an electrospun nanofiber are also necessary studies. Specifically, when high humidity is negatively correlated with the solidification time thus high humidity resists the spinning process due to the solution viscosity being increased. Some studies reported that solvents can be completely removed by evaporation if the humidity is enough low. While in highly humid environments the fibril formation was decreased (Huang et al., 2003). Temperature is another factor that affects the morphology of nanofibrous scaffolds. Two types of morphologies are observed based on temperature differences as follows beads formation, which is formed at low temperatures. At high temperatures, the fiber was condensed and flat fibers. By increasing the temperature, the viscosity of the polymer solution was decreased, leading to producing a small fiber diameter (Rodoplu et al., 2012).

### **2.3.2 Electrospun nanofibrous scaffolds for tissue engineering applications**

In the past decade, various researchers have studied the application of different synthetic polymers and natural polymer uses for tissue engineering applications to satisfy clinical needs. The synthetic polymer includes polylactic acid, polycaprolactone, poly amino acid, and polyvinyl alcohol, etc. For natural polymer

such as silk fibroin, chitosan, hyaluronic acid, and gelatin, etc. Which these polymers are biodegradable and biocompatible with promising potential in the biomedical field. However, the controlling of electrospinning parameters can be fabricated nanofiber for biomedical application. In addition, electrospun nanofibers can potentially direct cellular and molecular responses after implantation, for example, Neves et al. (2007) fabricated various fiber meshes based on poly(ethylene oxide) (PEO) and PCL can be produced by electrospinning. The fiber meshes keep having average diameters in the submicron range. The tensile test of the nanofiber meshes is very consistent which the tensile properties depend on the degree of alignment of the fibers in the mesh. Cell adhesion on fiber showed that the cells are viable when seeded osteoblastic cells to PCL fiber meshes and cultured up to 7 days. Normally, the osteoblastic cells respond to the patterns showing some preference in cell adhesion for the areas of random alignment of the fibers (Figure 2.14).

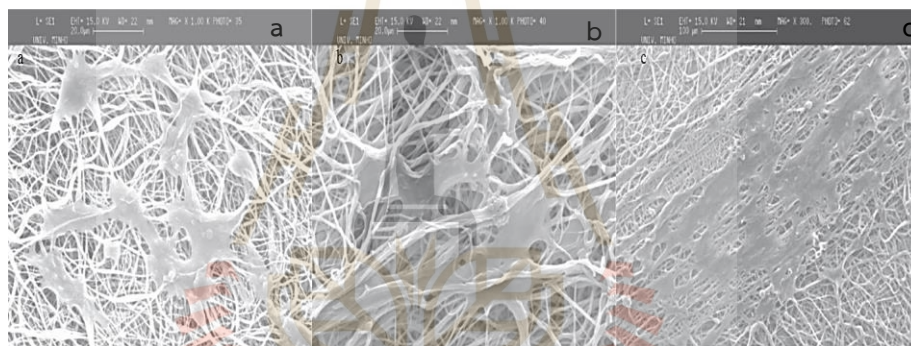


**Figure 2.14** Adhesion of osteoblastic cells to PCL fiber meshes after 7 days in culture: a) flat copper plate, b) screw collector and c) wire net collector (Neves et al., 2007).

Some researchers focus on designing scaffolds with homologous properties to human tissue at the nanoscale level. Several studies reported using electrospinning loosely connected 3D porous nanofibrous constructs with a large surface region can be produced to resemble the native ECM network. Gholipourmalekabadi et al. (2015) designed electrospun nanofibrous scaffolds by electrospinning method. There is a various concentration of silk fibroin solutions as follows 10, 12, and 14% w/v in formic acid, and tested their ability for tissue engineering in vitro and in vivo. Even though test cytotoxicity, formic acid was chosen to dissolve the lyophilized SF due to its interesting characteristics in the improvement of  $\beta$ -sheet crystallization. Among the prepared samples, ESFNS-10% showed more uniformity with the nanofibers scale and it is bead-free of all nanofibers. The morphology of the cells cultured on the nanofibrous scaffolds presented the adhesion properties and biocompatibility of the scaffolds. Bone tissue engineering presents to design a scaffold for delivering therapeutic agents

and cells to the injured tissue stimulating the new tissue formation. Li et al. (2006) have prepared silk fibroin nanofiber scaffolds containing bone morphogenetic protein 2 (BMP-2) and nanoparticles of hydroxyapatite (nHAP) with electrospinning. Cell culture with mesenchymal stem cells (hMSCs) on various conditions of electrospun silk-BMP-2 scaffolds. The results showed that electrospun SF-based scaffolds are suitable candidates for bone tissue engineering. Talebian et al. (2014) fabricated a hybrid nanofibrous scaffold with chitosan/1.2 wt% polyethylene oxide (PEO) and bioactive glass (BG) by an electrospinning technique. The results showed that BG-containing nanofibers could be induced the formation of hydroxyl carbonate apatite (HCA) on the surface of the scaffold after 14 days. Then the scaffold was immersed in SBF. The MTT assay was tested the cell viability of human mesenchymal stromal cells (hMSCs) on a nanofibers scaffold. The cell adhesion results showed that hMSCs were viable at a different time on the chitosan/PEO/BG nanofiber scaffolds. In addition, the BG enhanced the alkaline phosphatase (ALP) activity of hMSCs cultured on nanofiber scaffolds at day 14 compared to that on pure chitosan/PEO scaffolds. In this study, they have suggested chitosan/PEO/BG nanofibrous scaffold could be a potential candidate for application in bone tissue engineering (Figure 2.15).

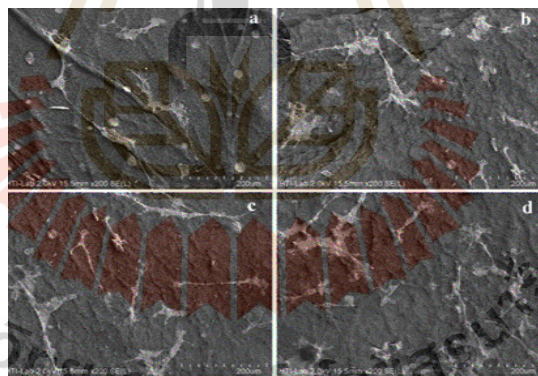


**Figure 2.15** FE-SEM images of hMSCs cultured on the chitosan/PEO/BG scaffolds after 1 (a), 3 (b), 5 (c) and 7 (d) days (Talebian et al., 2014).

Articular cartilage tissue has functionally reduced friction and increased the wear resistance of the tissue. Currently, cartilage injury is the most common crucial health issue. The electrospinning technique that can be used to mimic the pattern features of the extracellular matrix has gained considerable attention from scientists. Wise et al. (2009) have prepared polycaprolactone (PCL) scaffolds with electrospinning. Cell culture was tested with human mesenchymal stem cells (hMSCs) on the nanofibrous scaffold. The results showed that tissue engineering of the orient ECM environment to regulate tissue alignment could be optimized by orienting electrospun

nanofibers. The specific tissue engineering applications, such as scaffold creating the superficial zone of articular cartilage may be significant for improving the stem cells on nanofibrous scaffolds. Xue et al. (2013) studied engineered cartilage with precise three-dimensional (3-D) structures by applying electrospun of gelatin/polycaprolactone (GT/PCL) membranes into the round shape. Then seeded cell chondrocytes in the electrospun membranes. Histological analysis confirmed that the engineering of cartilage using the electrospun GT/PCL membranes as possible. For cell culture in vitro and in vivo showed the ear-shaped cartilage largely maintained its original shape, with a shape similarity up to 91.41% of the mold. These results demonstrated that the 3-D cartilage in a sandwich model using electrospun membranes was easy and effective. which has suitable to be applied for another tissue engineering. Li et al. (2009) have fabricated a nanofibrous scaffold (NFS) made from poly( $\epsilon$ -caprolactone) (PCL) and tested its ability to support in vitro chondrogenesis of MSCs. The electrospun PCL nanofibrous scaffold was showed fiber uniform, randomly oriented nanofibers with a diameter in the range of 700 nm. Cell culture on the electrospun scaffold with MSCs presence of TGF-B1 separated to a chondrocyte phenotype of chondrocyte-specific gene expression and synthesis of cartilage ECM proteins. The physical nature and improved mechanical properties of PCL scaffold indicate results that the PCL nanofibrous scaffold is a practical carrier for MSC transplantation and represents a scaffold for cell-based tissue engineering for cartilage repair (Figure 2.16).

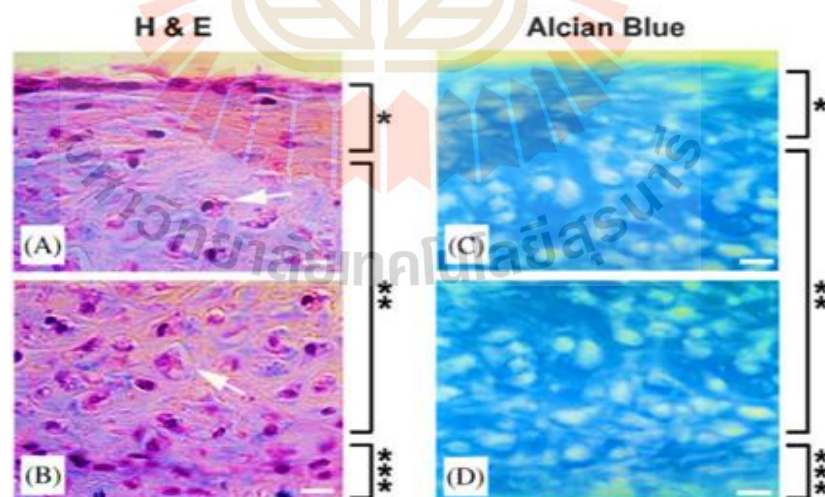


**Figure 2.16** Histological analysis of NFS MSC cultures maintained in a chondrogenic medium supplemented with TGF-b1 for 21 days. H&E staining showed flat fibroblast-like cells on the top zone (bracket, \*), round chondrocyte-like cells embedded in lacunae (arrows) in the middle zone (bracket, \*\*), and small, flat cells at the bottom zone (bracket, \*\*\*). Alcian blue staining showed the presence of sulfated proteoglycan-rich ECM in the construct (Li et al., 2009).

Vascular tissue engineering effort to recreate blood vessels comprise of endothelial and perivascular cells for clinical applications. The high porosity and length of nanofibers enhance nutrients and gas which is the key factor of vascular regeneration. ECM is the most important component of the vascular system. Thus, the tensile strength, elasticity, and compressibility of a blood vessel are important properties of designing vascular scaffolds (Rahmati et al., 2016). Yazdanpanah et al. (2015) used the electrospinning technique to fabricate nanofibrous scaffolds with poly(L-lactic acid) (PLLA) and gelatin. The results of tensile tests showed that the mechanical strength was increased and estimated burst pressure of properties PLLA/gelatin scaffolds are better than those of PLLA/gelatin and gelatin scaffolds. There is suggested these scaffolds in vascular tissue engineering. The knee meniscus is crucial to the long-term health of the knee joint. Because of the accident of injury and degeneration. The replacing damage of meniscus or lost meniscal tissue is very related to clinical (Grogan et al. 2020). Nanofibrous scaffolds are the most interesting to replace due to their biochemical composition and it has structural features similar within meniscus tissue. Rothrauff et al. (2016) designed aligned and random scaffolds prepare from poly- $\epsilon$ -caprolactone (PCL). The scaffolds possessed the most anisotropic mechanical properties. Whereas random scaffolds presented uniform properties in parallel and vertical directions. The results showed that a novel biomimetic scaffold constructed by electrospinning could be incorporated into the repair of a radial meniscus tear without effect on the tensile properties of the repair (Figure 2.17 and Table 2.2).

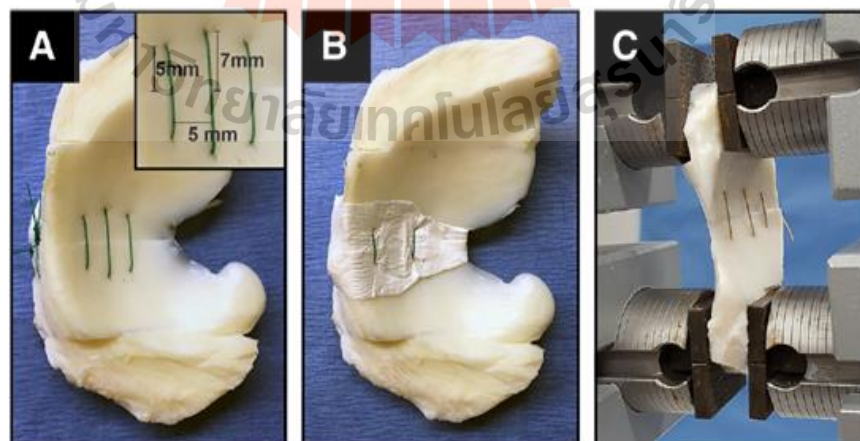


**Figure 2.17** Suture repair of meniscal tears and mechanical testing set-up. A) Suture repair of fully transected meniscus. Inset shows dimension of suture placement. B) Scaffold-augmented repair. C) Suture repaired meniscus clamped in materials testing machine prior to tensile loading protocol (Rothrauff et al., 2016).

**Table 2.2** Mechanical Properties of Native and Repaired Menisci Pulled to Failure (Rothrauff et al., 2016).

	Native	Suture Repair	Scaffold-Augmented
Ultimate Load (N) <sup>a</sup>	437.3±117.5	124.4±21.4	137.1±31.0
Ultimate Elongation(mm) <sup>b</sup>	5.12±1.55	10.14±4.61	12.09±5.89
Stiffness (N/mm)	141.0±42.4	18.4±4.7	20.8±3.6

Baek et al. (2015) constructed layers of aligned polylactic acid (PLA) electrospun scaffolds with human meniscus cells embedded in ECM hydrogel lead to the formation of new tissues that are similar to meniscus tissue. PLA electrospun scaffolds with aligned and random fibers were seeded with human meniscus cells received from vascular or avascular regions. Aligned electrospun PLA nanofibers showed mechanical properties that are better than other fibers. Cells from avascular and vascular regions of human menisci grew, attached, and infiltrated to the PLA nanofibrous scaffold. There are secreted major proteins found in the meniscal tissue. The method of compound nanofibrous scaffolds with human meniscus cells in an ECM hydrogel create thicker multilayered constructs in partial meniscus replacement. Skin injuries are generally caused by burns, trauma, surgical procedures, bedsores, diabetes, aging, etc. Researchers designed skin scaffolds that can improve skin healing by protecting the tissue from dehydration and infection. In addition, a scaffold provides cell attachment, cell proliferation, and migration, which finally lead to the development of new skin. Milan et al. (2016) studied the 3D dermal substitutes prepared using collagen nanofibers to provide a physiological environment for skin cell attachment and expansion. Which nanofibers can protect damaged skin tissue from fluid and protein loss.

## 2.4 Meniscus scaffolds for tissue engineering applications

Injury between plays sports activities or accidents has been associated with a meniscus injury. Especially, the concern is knee injuries that affect the meniscus of the joint. The knee menisci are semilunar-shaped fibrocartilaginous structures interposed between the femoral and tibial and it is essential for the knee joint. There is considerable research for developed meniscus scaffolds. Esposito et al. (2013) studied PLDLA/PCL-T 90/10 polymeric scaffold with solvent casting and particulate leaching. The result of mechanical properties was showed a high compressive modulus of 9.5 ±1.0 MPa. Cell culture with fibrochondrocytes from rabbit menisci and seeded directly

on the scaffolds. Which implantation consists of cell-free scaffolds or cell-seeded scaffolds that were introduced into the medial knee meniscus and the negative control group is rabbits no implant. Therefore, PLDLA/PCL-T 90/10 polymeric scaffold has potential for tissue engineering applications since this scaffold allowed the formation of fibrocartilaginous tissue. Which is a structure of importance for repairing meniscus injuries including replacement and the protection of the meniscus from degeneration (Figure 2.18).

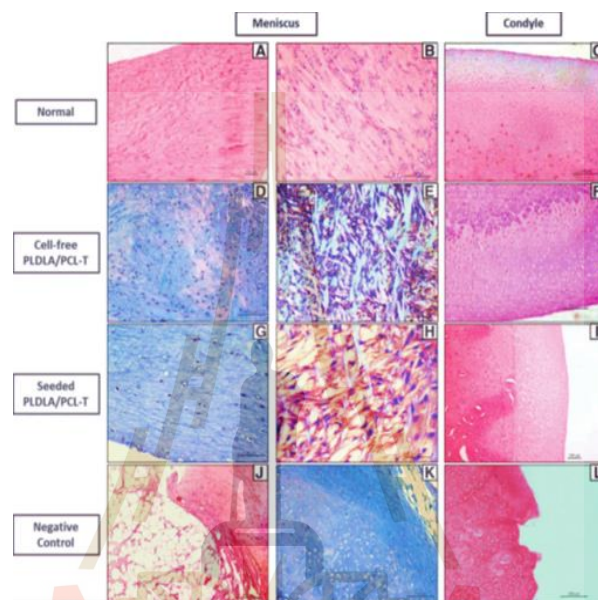


**Figure 2.18** Twenty-four weeks after implantation of PLDLA/PCL-T scaffold (Esposito et al., 2013).

Natsu-ume et al. (2005) designed a fibrin gel scaffold and cell culture with autologous fibrochondrocytes while treatment 2-week in vitro culture of cells before transplantation. The result was showed good cell proliferation with matrix synthesis, and they found that Neo-tissue formation. Kang et al. (2005) developed the current treatments of the meniscal damage in the knee joint. The meniscus scaffold was fabricated from polyglycolic acid (PGA) fiber meshes that were adding reinforcement by poly(lactic-co-glycolic acid). The compressive modulus of the PGA scaffold was higher than that of a non-reinforcement scaffold. The meniscal cells were seeded onto the polymer scaffolds and cultured in vitro for 1 week. Then, implantation scaffold to rabbit knee joints from which medial menisci were removed. Hematoxylin and eosin staining of the sections of the neo-menisci at 6 and 10 weeks presented the regeneration of fibrocartilage. Safranin-O staining showed that plenty of proteoglycans was presented in the neo-menisci at 10 weeks. Masson's trichrome staining revealed the presence of collagen. Immunohistochemical analysis showed that the presence of

collagen type I and II in neo-menisci at 10 weeks. This research showed the first time and the possibility of regenerating a meniscus in a rabbit model using the tissue engineering method (Figure 2.19).

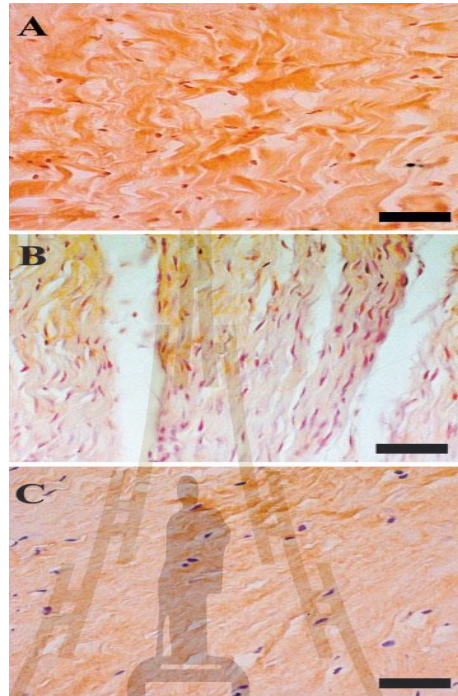


**Figure 2.19** Immunohistochemical staining for collagen type II of inner zone of (A) normal meniscus and tissue engineered meniscus at (B) 6 and (C) 10 weeks (Kang et al., 2005).

Shimomura et al. (2015) have prepared 5% (w/v) PCL mixed with tetrahydrofuran at ratio 1:1 and prepared 10% PEO mixed with 0.06% N,N-dimethylformamide and NaCl. After that, they mixed PCL:PEO at ratio 1:1 and using electrospinning for preparation PCL/PEO nanofibers. Then, they cultured cell and staining with Picrosirius red. The result showed that radial tear wrapped with the scaffold alone or cell-seeded with mesenchymal fibrochondrocytes scaffold exhibited a partial repair and scaffold provides adhesive properties that may make implantation practical mesenchymal fibrochondrocytes appear to enhance biological healing (Figure 2.20).

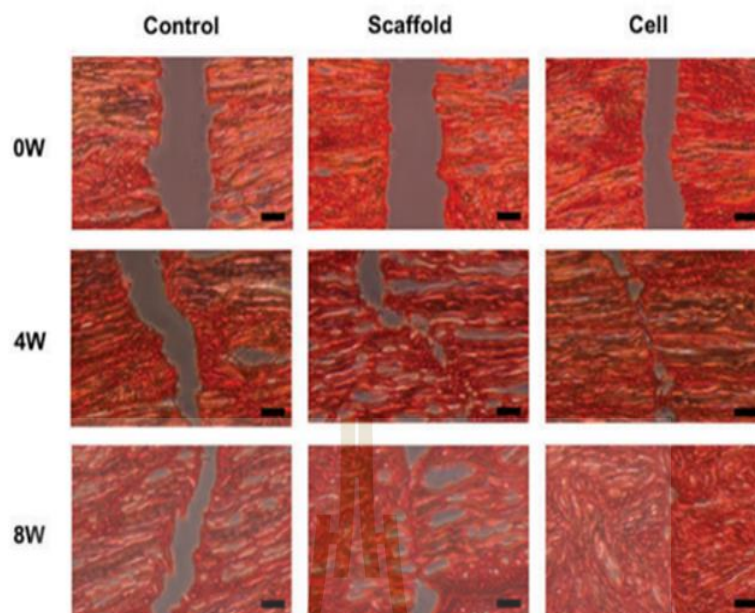


Figure 2.20 Picrosirius red staining (Shimomura et al., 2015).

Ruprecht et al. (2019) prepared scaffolds from medial menisci that were harvested from the knees of female pigs and frozen overnight, then freeze-dried (Figure 2.21). The porcine meniscus-derived matrix (MDM) scaffolds were provided a suitable environment for cell permeation, remodeling, and improve repair tissue. Thus, this scaffold has the potential to integrate into the meniscus joint and promote repair without external growth factors or an exogenous cell source.



Figure 2.21 Meniscus-derived matrix (MDM) was prepared from porcine medial meniscus (Ruprecht et al., 2019).

Mandal et al. (2011) designed 3D aqueous-derived silk scaffolds that were prepared into individual layers with varying pore sizes and orientations. The first two layers were fabricated salt leaching method, while the third layer was used the freeze-drying method. The mechanical properties tested the compressive modulus of silk meniscus scaffold layers with and without hMSCs cultured in differentiation media (Figure 2.22). The result showed higher the silk scaffolds/cells compressive modulus than silk scaffolds. Moreover, cultured hMSCs indicated that higher cellularization with improved ECM deposition. Whereas higher collagen, proteoglycan levels, and higher gene expression levels promote chondrocyte differentiation.

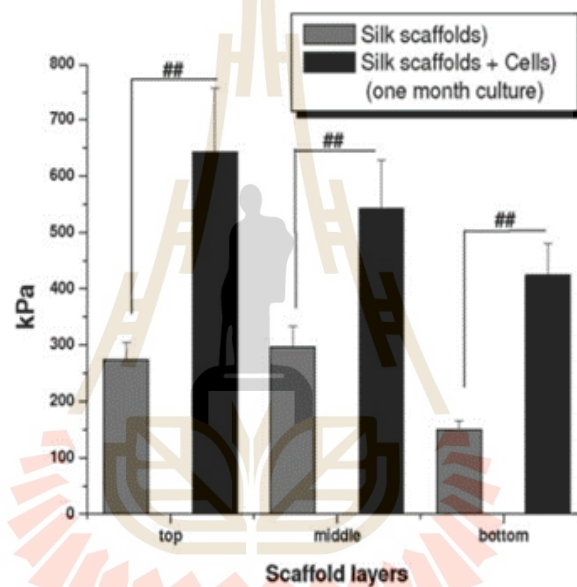


**Figure 2.22** Compressive modulus of individual silk meniscus scaffold layers (Mandal et al., 2011).

## CHAPTER III

### RESEARCH METHODOLOGY

#### 3.1 Preparation of *Bombyx mori* cocoons and degumming process

Silk cocoon from *Bombyx mori* species J108 was obtained from Queen Sirikit Sericulture Center, Nakhon Ratchasima were cut into small pieces, the dried pupae removed, and dirt separated from the cocoon fragments. Small pieces of cocoons were washed in distilled water and dried at 105°C for 4 h. After that, the weight of dried cocoons was recorded. To remove immunogenic sericin proteins, by 5 g of dried cocoons were dissolved in 1% (w/v) Na<sub>2</sub>CO<sub>3</sub> (ERBA CARLO, Italy) solution at 100±2°C for varied times of 10, 20, 30, and 40 minutes each. Then, the degummed silk was washed with distilled water several time until pH 7 and air dried overnight at 70°C. Finally, the weight of degumming fiber was recorded (Figure 3.1).

##### 3.1.1 Weight loss

Degumming performance was initially measured by determining the percentage weight loss of samples after degumming. Cocoon small pieces (5 g weight) were dried overnight at 70°C and weighed again to obtain a pre-degumming weight. Degumming silk was placed on the scales for 1 min to allow the reading to stabilize before the exact weight was recorded. Each degumming times condition was performed on triplicate 5 g samples. The weight loss was defined as follows (Allardyce et al., 2015)

$$\text{Weight loss (\%)} = (1 - (\text{mass of degummed fiber}) / (\text{mass of cocoons})) \times 100$$

##### 3.1.2 Residual sericin

Residual sericin content was obtained using the following equation. When the weight loss was 26.6%, the sericin was completely removed. (Ki et al., 2007)

$$\text{Residual sericin content (\%)} = (1 - (1 - 0.266) / (1 - d)) \times 100$$

where d is the weight loss.

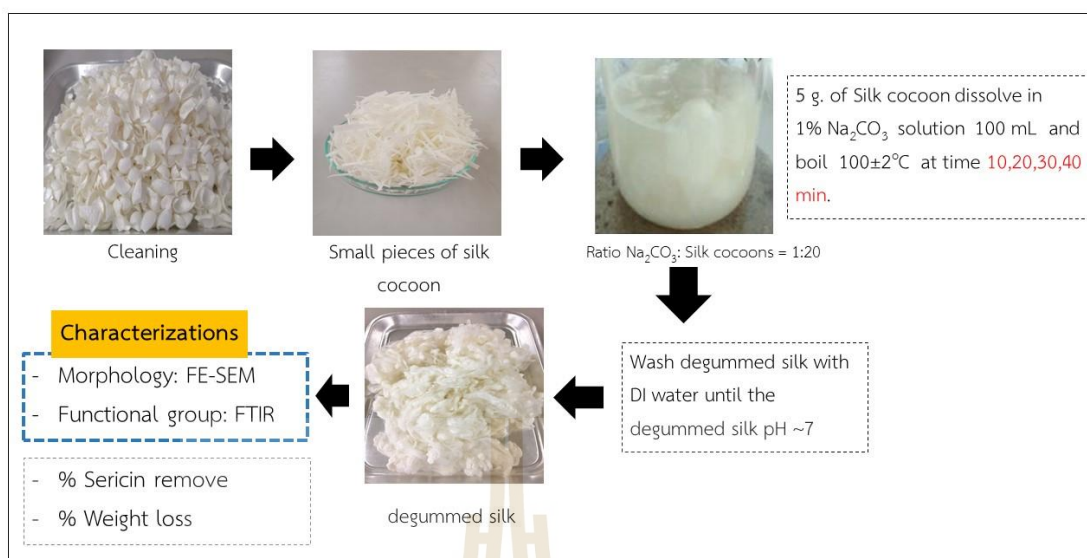


**Figure 3.1** The preparation process of degumming silk.

### 3.2 Preparation of silk fibroin extraction by $\text{CaCl}_2$ and $\text{LiBr}$ solvent

Silk fibroin dissolution by the extraction of degummed silk routes (Figure 3.1) using either 9.3 M  $\text{LiBr}$  (purchased from Sigma Aldrich, Singapore) solution at  $70^\circ\text{C}$  for 3 h and 4.14 M  $\text{CaCl}_2$  (purchased from Erba Carlo, Italy) solution at  $100^\circ\text{C}$  for 1 h. Then, silk fibroin solution was dialyzed ( $M_w = 6\text{--}8$  kDa) with deionized water for 4 days. After dialysis, SF solution was freeze-dried at  $-40^\circ\text{C}$ . The silk fibroin sponges yield was calculated according to the following formula: (Feng et al., 2020).

$$\text{Extraction yield (\%)} = (\text{weight of silk fibroin} / \text{initial weight of silk degummed}) \times 100$$

#### 3.2.1 Measurement of molecular weight

The molecular weight of the regenerated silk fibroin was determined by sodium dodecyl sulfate-polyacrylamide gel electrophoresis (SDS-PAGE). The hydrolyzed sample solution was added into a 3: 1 buffer sample, then boiled at  $100^\circ\text{C}$  for 5 minutes, then the sample was pipetted into a sequence of acrylamide gel respectively. The electrodes are mounted according to the poles. Electrophoresis was carried out at a voltage of 150V for 60 minutes. After electrophoresis, the gel was stained with 0.1% Coomassie Brilliant Blue R-250 staining solution for 30 to 60 minutes. The gel was rinsed with immersion in detaining solution (methanol, acetic acid, and distilled water at a ratio of 4:1:5) for 1 h. SDS-PAGE was recorded and defined.

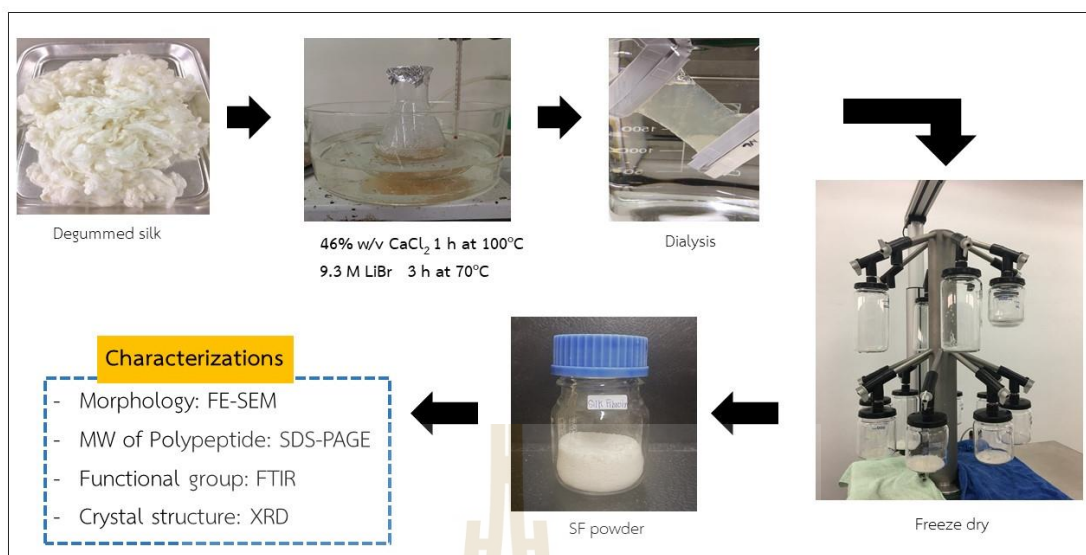


**Figure 3.2** The preparation process of silk fibroin extraction by CaCl<sub>2</sub> and LiBr solvent.

### 3.2.2 Characterization of Silk fibroin

#### 3.2.2.1 Fiber surface morphology

The surface morphology of degumming fiber was studied using field emission scanning electron microscope (FE-SEM) (Zeiss AURIGA FE-SEM/FIB/EDX). Fiber diameter was randomly measured from 100 fibers according to 10 different area of the sample. The average fiber diameter was then calculated using ImageJ software.

#### 3.2.2.2 Fourier transform infrared spectroscopy

Functional groups in the degumming fiber were analyzed by Fourier Transform Infrared Spectroscopy (FT-IR) (Bruker Tensor27). The spectra were recorded over a wave range of 4000–400 cm<sup>-1</sup> at resolution of 4 cm<sup>-1</sup>.

#### 3.2.2.3 X-ray diffraction

X-ray diffraction (XRD) patterns were obtained using a Bruker XRDD8 Advance with Cu-Kα (1.54 Å) radiation operated at a voltage of 40 kV and current of 40 mA. The detector was LYNXEYE. The scan 2θ range was from 5 to 50 degrees with a step size of 0.02° and time per step of 1.2 s. Percentage of crystallinity can be calculated as ratio of crystalline area to total area.

$$X_c = A_c / (A_c + A_a)$$

Where  $X_c$  = %crystallinity

$A_c$  = Area of crystalline phase

$A_a$  = Area of amorphous phase

### 3.3 Preparation of electrospun PVA nanofiber and electrospun SF/PVA nanofiber

#### 3.3.1 Polymer solution preparation

Polyvinyl alcohol (PVA) (MW 146,000-186,000, Sigma Aldrich) solutions 5.0% w/v and 10.0% w/v were prepared by adding PVA into 80°C distilled water. The solution was stirred with a magnetic stirrer until the solution was clear. The solution was then stirred continuously at room temperature for additional 24 h. Silk fibroin (SF) was prepared by degumming waste cocoons (*Bombyx mori* silk). 1% Na<sub>2</sub>CO<sub>3</sub> solution was boiled for 30 min to remove sericin, and washed with distilled water. Two g of the degummed silk was put into 10 g CaCl<sub>2</sub> solution (Carlo Erba Reagent). The degummed silk solution was stirred and heated at  $98 \pm 2^\circ\text{C}$  for 1 h. The solution was then dialyzed with deionized water. After dialysis, the SF solution was freeze dryer at -40°C.

#### 3.3.2 Preparation of blend SF/PVA

SF (12% w/v) was prepared in 98% w/v formic acid (Carlo Erba Reagent). SF in formic acid and 10% w/v PVA solution were mixed in the ration of 25:75 (v/v) respectively. The solutions were stirred on a magnetic stirrer for 4 h at room temperature.

#### 3.3.3 Electrospinning of 5% w/v, 10% w/v PVA and blended SF/PVA nanofiber

SF/PVA was loaded into a 10 mL syringe which was connected to a 20-gauge blended tip needle. The needle tip was placed 10 cm from the cylindrical corrector. The electrospinning parameter was set at 15 kV with a flow rate of 0.5 mL/h. All conditions were controlled, and the relative humidity (RH) varied at 50%, 60%, 70%, and 80%. The effect of the applied voltage in the electrospinning process was studied using variable voltages of 10, 15, 20, and 25 kV. In addition, the parameters were set at a flow rate of 0.5 mL/h and a humidity of 50% (Figure 3.3).

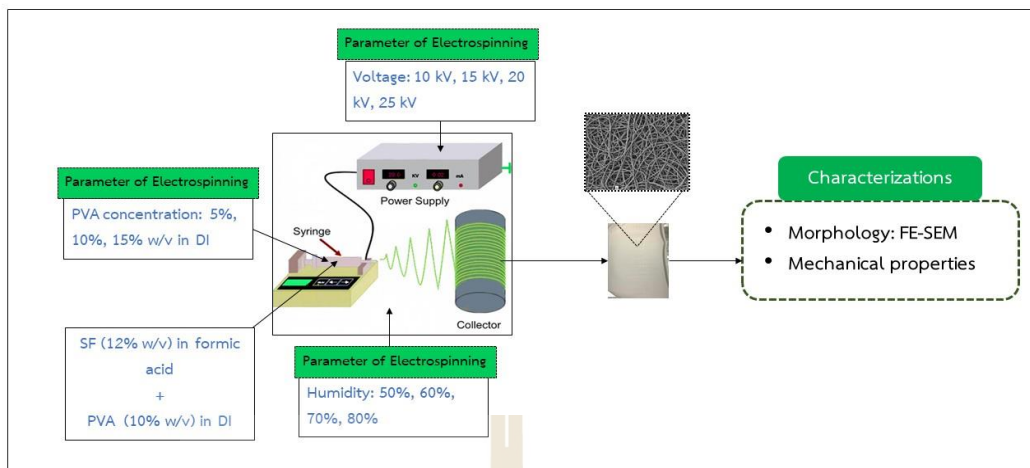


**Figure 3.3** The preparation process of electrospun PVA nanofiber and electrospun SF/PVA nanofiber.

### 3.3.4 Characterization of blended electrospun nanofiber

#### 3.3.4.1 Morphology

Fiber diameter and pore size of the nanofiber sheath were observed by Field Emission Scanning Electron Microscope (FE-SEM) (Zeiss AURIGA FE-SEM/FIB/EDX). In one microscope filed, twenty fibers were chosen to measure for diameter; 5 fields were taken in one electrospun nanofibrous sample and characterization of nanofiber diameter using image J analysis.

#### 3.3.4.2 Mechanical properties

The nanofibrous scaffold was tested at room temperature and cut the scaffold into 1.5 cm in width, 10 cm in length and 0.2-0.5 mm in thickness tensile test was done according to ASTM D882 by using a universal testing machine (Model 4502, Instron, Norwood, MA) with a load cell of 5 kN.

## 3.4 Fabrication of electrospun SF/PVA nanofibrous scaffold

### 3.4.1 Materials

Silk fibroin sponges, Poly(vinyl alcohol) (PVA) (Mw 146,000-186,000, 99% hydrolyzed), 99% Lithium bromide (LiBr), and Dimethyl sulfoxide (DMSO) was purchased from Sigma Aldrich, Singapore. 99% Formic acid, Sodium carbonate ( $\text{Na}_2\text{CO}_3$ ), and Calcium chloride ( $\text{CaCl}_2 \cdot 6\text{H}_2\text{O}$ ) were purchased from Erba Carlo, Italy. The MTT Assay Kit was purchased from Sigma Aldrich, Singapore. Fetal Bovine Serum (FBS), Trypsin-EDTA solution and Phosphate Buffered Saline (PBS) were purchased from Sigma Aldrich, Singapore. DMEM was purchased from Gibco, Life Technologies and TRIZOL reagent was purchased from Invitrogen, USA.

### 3.4.2 Electrospinning of SF/PVA solution

SF solution was prepared by dissolving 12% (w/v) SF in 99% formic acid. PVA was dissolved in deionized water at 80°C to prepare 10% (w/v) PVA solution. SF/PVA solution was prepared in different ratios; 100:0, 75:25, 50:50, 25:75 and 0:100 (v/v) and stirred for 2 hr. SF/PVA then loaded into 10 ml syringe which connected to 20-gauge blended tip needle (Table 3.1). The needle tip was placed at 10 cm from cylindrical corrector. Electrospinning parameter was set at 20 kV with flow rate of 0.5 ml/h at humidity of 50% and the roller receiver rotation speed of 200 rpm (Figure 3.4).

**Table 3.1** Composition of SF blend with PVA (SF/PVA).

Sample	SF (mL)	PVA (mL)	Ratio
a	100	0	SF/PVA 100:0
b	75	25	SF/PVA 75:25
c	50	50	SF/PVA 50:50
d	25	75	SF/PVA 25:75
e	0	100	SF/PVA 0:100

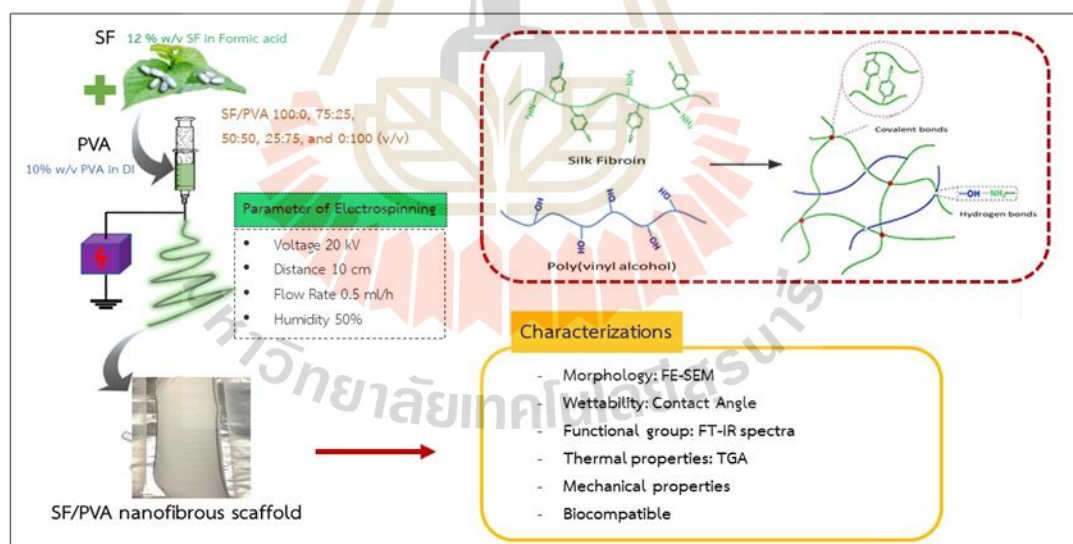


**Figure 3.4** The fabrication process of electrospun SF/PVA nanofibrous scaffold.

### 3.4.3 Characterization of blended electrospun nanofiber

#### 3.4.3.1 Viscosity

The viscosity of electrospinning solution which shear viscosities of the spinning fluids were measured at the shear rate of 0.1-200  $s^{-1}$ , 25°C with Brookfield viscometer (Brookfield LVDV3T, USA).

#### 3.4.3.2 Morphology

Fiber diameter of the nanofiber sheath were observed by Field Emission Scanning Electron Microscope (FE-SEM) (Zeiss AURIGA FE-SEM/FIB/EDX). The nanofiber was selectively measured in different surface area were investigated.

#### 3.4.3.3 Contact angle test

The electrospun nanofiber was observed using contact angle. The water was dropped onto the surface of the nanofiber with a needle syringe. Images of the drop was captured after the drop set onto the nanofiber. The contact angle was calculated by the software image J for analyzing the shape of the drop.

#### 3.4.3.4 Tensile properties

The nanofibrous scaffold was tested at room temperature and cut the scaffold into 1.5 cm in width, 10 cm in length and 0.2-0.5 mm in thickness tensile test was done according to ASTM D882 by using a universal testing machine (Model 4502, Instron, Norwood, MA) with a load cell of 5 kN and crosshead speed of 20 mm/min.

#### 3.4.3.5 Fourier transform infrared spectroscopy

Fourier transform infrared spectroscopy (FT-IR) (Bruker Tensor27) was used to identify the functional groups of SF/PVA nanofibrous scaffold. The spectra were recorded over a wave number range of 4000–400  $\text{cm}^{-1}$  at resolution of 4  $\text{cm}^{-1}$ .

#### 3.4.3.6 Thermogravimetric analysis

SF/PVA nanofiber was characterized by the TGA (model STA 6000, Perkin-Elmer) in non-isothermal mode. The heating rate was 10  $^{\circ}\text{C}/\text{min}$  under an inert nitrogen atmosphere over the temperature range of 50-700 $^{\circ}\text{C}$ .

#### 3.4.3.7 Cell viability

SF/PVA scaffolds were cut in to 4 x 4 mm and placed separately placed in 96 wells. Chondrocyte culture medium, contained with high glucose Dulbecco's modified Eagle's medium (DMEM/F12, Gibco, Life Technologies) supplemented with 10% FBS and antibiotic-antifungal mixture were then added into each well. After 30 minutes incubation,  $5 \times 10^3$  human chondrogenic progenitor cells (HCPCs) (Figure 3.1) were seeded into the scaffolds and cultured in a humidified, 37 $^{\circ}\text{C}$ , 5% carbon dioxide environment. The cell viability was performed using by 3-(4, 5-dimethyl thiazolyl-2)-2,5-diphenyl tetrazolium bromide (MTT) assay at day 1, 3, and 7 by analyzing with microplate reader (Thermo Scientific Microplate Spectrophotometer) at 590 nm. Cell viability percentage was calculated by comparing the absorbance of cells cultured on

different nanofibrous scaffolds to scaffold free control. All set of experiment were performed in triplicate samples.

#### 3.4.3.8 Quantitative analysis for gene expression

According to the results from mechanical and cell viability tests, 50:50 SF/PVA scaffold was used to assess chondrogenic gene expression. In brief, 50:50 SF/PVA nanofibrous scaffold sheets were cut to the 12 mm diameter spheres and sterilized under UV light for 30 minutes. Then, the sphere scaffolds were put in 24 well and incubated in culture media for 4 hours. After incubation,  $2.5 \times 10^4$  HCPCs were seeded in each scaffold and cultured for 7, 14, and 28 days. The culture media was refreshed every 3 days. At day 7, 14, and 28, total RNA was extracted from the HCPCs on the scaffolds for quantitative gene-analysis using RNeasy mini Kit (Qiagen, Hilden, Germany). Quantitative real time polymer chain reaction (qRT-PCR) was done with SYBR Green kit (Thermo Fisher Scientific, USA) and Fluorescein Kit (BIOLINE, London, UK). The target genes were type I collagen (COL1A1), type II collagen (COL2A1) and aggrecan (ACAN), with 18S rRNA as a housekeeping gene (Figure 3.5 and Table 3.2).

**Table 3.2** Sequences of primer sets for qRT-PCR.

Genes		Primer sequence (5' to 3')
Type I collagen (COL1A1)	Sense	GGAGGAGAGTCAGGAAGG
	Antisense	GCAACACAGTTACACAAGG
Type II collagen (COL2A1)	Sense	GGCAGAGGTATAATGATAAG
	Antisense	ATGTCGTCGCAGAGG
Aggrecan (ACAN)	Sense	ATACCGTCGTAGTTCC
	Antisense	TCCTTGCTCCATAGC
18S rRNA	Sense	ATACCGTCGTAGTTCC
	Antisense	GTCTCGTTCGTTATCG

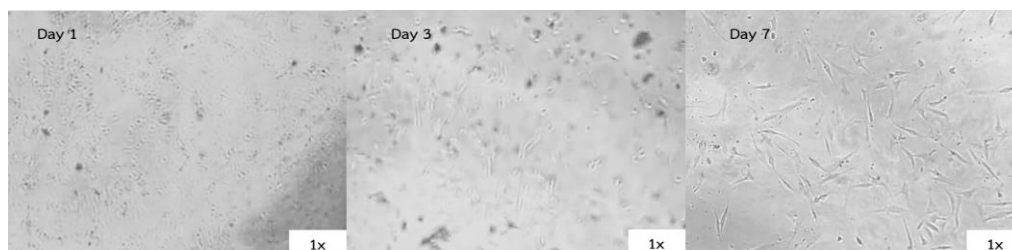


**Figure 3.5** Representative clonally derived human chondrogenic progenitor cells (HCPCs) on day 1, day 3, and day 7.

## CHAPTER IV

### RESULTS AND DISCUSSION

#### 4.1 The effect of solvent for silk fibroin extraction on physical properties and biological properties of electrospun nanofibrous scaffold

##### 4.1.1 Time on degumming silk

It is well known that the sericin content in *Bombyx mori* cocoons reported for about 20-30 wt.% (Wang et al., 2015) and weight loss measurements have been widely used to observe the degumming silk efficiency. Weight loss measurements indicated a more efficient removal of sericin, but excessive weight loss may indicate substantial hydrolysis of fibroin. This study used  $\text{Na}_2\text{CO}_3$  solution for the degumming silk at varied times when compared using a t-test ( $p < 0.05$ ). Overall, the lowest weight loss value of 23.71% ( $p = 0.048$ ) corresponded to degumming time at 10 min. While the degumming time for 20, 30, and 40 min, the weight loss value of 25.03%, 25.26%, and 25.40%, ( $p = 0.044$ ,  $p = 0.063$ , and  $p = 0.058$ ) respectively (Table 4.1). The residual sericin remaining on the silk fibers correspondingly declined to a low level with increasing time. The sericin content for 10 to 40 min has values of 3.79%, 2.09%, 1.79%, and 1.60%, respectively. It indicates the effective removal of sericin. In this study, we selected degumming time at 20 min because the t-test has a  $p$ -value  $< 0.005$ , weight loss, and sericin content were most suitable for using silk fibroin extraction. Cao et al. (2013) reported the degumming time of 20, 40, or 60 min had no further effect on the degumming rate. That is indicating all the sericin was removed from around the fibroin fiber. Teuschl et al. (2014) suggested that the time required for suitable degumming is between 20 to 40 min. More et al. (2018) reported almost 100% degumming was complete within 30 min and thereafter increase was slow. Therefore, a degumming time of 20 min was used the silk fibroin extraction in the subsequent experiments. The results of fiber surface morphology were shown by an FE-SEM image in which the silk cocoon before being degummed still exhibits sericin residues, mainly located at the outer structures of the silk fiber (Figure 4.1). Sericin appears as a non-uniform coating on the surface of the silk fibers. The FE-SEM image (Figure 4.2) of silk extracted with a sodium carbonate solution at the varied times showed sericin appears as a non-uniform coating on the surface of the silk fibers for 10 min. Degumming time after 20

min showed sericin slight coating on the surface of the silk fibers and the fiber surface was highly smooth, and clean fibroin appeared.

**Table 4.1** Time of degumming silk.

Time of Degumming (min)	Weight loss (%)	<i>P</i> -value	Sericin remove (%)
10	23.71	0.048	96.21
20	25.03	0.044	97.91
30	25.26	0.063	98.21
40	25.40	0.058	98.40

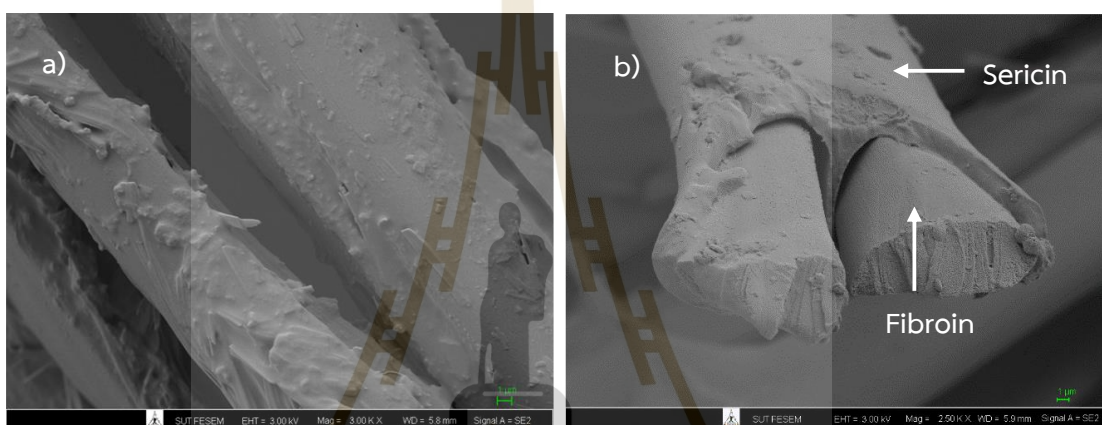


**Figure 4.1** FE-SEM images of cocoon a) outer fiber of cocoon and b) silk fiber showing the two filaments of fibroin and sericin coating.

The effect of time on degumming processes was investigated by FT-IR. The IR spectrum silk cocoon and degummed silk fibers presented in Figure 4.3 show that the peaks from wavenumber 1000 to 1800  $\text{cm}^{-1}$  are due to fingerprint regions for all silk fibers. The absorption bands at 1508  $\text{cm}^{-1}$  correspond to amide II, assigned to the  $\beta$ -sheet structure (crystalline) (Chung et al., 2015), and 1217  $\text{cm}^{-1}$  corresponds to amide III, assigned to the random coil/ $\alpha$ -helical structure (Murphy et al., 2008). Nevertheless, In the amide I band, the silk cocoon and the degummed silk fibers exhibit absorption peaks at 1697  $\text{cm}^{-1}$  (random coil/ $\alpha$ -helical structure) and 1639  $\text{cm}^{-1}$  ( $\beta$ -sheet structure) (Callone et al., 2016), respectively, indicating the amount of  $\beta$ -sheet structure is increased after degumming. Therefore, the FTIR spectra indicated that the molecular conformation of the silk fibers does not change after different degumming methods, and they assume a  $\beta$ -sheet and random coil/ $\alpha$ -helical coexisting conformation.

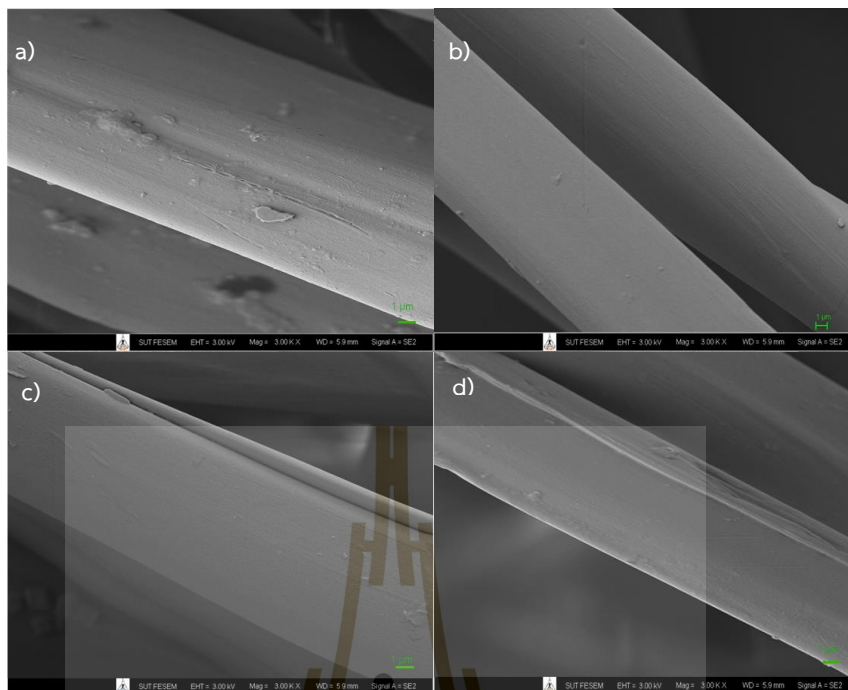


**Figure 4.2** FE-SEM images of degumming silk a) degumming time 10 min, b) degumming time 20 min, c) degumming time 30 min, and d) degumming time 40 min.

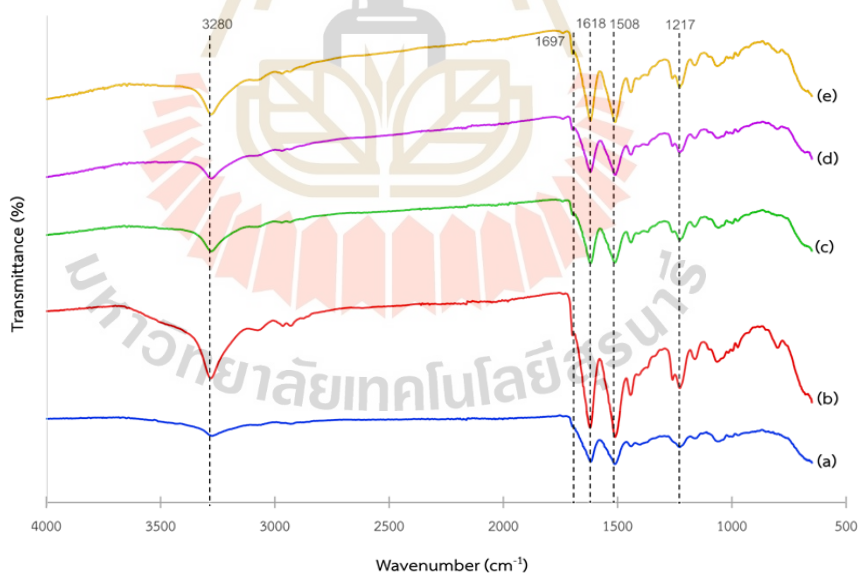


**Figure 4.3** FTIR spectra of a) raw cocoon, b) degumming time 10 min, c) degumming time 20 min, d) degumming time 30 min, e) degumming time 40 min.

#### 4.1.2 Effect of silk fibroin extraction by $\text{CaCl}_2$ and $\text{LiBr}$ solvent

The dissolving ability of  $\text{CaCl}_2$  and  $\text{LiBr}$  solvents was determined by the time and temperature suitable to completely dissolve silk fibroin.  $\text{CaCl}_2$  took 1 h at  $100^\circ\text{C}$

to completely dissolve silk fibroin while LiBr can dissolve silk fibroin at lower temperature (70°C) but longer time (3h) as shown in Table 4.2. Cheng et al. (2015) reported the better dissolving ability of LiBr solvent compared to CaCl<sub>2</sub> solvent by using much less time to dissolve silk fibroin at 80°C. The yield rate of silk fibroin obtained by using LiBr solvent was 77.47% which was higher than the one using CaCl<sub>2</sub> solvent (50.71%) as reported in our previous study (Raksa et al., 2021). After lyophilized silk fibroin, the surface morphology of silk fibroin in different solvent systems were observed by FE-SEM (Figure 4.4). The result showed elongated or needle-like shapes of silk fibroin which no significant difference of morphology of silk fibroin obtained from different solvent system.

**Table 4.2** Silk fibroin yields of different extraction method.

Extraction Condition	Yield (%)
4.14 M CaCl <sub>2</sub>	50.71
9.3 M LiBr	77.47



**Figure 4.4** FE-SEM image of silk fibroin a) and b) silk fibroin extracted by LiBr solvent using magnification 250x and 1000x and c) and d) silk fibroin extracted by CaCl<sub>2</sub> solvent using magnification 250x and 1000x.

The pattern of extracting proteins on SDS-PAGE was shown in Figure 4.5 and Table 4.3 showed the molecular weight of silk fibroin dissolved following different methodologies. Silk fibroin is composed of two main protein components: the heavy chain (350 kDa) fibroin (H-chain) and the light chain (25 kDa) fibroin (L-chain) (Inoue et al., 2000). The H-chain is hydrophobic and responsible for the formation of  $\beta$ -sheet structures. While the L-chain composed of covalently linked by a disulfide bond at the carboxy-terminus of the two subunits (Feng et al., 2020; Inoue et al., 2000) and comprise a relatively high amount of leucine, isoleucine, valine, and acidic amino acid. L-chain is more hydrophilic properties which are suitable for cell growth (Tanaka et al., 2000; Wang et al., 2021; Zhou et al., 2001). Yamada et al. (2001) showed SDS-PAGE to analyze the silk fibroin, and the result indicated clear protein bands having molecular weights of about 25 and 350 kDa, which corresponded to the L chain and H chains of the silk fibroin. Our result showed the silk fibroin molecule by LiBr and CaCl<sub>2</sub> solvent was degraded to a mixture of polypeptides of different sizes, which is corresponded with some of the results presented by Yamada et al. (2001). The results were showed the solvents by LiBr and CaCl<sub>2</sub>, seemed to have a similar degradation and molecular weight distribution. It can be seen the band of polypeptides with a molecular weight 250 kDa and the band corresponding to the L-chain fibroin at the position around 25 kDa in the silk fibroin dissolved by CaCl<sub>2</sub> solvent and with LiBr solvent. The molecular weight of silk fibroin was affected by many factors between the solution preparing process. Not only did the different solvents have different abilities to degrade SF with different molecular weights (Wang et al., 2012; Cho et al., 2012). Denaturation can be led about by a variety of non-physiological reagents or conditions including, chaotropic ions, organic solvents, solutes of the urea, temperature, pressure, and interfacial forces (Pain et al., 1983).

The silk fibroin chain is a hydrophilic-hydrophobic-hydrophilic polymer and will fold into a 20-nm micelle with hydrophilic and hydrophobic interactions in aqueous solutions. Cho et al. (2012) indicated that when the regenerated silk fibroin chain was gathered after dissolution. It had a size range of 10–30 nm compared to 100–300 nm when the chain was hydrolyzed. Cheng et al. (2015) studied the micelle size of the regenerated silk fibroin (RSF) protein that was larger than 30 nm. This presented that all of the RSF protein was hydrolyzed during dissolution. This was also verified by SDS-PAGE. SDS-PAGE analysis indicated that the RSF solutions from different solvents had similar molecular weight distributions. Hence, the formation of micelles with similar size distributions. For inorganic salt generates ions in water and increases the polarity of the water molecules. This breaks the intermolecular forces of

silk fibroin. Consequently, different solvents produced different hydrolyzed silk fibroin molecular chains and led to different self-assemblies of RSF (Cheng et al., 2015).

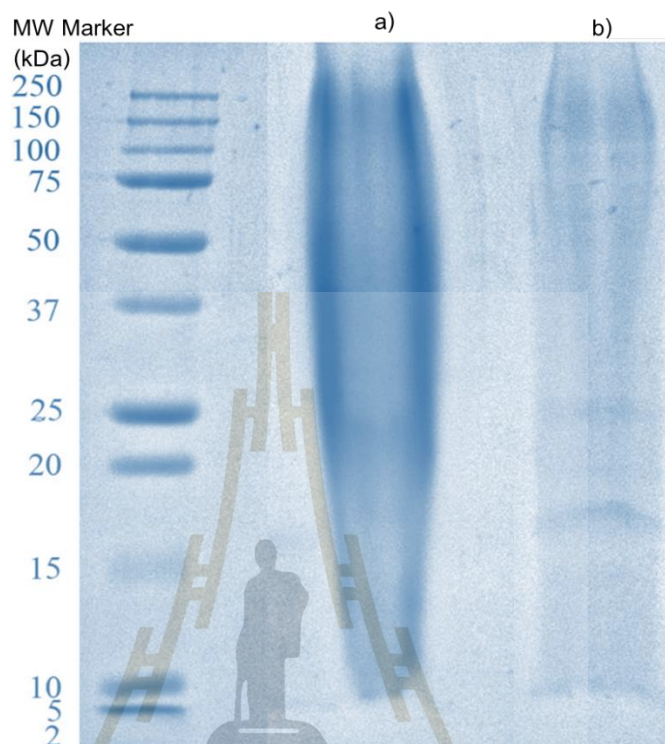


**Figure 4.5** SDS-PAGE analysis of silk fibroin dissolved following different methodologies. 46% w/v  $\text{CaCl}_2$  (lane a) and 9.3 M LiBr (lane b).

**Table 4.3** Molecular weight of silk fibroin dissolved following different methodologies.

SF( $\text{CaCl}_2$ )	SF(LiBr)
10-15 kDa	10-15 kDa
25 kDa (L-chain)	25 kDa (L-chain)
>250 kDa (H-Chain)	>250 kDa (H-Chain)

The structure of the silk fibroin in different solvents was analyzed by FTIR spectroscopy (Figure 4.6). Silk I and silk II are two kinds of silk fibroin molecular structures, and they are frequently used to analyze the silk fibroin structure. Silk I (the black solid line in Figure 4.6) is composed of random coils and an  $\alpha$ -helix, which shows a peak at  $1645\text{-}1650\text{ cm}^{-1}$  that responds to amide I and  $1530\text{ cm}^{-1}$  that responds to an amide II (Cheng et al., 2015). Silk II (the black dotted line in Figure 4.6) mainly is  $\beta$  sheets, which show an amide I bond at  $1630\text{ cm}^{-1}$  and an amide II bond at  $1500\text{ cm}^{-1}$

(Lu et al., 2011; Li et al., 2001; Chen et al., 2007). The FTIR spectra showed that the amide I band of SF extracted by LiBr solvent appeared at  $1650\text{ cm}^{-1}$  and SF extracted by  $\text{CaCl}_2$  solvent showed shifted peak at  $1645\text{ cm}^{-1}$ . Though all absorption bands were assigned to a random coil (Silk I) (Chen et al., 2001; Cheng et al., 2015). The amide II and amide III bands of both solvents appeared at  $1530\text{ cm}^{-1}$  and indicated  $\beta$ -sheet structures (silk II) and showed a peak at  $1235\text{ cm}^{-1}$  ( $\beta$ -sheet but with a certain amount of random coil structure) (Bawazeer and Alsouf, 2017), respectively.

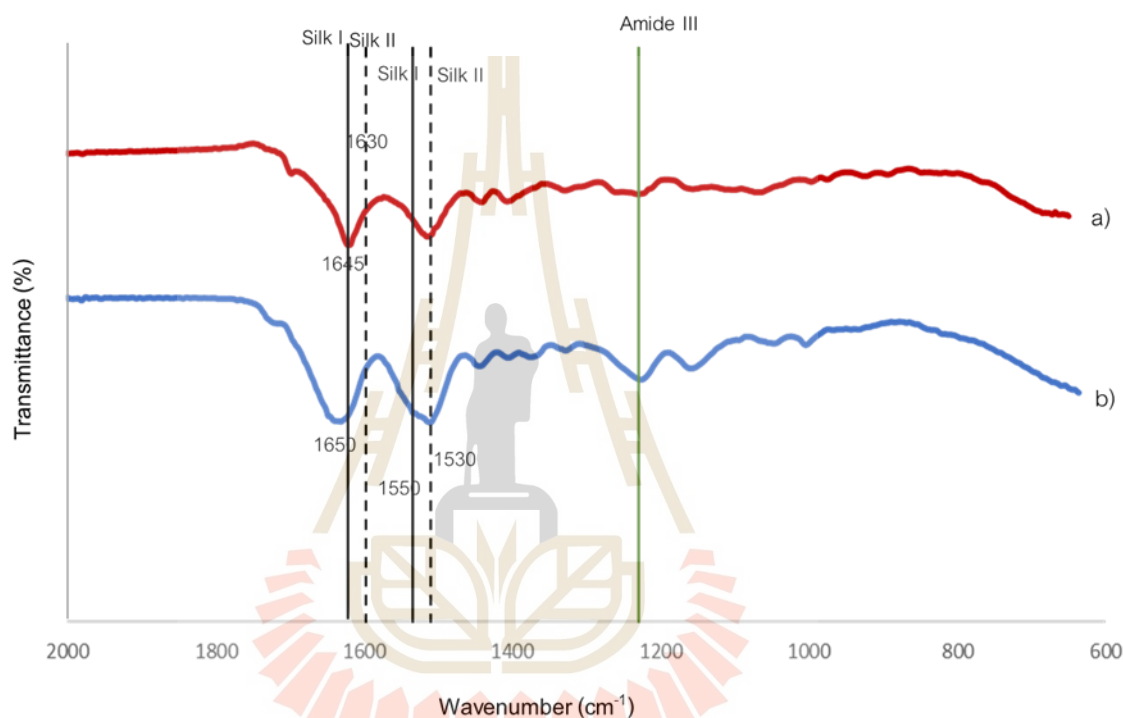


**Figure 4.6** FT-IR spectra of silk fibroin extracted by a)  $\text{CaCl}_2$  solvent and b) LiBr solvent.

X-ray diffraction (XRD) spectra of silk fibroin extracted by  $\text{CaCl}_2$  and LiBr solvents are shown in Figure 4.7. SF mainly occurs in crystalline or amorphous (random coil) form under different conditions. XRD peaks appear at  $2\theta = 9.9^\circ$  for silk I and  $2\theta = 20.2^\circ$  and  $24.1^\circ$  for silk II (Wang and Zhang, 2014). Silk I (random coil) and silk II are attributed to the  $\beta$ -sheet crystalline structure of fibroin (Andiappan et al., 2013; Abdel-Fattah et al., 2015; Qi et al., 2017). Furthermore, when silk fibroin is extracted using  $\text{CaCl}_2$  solvent, it exhibits a crystallinity of 31.40%, whereas extraction with LiBr solvent results in a higher crystallinity of 32.71%.

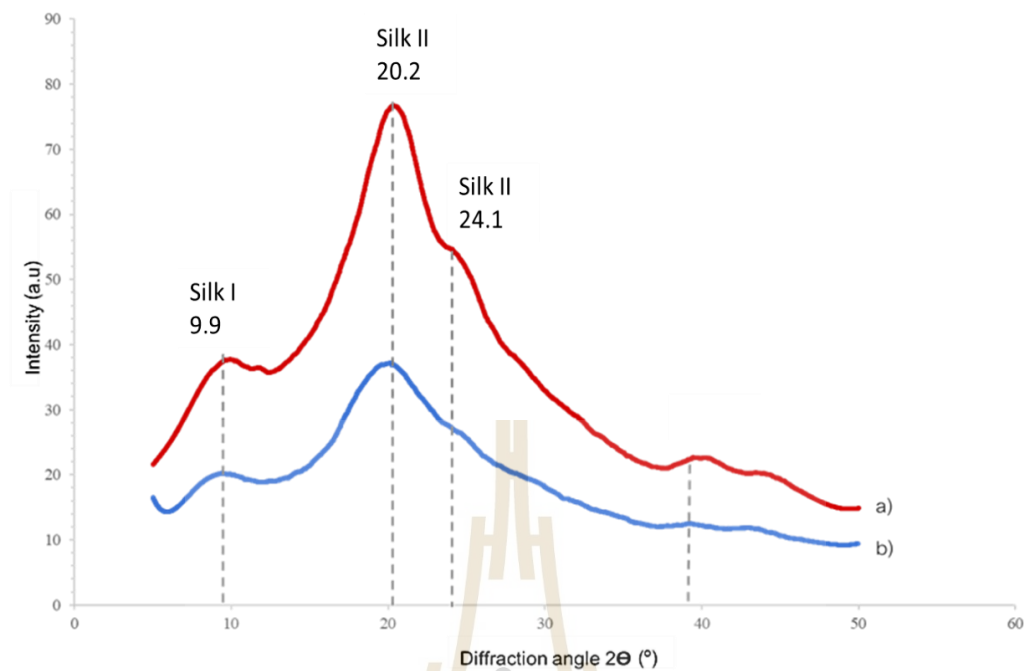


**Figure 4.7** XRD patterns of silk fibroin extracted by a)  $\text{CaCl}_2$  solvent and b) LiBr solvent.

## 4.2 The effect of electrospinning parameters on the morphology and mechanical properties of electrospun nanofibrous scaffold

### 4.2.1 The effect of PVA concentration

FE-SEM in Figure 4.8 and Table 4.4 showed the combination of beaded fiber in the electrospun nanofiber ( $132 \pm 24$  nm) prepared using a 5% w/v of PVA solution, whereas the larger fibers without beads were obtained in the case of the system prepared using the 10% w/v of PVA solution ( $181 \pm 27$  nm). When the concentration of PVA was increased to 15% w/v, the polymer solution did not flow through the tip. The bead formation in the fiber occurred due to the evidence of droplets during electro spray and, thereafter, they were deposited on the fiber. In the case of more concentrated polymer solutions, the charged jet did not break up into small droplets. The smallest PVA fiber was evident when the lower concentration PVA solution was used. This is because the lowest solution viscosity could accelerate the stretching of the polymer during electrospinning. Adding the higher PVA to the solution affected the viscosity of the solution and resulted in increasing the fiber diameter. The charged jet from high concentrate solution could withstand the coulombic stretching force therefore the smooth with larger electrospun fibers could be obtained. In addition, the low solvent in the charged jet of concentrate polymer solution dried more easily, which complicated the elongation and thinning of fibers (Supaphol et al., 2008). The high-concentration solution exhibited high viscosity and also high surface tension;

thereafter, the stretching ability was reduced. Typically, the solution viscosity increases with increasing solution concentration according to a power-law relationship, and an increase in the solution viscosity should result in the formation of fibers of larger diameters (Mit-uppatham et al., 2004). The polymer concentration is associated with solution viscosity, which increases with the increase of the polymer concentration and then leads to a larger fiber diameter. However, if the concentration is too low, continuous polymer fibers cannot be achieved, and polymer beads are obtained. When the concentration is too high, the polymer solution becomes very viscous and fibers are obtained along with many drops. Highly viscous solutions have difficulty flowing through the syringe tip. Therefore, an appropriate polymer concentration is very important to the electrospinning process (Hong, Y., 2016).

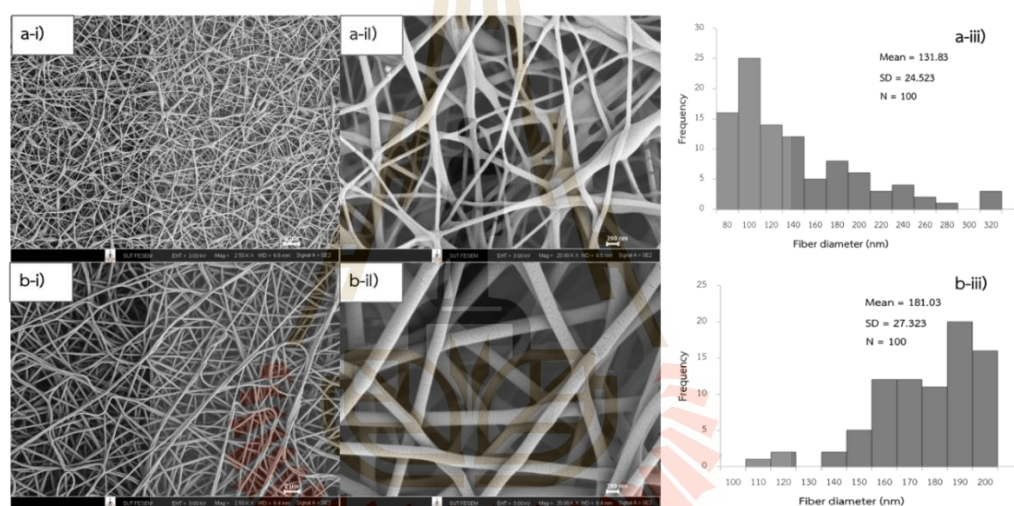


**Figure 4.8** FE-SEM images and histograms of electrospun of PVA nanofiber at different concentration; (a-i, a-ii, a-iii) = 5% w/v, (b-i, b-ii, b-iii) = 10% w/v (Magnification 2500x and 20000x).

**Table 4.4** Some Properties of the electrospun PVA nanofiber.

Concentration of PVA solution (% w/v)	Viscosity (cP)	Fiber Diameter (nm)	Observation
5	984	132	Beaded formation
10	2427	181	The formation of continuous fibers was observed
15	8305	-	No formation of fibers is observed, the polymer solution did not flow through the tip

The breakage mechanism and fiber morphology of electrospun nanofiber are the main reasons for the increase in tensile strength with an increase in polymer concentration. The presence of beads in the nanofiber mats at low concentrations causes fewer fiber-to-fiber interactions and increased weakness of individual fibers, resulting in generally low tensile strength values. Beads act as defects in a fiber. Hence, from the present study, it has been observed that the weak points increase with the increased beads of nanofibers. As the concentration is increased, smoother fibers with improved diameter uniformity are formed (Tarus et al., 2019). This results in increased fiber cohesion points, thereby increasing the tensile strength as shown in Figure 4.9. From the stress-strain curves, the initial difference in tensile strength values between the 5% w/v PVA nanofibers and the presence of beads on the fibers led to fewer fiber cohesion points. The tensile strength is approximately 3.30 MPa with an elongation at break of 8.53%. When the polymer concentration was increased to 10% w/v PVA, the large diameters of the smooth electrospun nanofibers showed a tensile strength of 4.66 MPa and an elongation at break of 70.10%, which means the tensile properties of 10% w/v PVA were higher than 5% w/v PVA. Thus, the concentration was influenced by nanofiber morphology, which in turn affects the mechanical properties (Mittupatham et al., 2004). It is expected that as the solution concentration of PVA is further increased, an optimum point would ultimately be reached where further concentration increases would lead to diminishing tensile properties. This would be due to the increasing diameter causing reduced fiber surface area to volume ratio, thereby decreasing fiber interaction points.

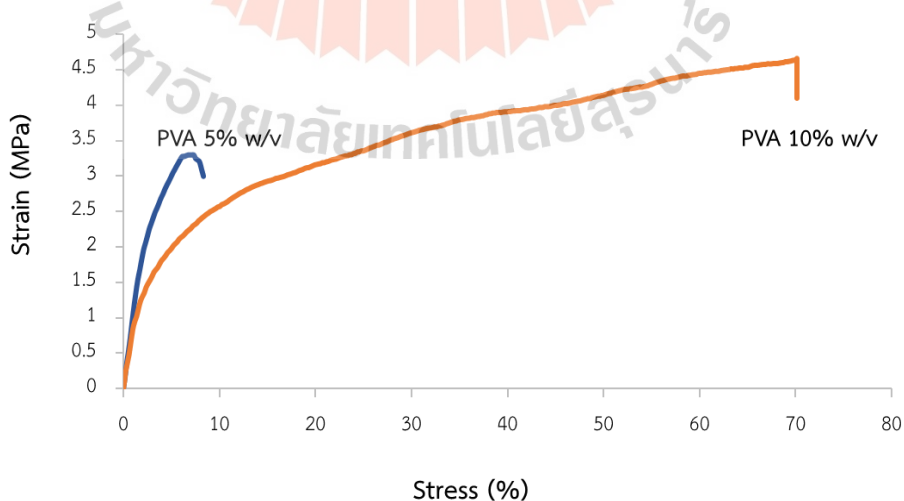


**Figure 4.9** The stress-strain curve of nanofiber prepared using different concentration of PVA solutions.

#### 4.2.2 The effect of humidity

The morphology of SF/PVA (25:75 v/v) blended nanofiber studied by FE-SEM was shown in Figure 4.10. With increasing relative humidity, the fiber became more nonuniform in shape and thickness. Uneven fiber diameter with increasing relative humidity was also found in electrospun silk fibroin. Wider fiber diameter distribution was observed at higher relative humidity. Pelipenko et al. (2018) reported the influence of humidity on diameter of PVA nanofiber. With increasing relative humidity from 4% to 70%, fiber diameter was decreased from  $667 \pm 83$  nm to  $74 \pm 99$  nm. In contrast, for SF nanofiber, fiber diameter was increased from 30 to 120 nm. When the relative humidity (RH) was increased from 25% to 30% (Kim et al., 2013). From our study, the relative humidity of 50%-80% in Figure 4.10 and Table 4.5, the electrospun SF/PVA nanofiber showed smooth surface without any bead formation and the average fiber diameter size in the range 111 to 90 nm. The average pore size of nanofiber shows a small interconnecting fiber in the range 360 to 290 nm, it was decreased when the relative humidity increased. The distance of interconnecting pore nanofiber was less than cell size which was the diameter size of a cell infiltrated about 100  $\mu$ m to 1 cm (Wu and Hong, 2016). Nevertheless, an inherent limitation of electrospun scaffolds is the relatively small pore size that does not promote cellular infiltration and tissue ingrowth into the scaffold (Rnjak-Kovacina and Weiss, 2011). At higher number of water molecules in the atmosphere during the electrospinning process, the water evaporation in the polymeric jet is slower, therefore, solidifies more slowly. Moreover, high relative humidity supported to the absorption of water molecules, which may increase the wettability of the polymer jet and as resultant to obtain small fibers. On the other hand, Pelipenko et al. (2013) reported at low RH conditions, the polymer jet solidifies soon after it comes out of needle tip. Therefore, it is exposed to voltage induced stretching for a short time only. At higher RH solidification occurs more slowly and polymer jet is consequently exposed to voltage induced stretching for a longer time, resulting in the formation of thinner fibers. The changes in nanofiber morphology can be explained with the combination of solvent evaporation rate (solidification velocity) and bead-on-a-string formation during the capillary breakup of viscoelastic fluid (Tripatanasuwan et al., 2007). PVA and silk have different viscoelastic property and water absorbability. This may lead to larger fiber diameter of silk fibroin nanofiber and smaller fiber diameter of PVA nanofiber when the relative humidity was increased. This resulted in wide distribution of fiber diameter of electrospun SF/PVA nanofiber. However, with low relative humidity, there is less interconnecting pore distribution on the surface. Because fast solvent evaporation at lower relative humidity has less

chance to condense the moisture on the surface of electrospun fibers. Mechanical properties of SF/PVA nanofiber at different relative humidity were shown in Table 4.5 and stress–strain curves of electrospun SF/PVA nanofiber at different relative humidity are shown in Figure 4.11. The results show that the highest tensile strength was obtained from the nanofiber electrospun at lowest relative humidity. Solvent evaporation rate was higher with lower relative humidity leading to higher concentration of polymer solution being electrospun. The higher concentration results in higher tensile strength. A decrease in tensile strength with increasing RH was also reported by Tang et al. (2009) for the electrospun polyether sulfone nanofiber. In general, electrospun nanofiber has higher tensile on surface forms shortly after the polymer jet comes into contact with the surrounding environment. Therefore, fiber to fiber adhesion will be weaker as residual solvent is essential to link fibers junctions together. This reduced strength of nanofiber at higher humidity. When the relative humidity was increased, more water molecules present in the atmosphere. If the water molecule penetrates into polymer molecules, it can react as plasticizer resulting in higher elongation at break. Thus, at the highest relative humidity, and highest elongation at break were obtained from our study strength at break when electrospun at lower humidity. At low RH, the nanofiber surface was smooth and bead free. At high RH, the fibers exhibited a soft texture indicating poor fiber–fiber bonding (Tang et al., 2009; Zaarour et al., 2018). The reason for this poor bonding at high humidity is due to the phase separation promoted by the presence of water. Fiber on surface forms shortly after the polymer jet comes into contact with the surrounding environment. Therefore, fiber to fiber adhesion will be weaker as residual solvent is essential to link fibers junctions together. This reduced strength of nanofiber at higher humidity. When the relative humidity was increased, more water molecules present in the atmosphere. If the water molecule penetrates into polymer molecules, it can react as plasticizer resulting in higher elongation at break. Thus, at the highest relative humidity, and highest elongation at break were obtained from our study.

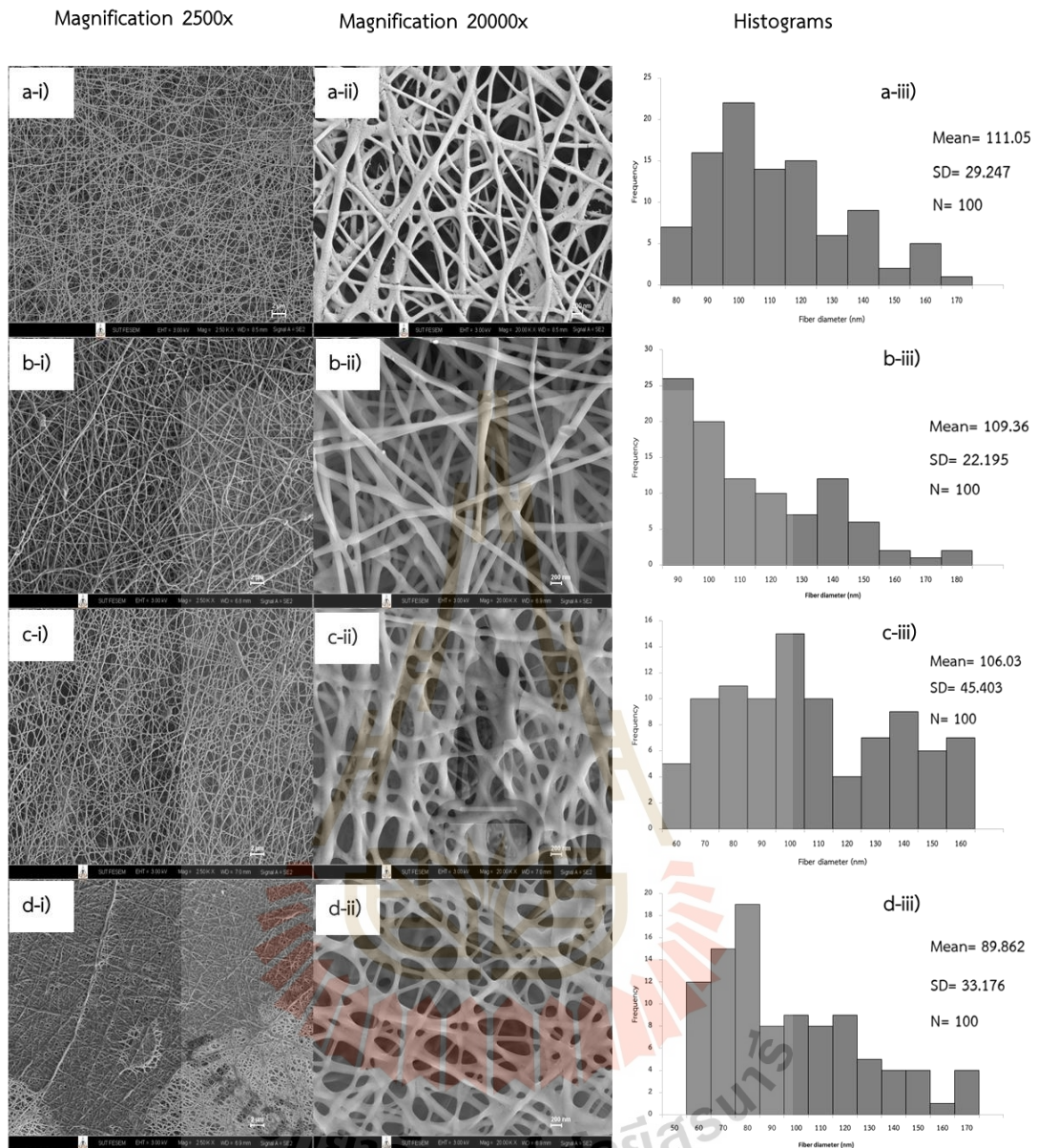


**Figure 4.10** FE-SEM images and histograms of electrospun SF/PVA blended nanofiber at different relative humidity; (a-I, a-II, a-III) = 50%, (b-I, b-II, b-III) = 60%, (c-I, c-II, c-III) = 70%, (d-I, d-II, d-III) = 80%.

**Table 4.5** Mechanical properties and Fiber diameter size of SF/PVA blended nanofiber at different relative humidity.

Relative humidity	Tensile strength at break (MPa)	Elongation at break (%)	Average fiber diameter (nm)
50	4.00±0.02	27.23±1.64	111±29
60	3.20±0.18	23.47±0.88	109±22
70	2.80±0.08	36.08±1.39	106±45
80	2.78±0.10	41.11±1.25	90±33

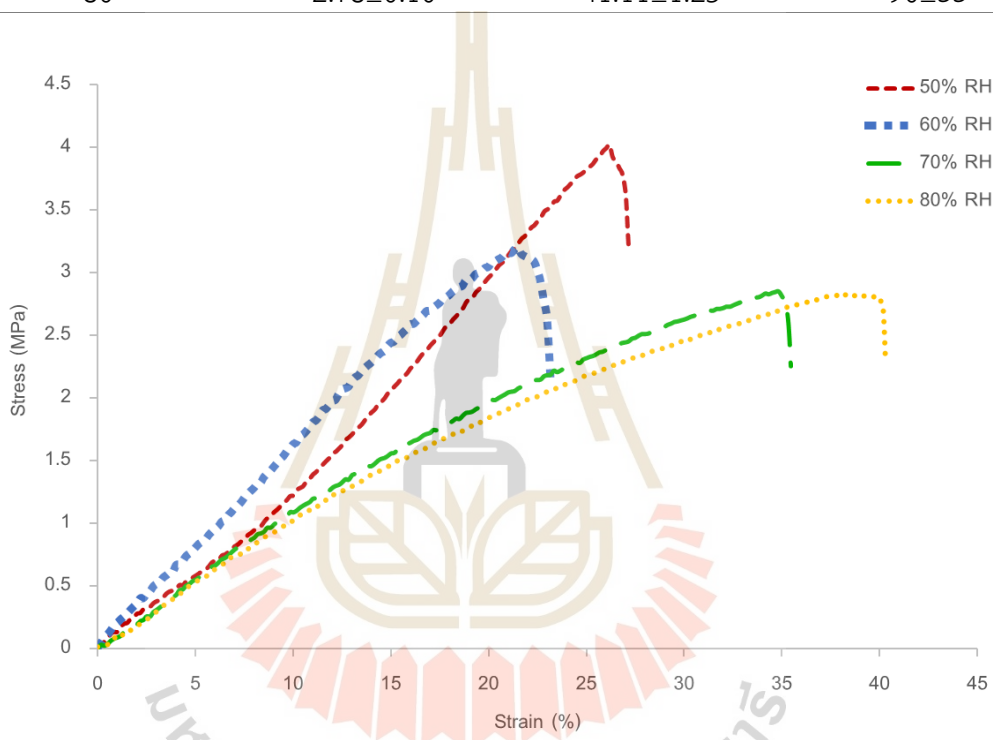


**Figure 4.11** Stress–strain curves of electrospun SF/PVA nanofiber at different relative humidity.

#### 4.2.3 The effect of voltage

In this study, the polymer blend of the SF/PVA (25:75 v/v) was fabricated into nanofiber under the applied voltages of 10, 15, 20, and 25 kV over a tip-to-collector distance of 10 cm. The FE-SEM images in Figure 4.12 reveal the electrospun SF/PVA nanofiber and fiber diameter distributions obtained at different applied voltages. Electrospun SF/PVA nanofibers showed a random nanofiber, no bead, and a smooth surface fibrous structure. At 10 kV, Figure 4.12(a-iii) showed an average fiber diameter of 362 nm. When the applied voltage was increased to 15, 20, and 25 kV (Figure 4.12 (b-iii), (c-iii), and (d-iii)), the average fiber diameter was decreased (175, 135, and 110

nm). It was due to adjusting the applied voltage having multiple effects on the electrospinning procedure since it affects the number of charges applied to the solution. Increasing the voltage will accelerate the electrospinning jet, which may result in a larger volume of solution being pulled from the needle tip. If the solution feed rate is held constant, the Taylor cone will be smaller and less stable (Zhong et al., 2002) and may finally recede into the needle (Deitzel et al., 2001). Lee et al. (2004); Buchko et al. (1999) reported that the large voltage applied will result in a greater stretching of the solution, which in turn should result in thinner fibers. Electrospinning a solution with low viscosity at a higher voltage may also favor the production of secondary jets, resulting in smaller fiber diameters. Normally, in nanofibrous scaffolds for tissue engineering applications, there should be no beads in the electrospun SF/PVA nanofibers. Furthermore, the nanofiber diameters must be similar to the natural extracellular morphology in order to promote cell growth (Haider et al., 2018). Badami et al. (2006) showed that fibers with small diameters (140 nm or less) could hinder cell infiltration and proliferation due to that reduced fiber diameter results in a smaller pore size in scaffolds (Eichhorn and Sampson, 2005). In addition, electrospun scaffolds with a diameter of fiber that is greater than 1600 nm revealed a reduction in the amount of cell attachment and proliferation of fibroblast of electrospun scaffolds (Pham et al., 2006). As for Figure 4.12(d-ii), it shows branch-shaped fibers are observed when the voltage increases, which can be explained as follows: when high voltages induce multiple jets of electrospinning, reducing the electrostatic forces and stretching the fibers, as a result, shrunk fibers are obtained (Lui et al., 2019).

The mechanical properties of the scaffolds used in tissue engineering are one of the most important aspects that need to be taken into consideration. The tensile properties are the most common ones for the meniscus which tensile properties are cross-section and position-dependent due to varied fiber densities and orientations. As a result, the axial compressive force is thus distributed as a circumferential tensile load. The purpose of the tensile test is to quantify the circumferential tensile properties of scaffolds under an axial load at the knee. The scaffold structure can greatly impact the tensile and compressive test results. The mechanical properties of electrospun SF/PVA nanofiber at different applied voltage (10, 15, 20, and 25 kV) was shown in Figure 4.13 and stress–strain curves of electrospun SF/PVA nanofiber show in Table 4.6. The results showed that the highest tensile strength (5.78 MPa) was obtained from the electrospun nanofiber at voltage of 20 kV. In addition, at 10 and 15 kV shown ultimate tensile strength of 4.15 and 4.78 MPa while the voltage of 25 kV had tensile strength of 5.26 MPa. It can be observed that increasing the voltage increases the

ultimate tensile strength and elongation at break of the electrospun nanofibers was increased while the highest voltage (25 kV) had a slight decrease in tensile strength. Because the expelled polymer jet is randomly welded together, it reaches the collector and causes the union of fibers to form stronger and more tensile strength connections, affecting the morphology and mechanical properties (Reneker and Yarin., 2008; Carg et al., 2011). Nguyen et al. (2010) reported conglutination is common when high voltages are used in the electrospinning of scaffolds and allow for increased tensile strength due to the formation of a network of interlaced fibers. Furthermore, Wei et al. (2009) modeled the mechanical properties of an electrospun nanofiber network and discovered that the conglutination of fibers increases tensile strength significantly. Load transfer between fibers occurs via van der Waals interactions as well as mechanical interlocking, where introducing fusion points (by increasing the voltage) improves load transfer and tensile strength (You et al., 2006). However, at 25 kV of the electrospun nanofiber, show a tensile strength decrease may be due to the morphology of the electrospun nanofiber in Figure 4.12(d-ii) exhibits producing points of contact between fibers and branched structures, which could affect the tensile strength (Doshi and Reneker, 1995). Therefore, the electrospun SF/PVA nanofiber (25:75 v/v), the applied voltage at 20 kV had the highest tensile strength which could be used for tissue engineering in next studies.



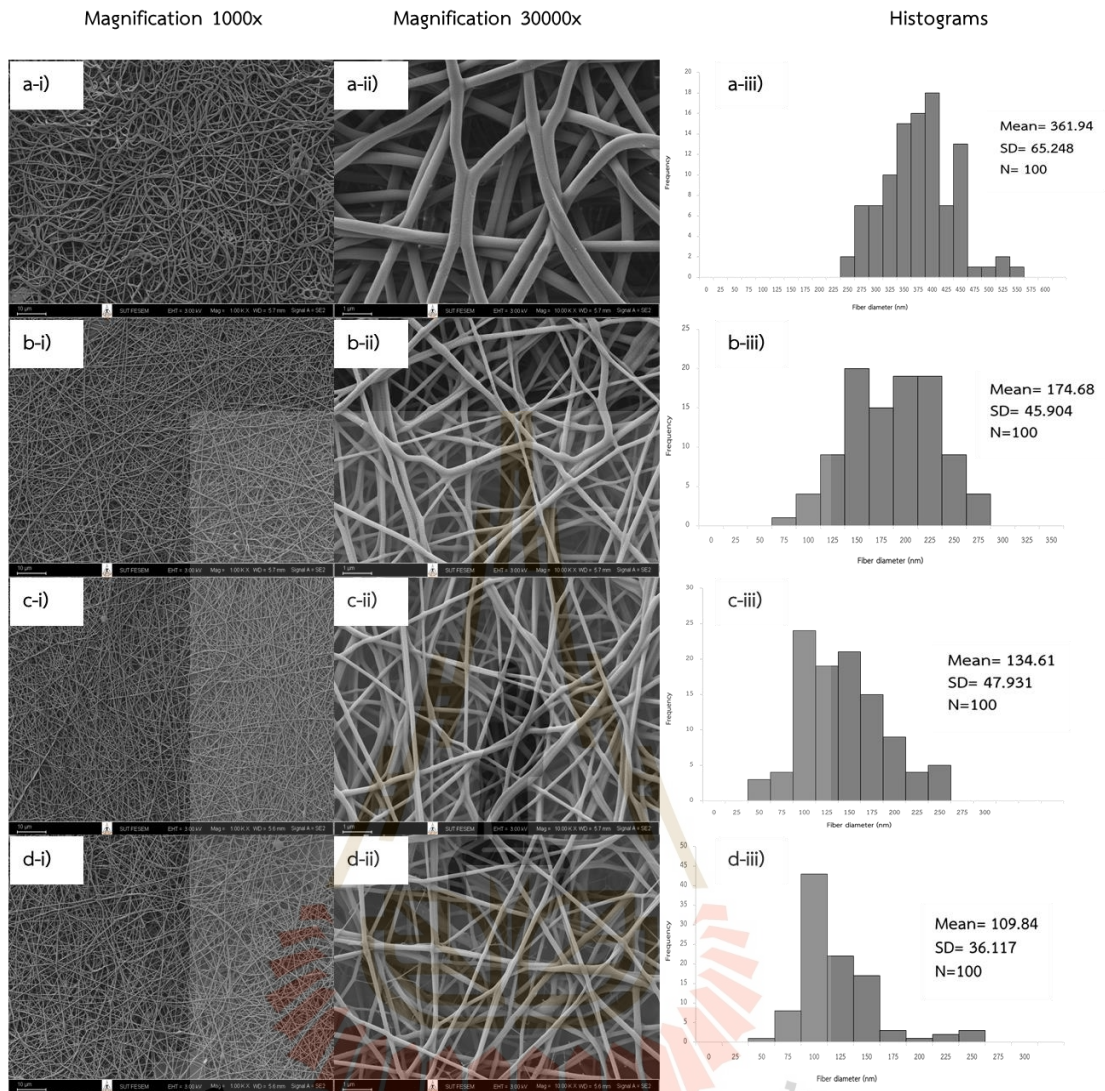


**Figure 4.12** FE-SEM images and histograms of electrospun SF/PVA blended nanofiber at different applied voltage; (a-i, a-ii, a-iii) = 10 kV, (b-i, b-ii, b-iii) = 15 kV, (c-i, c-ii, c-iii) = 20 kV, (d-i, d-ii, d-iii) = 25 kV.

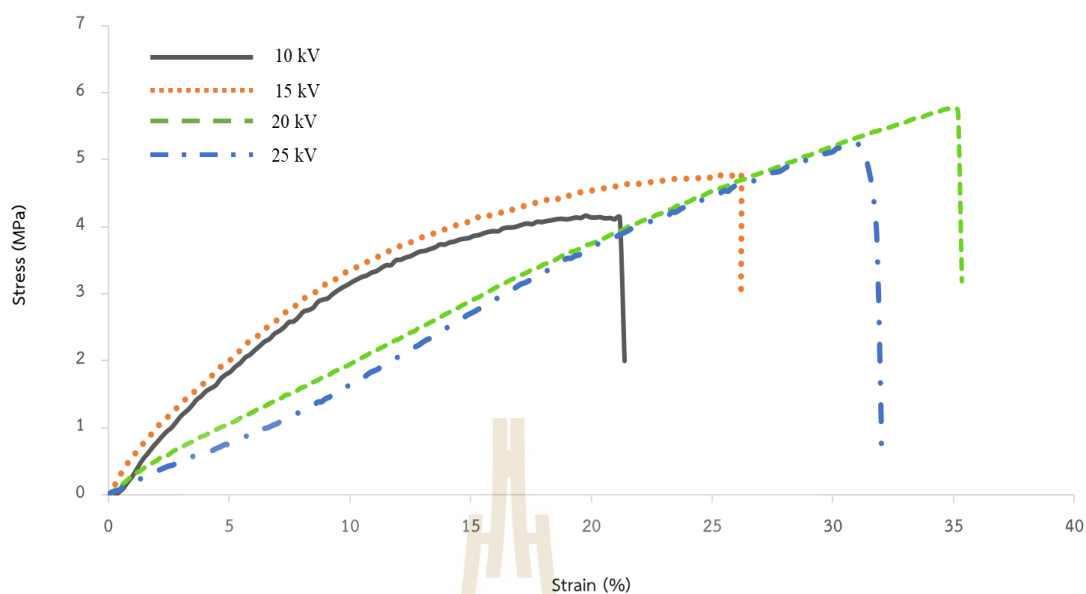


**Figure 4.13** Stress–strain curves of electrospun SF/PVA nanofiber at different applied voltage.

**Table 4.6** Mechanical properties and Fiber diameter size of SF/PVA blended nanofiber at different applied voltage.

Applied Voltage (kV)	Tensile strength at break (MPa)	Elongation at break (%)	Average fiber diameter (nm)
10	4.15±0.44	22.35±1.55	362±65
15	4.79±0.16	26.12±0.93	175±45
20	5.78±0.07	34.99±4.40	135±47
25	5.26±0.24	32.27±2.02	110±36

### 4.3 The effect of silk fibroin content on physical properties and mechanical properties of electrospun SF/PVA nanofibrous scaffold

#### 4.3.1 Measurements of Viscosity

The viscosity of both solvents in the SF/PVA solution plays an important role in determining the nanofiber shape formation, size, and morphology of the fibers. Pal et al. (2017) reported that adequate chain entanglement was essential among the polymers for the initiation of uninterrupted electrospinning yielding fibers in diameter submicron range. The viscosity with low values or high values may result in beaded nanofibers and the viscosity value in the range of 100 to 2000 cP was suitable for spinning (Amariei et al., 2017). In this study, it was observed (Figure 4.14) that

SF(CaCl<sub>2</sub>)/PVA and SF(LiBr)/PVA blend solution displayed higher viscosity when the PVA amount was increased and the stability of the nanofibrous scaffold produced was complete but had thicker fiber diameters (Figure 4.10 and Figure 4.15). Both solvents in the SF/PVA blended solution showed spinnability except for the SF/PVA solution at a ratio of 100:0 because of a viscosity value of less than 100 cP. The viscosity was below 100 cP which resulted in the breakage of the solution into droplets giving an increase to multiple beaded fibers. This is probably the interfacial tension dominates over the viscous force (Roy et al., 2018). Therefore, these results could be linked to a high volume of polymer chain entanglement. Whereas, with increasing in silk fibroin concentration in the blended solution no significant change in viscosity.

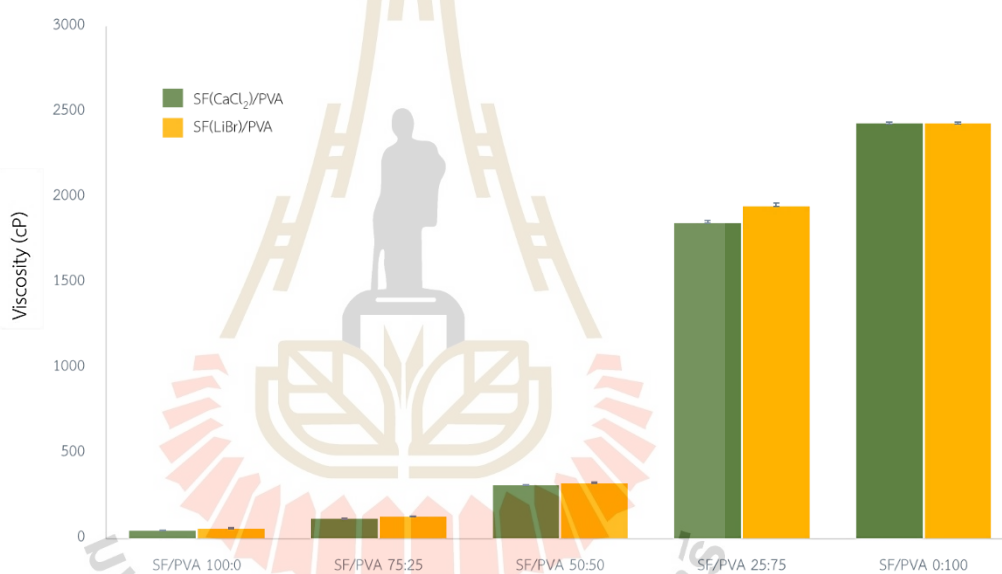


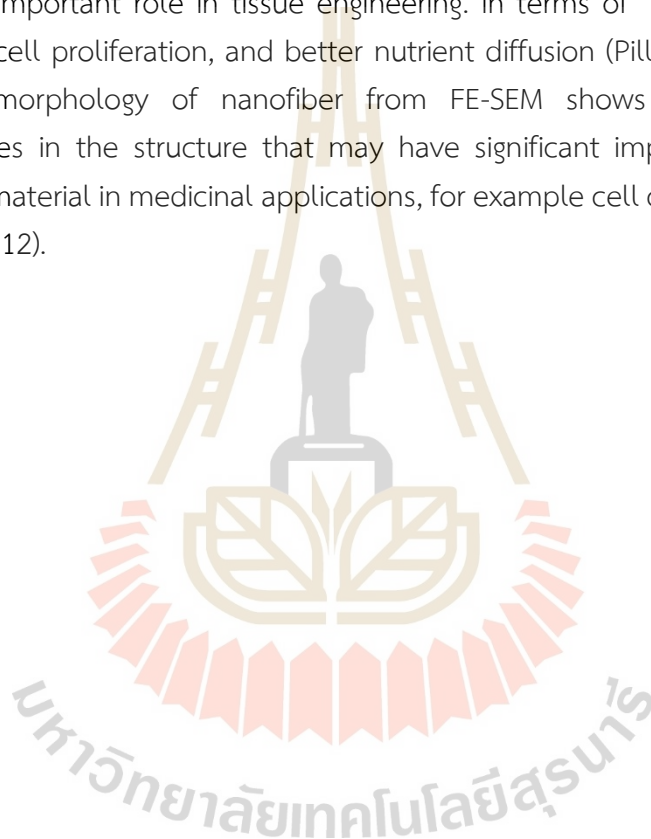
**Figure 4.14** Viscosity of SF/PVA solution at different ratios (the green line represents the viscosity value of SF(CaCl<sub>2</sub>)/PVA and the yellow line represent the viscosity value of SF(LiBr)/PVA).

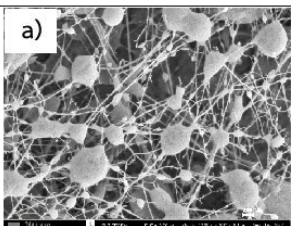
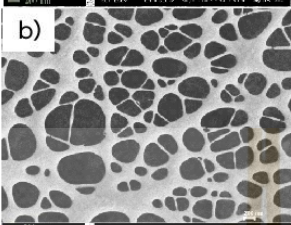
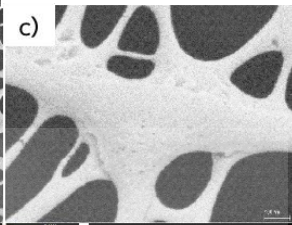
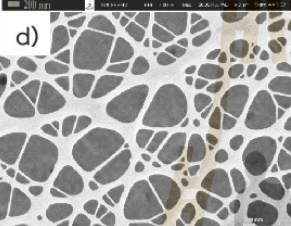
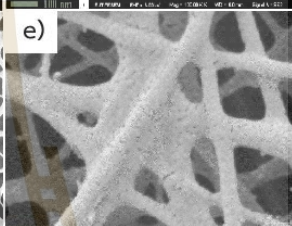
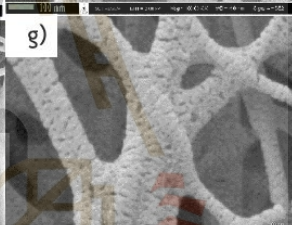
### 4.3.2 Effect of CaCl<sub>2</sub> solvent for extraction silk fibroin on SF(CaCl<sub>2</sub>)/PVA nanofibrous scaffold

#### 4.3.2.1 Morphology

Figure 4.15 shows the field emission scanning electron microscope images of SF(CaCl<sub>2</sub>)/PVA blended nanofiber at various ratio between SF to PVA including 100:0, 75:25, 50:50, 25:75, and 0:100. Each nanofiber shows a different shape and diameter size. The blended SF/PVA of 100:0 with diameter size in range of 34±11 nm. contained beaded formation on nanofiber. The beads formation may be caused by low molecular

weight, charge density, or high surface tension. The morphology of SF(CaCl<sub>2</sub>)/PVA at ratio of 75:25, 50:50, and 25:75 showed an interconnecting network structure on the fiber surface and bead free, which their mean diameter were 54±17, 62±21, and 74±18 nm, respectively. Whereas, blended SF(CaCl<sub>2</sub>)/PVA of 0:100 showed random and bead free nanofiber with smooth surface, and diameter size in range of 183±31 nm. However, on blending SF and PVA, the nanofiber diameter was increased when SF content was decreased. The small diameter of SF(CaCl<sub>2</sub>)/PVA nanofiber led to an increase in surface area. This interconnecting network structure on fiber surface of the scaffold nanofiber will play an important role in tissue engineering. In terms of a place for good cell attachment, cell proliferation, and better nutrient diffusion (Pillai et al., 2016). In this study, the morphology of nanofiber from FE-SEM shows the appearance of heterogeneities in the structure that may have significant impact on behaviour of nanofibrous material in medicinal applications, for example cell culture or drug release (Sirc et al., 2012).



Composition	Magnification 20000X	Magnification 100000X	Fiber Diameter (nm)
SF(CaCl <sub>2</sub> )/PVA 100:0			34±11
SF(CaCl <sub>2</sub> )/PVA 75:25			54±17
SF(CaCl <sub>2</sub> )/PVA 50:50			62±21
SF(CaCl <sub>2</sub> )/PVA 25:75			74±18
SF(CaCl <sub>2</sub> )/PVA 0:100			183±31

**Figure 4.15** FE-SEM images of SF/PVA nanofibrous scaffold various ratios and different magnification; a) SF/PVA 100:0, b) and c) SF/PVA 75:25, d) and e) SF/PVA 50:50, f) and g) SF/PVA 25:75, h) and i) SF/PVA 0:100.

#### 4.3.2.2 Wettability

Hydrophilicity is an important role for biocompatibility of scaffold for tissue engineering. The hydrophilicity of the different blended nanofiber was shown in Figure 4.16 Contact angle of SF(CaCl<sub>2</sub>)/PVA nanofibrous scaffold and Table 4.7. Contact angle of the SF(CaCl<sub>2</sub>)/PVA nanofibrous scaffold showed the value in range of 40° -65°. The increase in contact angle was observed with an increase SF content. This is due to the hydrophobicity of the SF/PVA nanofiber. Normally, SF is mostly composed of hydrophobic amino acids domains of the H-chain that contains a repetitive hexapeptide sequence of Gly-Ala-Gly-Ala-Gly-Ser and repeat units of Gly-Ala/Ser/Tyr dipeptides. The hydrophobic amino acid domains of H-fibroin fold and bond together via hydrogen bonds, Van der Waals forces, and hydrophobic interactions, to form anti-parallel  $\beta$ -sheet crystalline structures. (Qi et al., 2017; Nguyen et al., 2019). This structural characteristic provides enough hydrophobicity to increase contact angles of the SF(CaCl<sub>2</sub>)/PVA nanofiber. Polymers with an air-water contact angle around 60° - 65° leads to cell attachment and cell proliferation (Bhattacharjee et al., 2015). The highest level of cell attachment (NIH 3T3 fibroblasts) at hydrophilic surfaces was obtained from nanofiber with contact angles in the range of 20°-60° (Wei et al., 2020). Therefore, the hydrophilicity of nanofiber prepared from our study was suitable for scaffold tissue engineering application.





Figure 4.16 Contact angle of SF(CaCl<sub>2</sub>)/PVA nanofibrous scaffold.

**Table 4.7** Contact angle and Tensile properties of SF(CaCl<sub>2</sub>)/PVA nanofibrous scaffold various ratio.

Composition	Contact Angle (°)	Ultimate Tensile Strength (MPa)	Elongation at Break (%)
SF(CaCl <sub>2</sub> )/PVA 100:0	65±3.6	-	-
SF(CaCl <sub>2</sub> )/PVA 75:25	60±4.3	0.94±0.06	10.8±1.1
SF(CaCl <sub>2</sub> )/PVA 50:50	55±2.3	9.45±2.44	39±4.8
SF(CaCl <sub>2</sub> )/PVA 25:75	51±2.5	5.78±0.92	35.3±11
SF(CaCl <sub>2</sub> )/PVA 0:100	40±1.3	4.97±0.8	112.57±4.8

#### 4.3.2.3 Tensile Properties

Mechanical properties of SF(CaCl<sub>2</sub>)/PVA nanofibrous scaffold at different ratios were shown in Table 4.7 and stress-strain curves of all nanofiber were shown in Figure 4.17. The result of SF(CaCl<sub>2</sub>)/PVA 0:100 nanofibrous scaffold exhibited relatively low mechanical strength. The SF(CaCl<sub>2</sub>)/PVA of 50:50 showed higher tensile strength than another nanofiber. Silk fibroin showed an improvement in the tensile strength of the electrospun fibrous scaffold. These improvement in mechanical properties is attributed to well oriented  $\beta$ -sheet crystallite structure and the shear alignment of the fiber chains (Altman et al., 2003). This is essential property for the meniscus scaffold for tissue engineering. However, when SF content was increased to very high ratio of SF(CaCl<sub>2</sub>)/PVA; the SF/PVA blended nanofiber was more difficult to be processed and nonuniform thickness of the nanofibers were obtained with the lowest tensile strength and elongation at break.

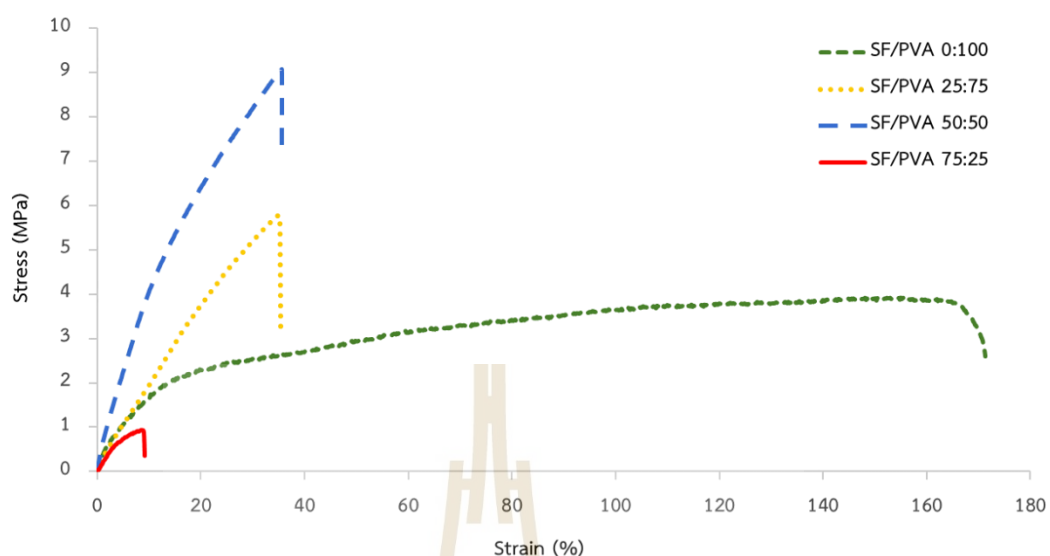


**Figure 4.17** Stress-Strain curve of SF(CaCl<sub>2</sub>)/PVA nanofibrous scaffold at different ratio.

#### 4.3.2.4 Fourier Transform Infrared (FT-IR) Analysis

FT-IR spectra of the different nanofibrous scaffold was investigated as shown in Figure 4.18. The main characteristic peaks of SF contain conformation of  $\beta$ -sheet structure which conformation shows characteristic peaks; absorption frequencies to  $\beta$ -sheet form at  $1625\text{-}1620\text{ cm}^{-1}$ ,  $1510\text{-}1500\text{ cm}^{-1}$ , and  $1245\text{-}1240\text{ cm}^{-1}$ , representing amide I, amide II, and amide III, respectively. The amide I band mainly comes from C=O stretching with minor contributions from N-H in-plane bending while the amide II band is mainly caused by C-N stretching and N-H in-plane bending of the SF backbone (Ling et al., 2013). The spectrum of PVA was obtained at  $3300\text{ cm}^{-1}$  (-OH stretching),  $2960\text{-}2920\text{ cm}^{-1}$  (-CH stretching) and  $1750\text{-}1720\text{ cm}^{-1}$  (-C=O stretching),  $1470\text{-}1450\text{ cm}^{-1}$  (CHOH bending),  $1250\text{ cm}^{-1}$  (C-O stretching), and  $1090\text{-}1080\text{ cm}^{-1}$  (C-O out-of-plane bending), respectively (Bhattacharjee et al., 2015). These bands assigned to PVA became stronger with increasing PVA contents. The characteristic absorption bands of SF(CaCl<sub>2</sub>)/PVA blended nanofiber showing the wave number ranges of amide I, amide II, and amide III were shifted from  $1625\text{-}1620\text{ cm}^{-1}$  to  $1630\text{-}1627\text{ cm}^{-1}$ ,  $1510\text{-}1500\text{ cm}^{-1}$  to  $1515\text{-}1512\text{ cm}^{-1}$ , and  $1245\text{-}1240\text{ cm}^{-1}$  to  $1250\text{-}1248\text{ cm}^{-1}$ , respectively. Furthermore, the width of the OH region  $3350\text{-}3300\text{ cm}^{-1}$  was extended by blending SF and PVA which could characterize the increase of the intensity of hydrogen bonding in FTIR spectra (Niu et al., 2019). This may confirmed the chemical interactions between the amino group of silk fibroin and the hydroxyl group of polyvinyl alcohol. However, it should be noted that FT-IR technique alone could hardly prove the extent of the SF/PVA chemical

interactions. This is because the moisture product impurity can also give rise to the broadened IR signal between the 3350-3300  $\text{cm}^{-1}$  region.

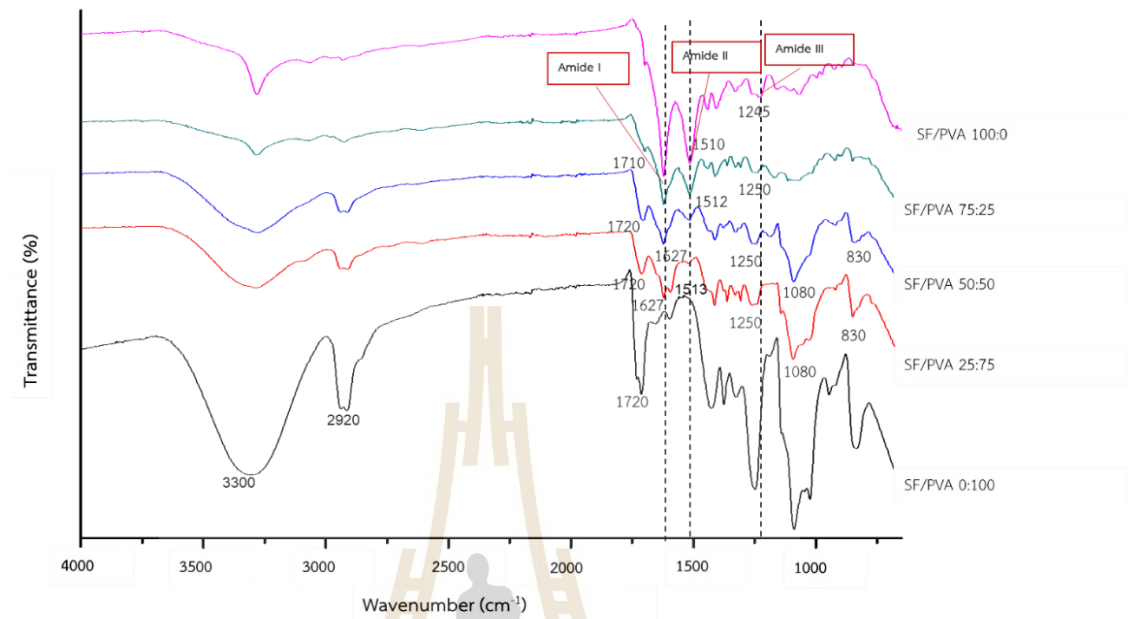


Figure 4.18 FT-IR spectra of SF( $\text{CaCl}_2$ )/PVA nanofibrous scaffold at different ratio.

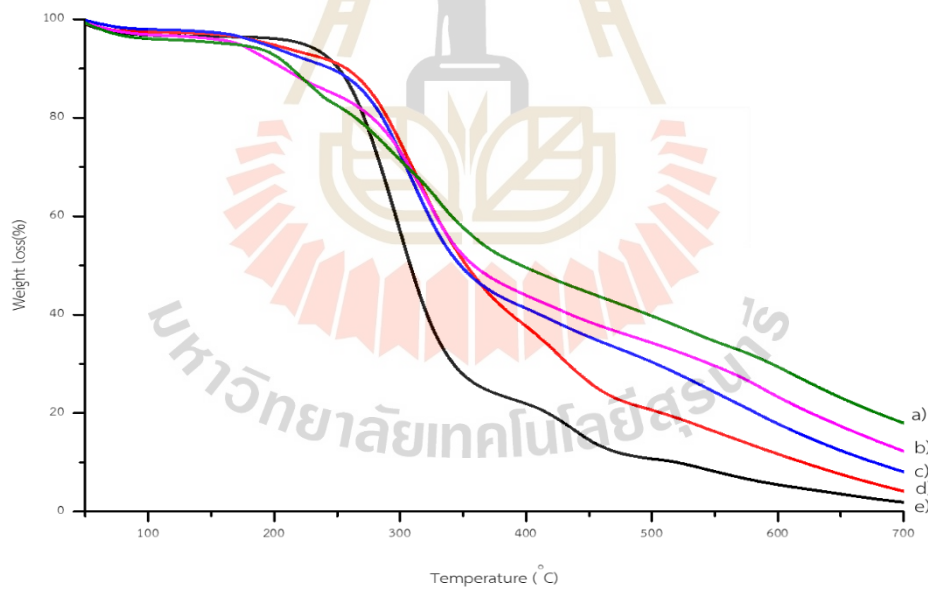


Figure 4.19 TGA thermograms of SF( $\text{CaCl}_2$ )/PVA nanofibrous at various ratios; a) SF( $\text{CaCl}_2$ )/PVA 100:0, b) SF( $\text{CaCl}_2$ )/PVA 75:25, c) SF( $\text{CaCl}_2$ )/PVA 50:50, d) SF( $\text{CaCl}_2$ )/PVA 25:75, and e) SF( $\text{CaCl}_2$ )/PVA 0:100.

#### 4.3.2.5 Thermal Stability

Figure 4.19 shows the thermal stability of SF(CaCl<sub>2</sub>)/PVA nanofibrous scaffold at various ratios. The TGA thermogram of all electrospun nanofiber showed the first step of weight loss around 50-180°C caused by the evaporation of water molecules in fiber about 4%. Thermograms of SF(CaCl<sub>2</sub>)/PVA 100:0 and SF(CaCl<sub>2</sub>)/PVA of 0:100 showed the second step decomposition around 200-360°C and 290-350°C, respectively. Decomposition of SF may be related with the breakdown of side-chain groups of amino acid residues as well as the cleavage of peptide bonds of silk fibroin (Raksa et al., 2020) and degradation of PVA that is an amorphous polymer. The third step after 350°C is the degradation of the crystalline region in PVA. The second degradation step of SF(CaCl<sub>2</sub>)/PVA blended nanofiber around 200-380°C may be attributed to the major composition of the silk protein. The third step showed degradation of polymer chain above 390°C. When SF content was increased, it causes an increase in the thermal stability of the blended nanofiber. Usually, sterilization is an important for scaffold and the suggestion for sterilization in an autoclave use steam heated to 121°C or 134°C. To achieve sterility, a holding time of at least 15 minutes at 121°C or 3 minutes at 134°C is required (Baume et al., 2016). The thermal stability of the prepared SF/PVA nanofiber in this study was therefore suitable with sterilization in an autoclave.

### 4.3.3 Effect of LiBr solvent for extraction silk fibroin on SF/PVA nanofibrous scaffold

#### 4.3.3.1 Morphology of Nanofibers

Nanofiber structure is very important for successful cell attachment and cell proliferation (Gittens et al., 2011 and Xu et al., 2004). FE-SEM images of SF(LiBr)/PVA nanofibers in different ratios demonstrated that the scaffolds consisted of randomly distributed fibers (Figure 4.20(a-e)). Figure 4.20 a shows the results of the 100:0 blended SF/PVA nanofibrous scaffold with a diameter size of 69±32 nm with some bead formation on the nanofibers. Bead formation occurs in electrospun nanofibers when the surface tension in the charged jet is high enough to convert the jet into droplets to reduce surface area (Fong et al., 1999). Nevertheless, on blending between SF and PVA, the nanofiber diameter increased considerably under the same processing conditions, showing uniform nanofibers, random network structure, and fiber without beads. Figure 4.20(b-d) showed the diameters of SF(LiBr)/PVA nanofibrous scaffolds at the ratios of 75:25, 50:50, and 25:75 were 78±33 nm, 82±31 nm, and 95±37 nm, respectively. In Figure 4.20(e), the nanofibers from pure PVA had a smooth surface with a diameter of 429±61 nm while the blended SF(CaCl<sub>2</sub>)/PVA nanofiber in our previous

study, it was shown that a smaller fiber diameter than the SF(LiBr)/PVA nanofiber (Raksa et al., 2021). This may be associated with increasing the solution viscosity with the increase of PVA content and also decreasing the stretching of the electrospun jet, which led to the larger formation of the fibers. These findings are in good agreement with those obtained by Phachamud et al. (2011) reported a higher concentration of PVA in solution affected the viscosity of the solution and resulted in an increase in the fiber diameter. Due to this, the charged jet from a high concentration solution could withstand the coulombic stretching force thus the smooth with larger fibers could be obtained. In addition, the morphology of electrospun nanofiber from FE-SEM shows the conformation of random nanofiber structure that may have a significant effect on the behavior of nanofibrous scaffold in tissue engineering applications, such as cell attachment, cell proliferation, and ECM (collagen and GAG) secretion on SF/PVA hybrid nanofiber (Pillai et al., 2016) and cell attachment of the crosslinked on PVA/SF scaffold (Sayed et al., 2019). Randomly oriented nanofibers have certain physical properties which are similar to the superficial layer of collagen fibers of a meniscus. The porosity, hydrophilicity, and swelling properties can promote cell adhesion and cell proliferation (Lü et al., 2012). Besides, there is an evidence reported higher MSCs viability and growth rate on random nanofibers compared to those on aligned nanofibers (Jahani et al., 2012 and Pandey et al., 2018).

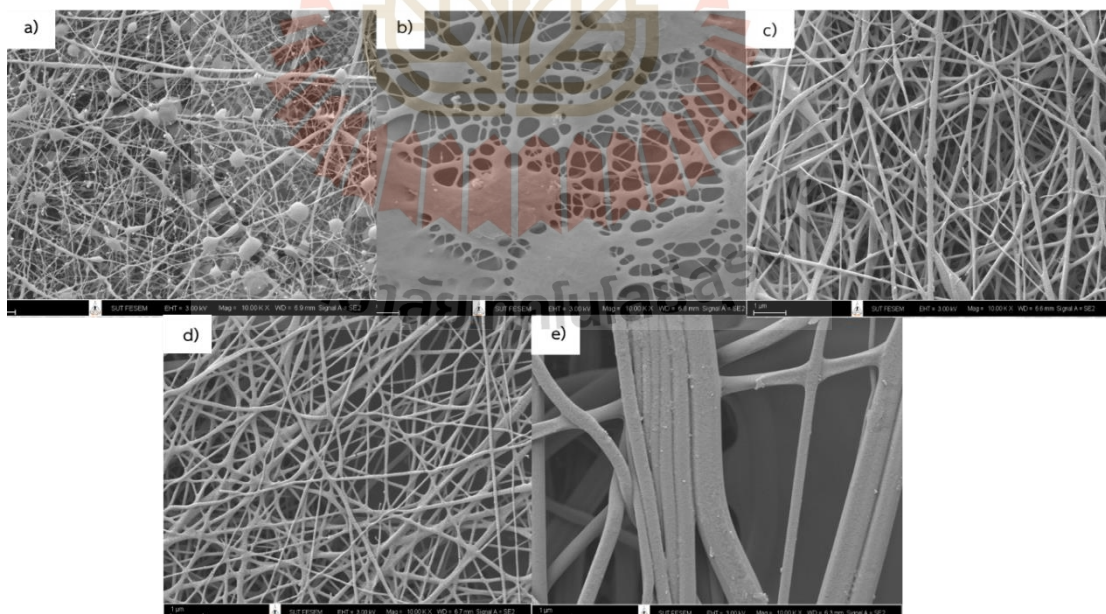


**Figure 4.20** FE-SEM images of SF(LiBr)/PVA nanofiber different ratios at magnification 10000x (a) SF(LiBr)/PVA 100:0, (b) SF(LiBr)/PVA 75:25, (c) SF(LiBr)/PVA 50:50, (d) SF(LiBr)/PVA 25:75, and (e) SF(LiBr)/PVA 0:100.

#### 4.3.3.2 Wettability

The wettability plays an important role in biocompatibility of the scaffolds. It affects cell attachment, cell adhesion, and cell proliferation (Wang et al., 2012). Therefore, the contact angles of SF(LiBr)/PVA nanofibrous scaffold in different ratios were studied to determine the wettability. Figure 4.21 shows the results obtained, the contact angle images, and the contact angle measurements. The blended SF(LiBr)/PVA nanofibrous scaffold of various ratios (100:0, 75:25, 50:50, 25:75, and 0:100) exhibited the water contact angles at  $66\pm 2.8^\circ$ ,  $64\pm 5.1^\circ$ ,  $56\pm 3.0^\circ$ ,  $53\pm 3.7^\circ$ , and  $40\pm 2.3^\circ$ , respectively. The contact angles of the electrospun nanofibrous scaffold increased with an increasing silk fibroin content. This is the result of the hydrophobic group of SF in the blended nanofiber. SF is composed of hydrophobic heavy chains (glycine, alanine, and serine), and SF contributes to a highly crystalline  $\beta$ -sheet structure (Nguyen et al., 2019). The electrospun nanofibrous scaffold from SF(CaCl<sub>2</sub>)/PVA nanofibrous scaffold in our previous study showed the results of contact angles with the value in a range of  $40^\circ$  -  $65^\circ$  which is similar to SF(LiBr)/PVA nanofibrous scaffold. Therefore, both SF/PVA nanofibrous scaffold were suitable for cell attachment and proliferation and have a higher affinity for hydrophilic than the hydrophobic surface. Bhattacharjee et al. (2015) reported that the contact angles suitable for cell attachment and cell proliferation of osteoblast cells (MG-63) on SF/PVA nanofibrous scaffold were approximately  $65^\circ$  to  $67^\circ$ . Hence, the hydrophilicity of the nanofibrous scaffold prepared in our study was suitable for meniscus tissue engineering application.

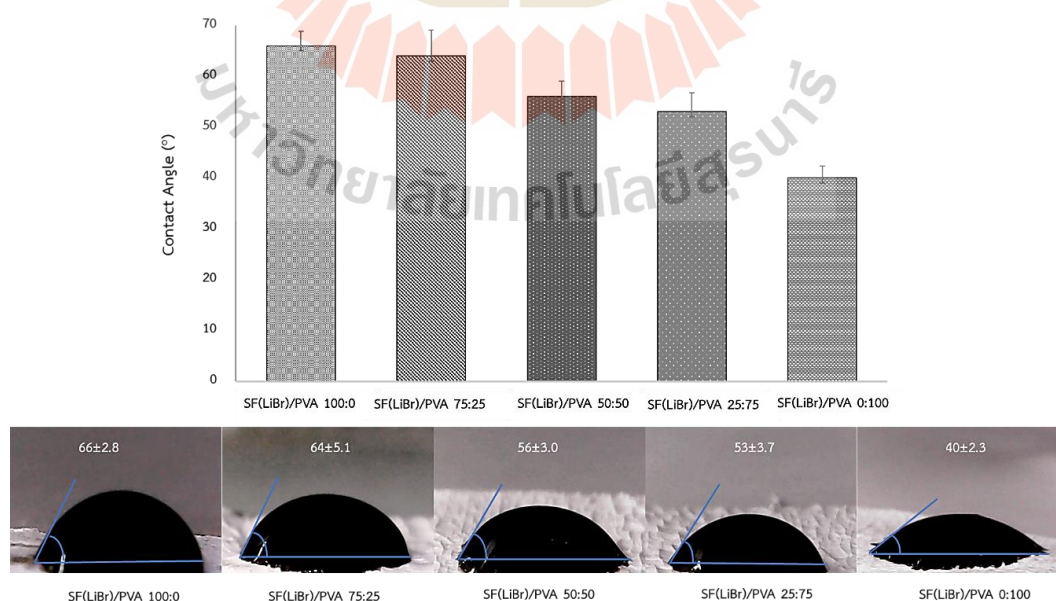


**Figure 4.21** Contact angle of SF(LiBr)/PVA electrospun nanofibrous scaffold different ratio.

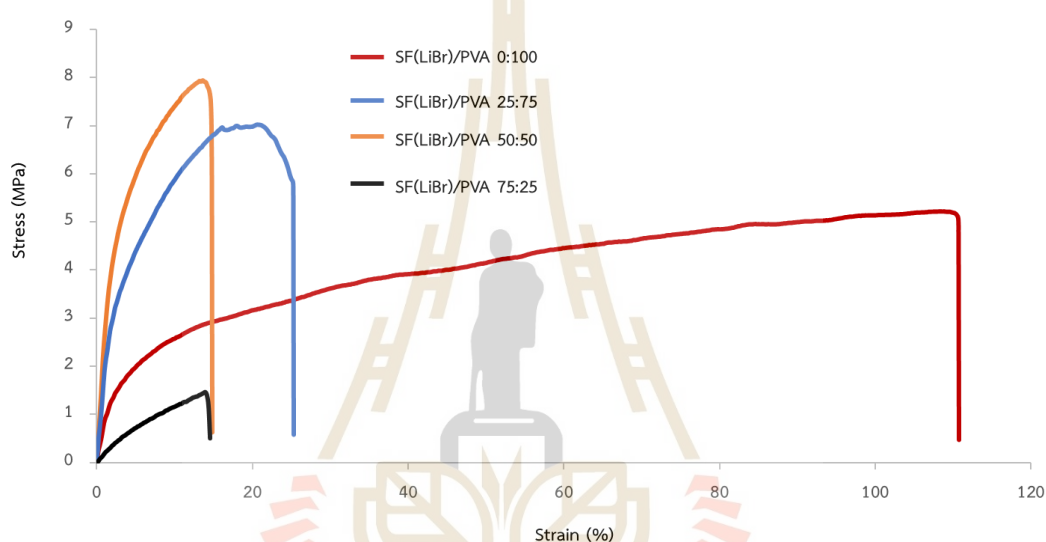
#### 4.3.3.3 Tensile properties

Mechanical properties of nanofibrous scaffold at different ratios are shown in

Table 4.8 and Figure 4.22. The results show that the SF(LiBr)/PVA electrospun nanofibrous scaffold at the ratio of 0:100 exhibited a rather low tensile strength of  $5.21 \pm 4.21$  MPa. Due to the fact that PVA has elastic nature, it showed the highest elongation at break among all nanofibrous scaffolds of  $108.36 \pm 5.03$  MPa. The SF(LiBr)/PVA nanofibrous scaffold of 50:50 showed the highest tensile strength with the value of  $7.93 \pm 2.44$  MPa compared to other electrospun nanofibrous scaffold. The blending with SF improved the tensile property of the electrospun nanofibrous scaffold and the increase of SF led to the creation of inter-fiber bonds which may improve the strength. Nevertheless, the SF(LiBr)/PVA nanofibrous scaffold of 75:25 was unable to fabricate according to inappropriate viscosity. The tensile strength of SF/PVA scaffolds increased by increasing of SF content, could be from  $\beta$ -sheets formation in the structure of SF that enhances the tensile strength of electrospun nanofibers (Altman et al., 2003). Anyway, when increased content of SF beyond 50:50 blended ratio, the tensile strength decreased. From morphological study, beads formation was observed through nanofibrous scaffold which 100:0 and 75:25 SF/PVA blended ratio and caused poor tensile strength. The beads formation in higher SF concentration can be explained by electrical force of electrospinning cannot overcome the gravity force of low viscosity solution therefore solution dropped on the collector and unable to form the fibers (Mohammad Ali Zadeh et al., 2014). The mechanical properties and structural absoluteness of the nanofibrous scaffold were significant parameters for the meniscus tissue engineering application. The load-bearing capacity of biological tissues is a consequence of geometry, deformation, and movement properties; the meniscus is an important load-bearing structure that minimizes contact stress by generating hoop stresses, hence minimizing contact area (Fukubayashi et al., 1980; Lee et al., 2006). As a result, the form of the meniscus is particularly crucial for loading. The mechanical strength of nanofibrous scaffolds is determined by their tension resistance in order to maintain scaffold integrity during implantation (Tran et al., 2018). Previous research reported a wide range for the meniscal circumferential ultimate tensile strength between  $\sim 3$  to 60 MPa (Bullough et al., 1970; Abdelgaied et al., 2015; Tissakht et al., 1995) which depends on the area of the meniscus. For our purpose of meniscus tissue engineering, as a biological augmentation with suture repair, the tensile strength of our SF/PVA (50:50) scaffold is acceptable.

**Table 4.8** Tensile properties of SF(LiBr)/PVA nanofiber various ratio.

Composition	Ultimate tensile strength (MPa)	Elongation at Break (%)
SF(LiBr)/PVA 100:0	-	-
SF(LiBr)/PVA 75:25	1.46±6.1	13.92±6.1
SF(LiBr)/PVA 50:50	7.93±2.4	13.66±8.6
SF(LiBr)/PVA 25:75	7.02±1.8	20.54±4.4
SF(LiBr)/PVA 0:100	4.97±0.8	112.57±4.8

**Figure 4.22** Stress-strain curve of SF(LiBr)/PVA nanofiber.

#### 4.3.3.4 FTIR spectroscopy

FTIR spectroscopy was used to assess the chemical groups of the polymers. Figure 4.23 shows the FTIR spectra of SF(LiBr)/PVA nanofibrous scaffold at different ratios. The nanofiber of SF(LiBr)/PVA (0:100) showed a spectrum at  $3300\text{--}3200\text{ cm}^{-1}$  associated with the O–H stretching from the intermolecular and intramolecular hydrogen bonds. The vibrational band observed between  $3000\text{--}2800\text{ cm}^{-1}$  was the result of the C–H stretching from alkyl groups. The peaks between  $1720\text{ cm}^{-1}$  and  $1625\text{ cm}^{-1}$  were due to the C=O and C–O stretching from the remaining acetate groups in PVA. The peaks were at  $1470\text{--}1450\text{ cm}^{-1}$ ,  $1260\text{--}1240\text{ cm}^{-1}$ , and  $1100\text{--}1080\text{ cm}^{-1}$  from CH–OH bending, C–O stretching, and C–O out-of-plane bending, respectively (Alhosseini et al., 2012 and Bhattacharjee et al., 2015). The SF(LiBr)/PVA nanofibrous scaffold of ratio 100:0 showed three characteristic vibrational bands at  $1625\text{--}1620\text{ cm}^{-1}$  (amide I, secondary NH bending),  $1510\text{--}1500\text{ cm}^{-1}$  (amide II, C=O stretching), and  $1235\text{--}1230\text{ cm}^{-1}$  (amide III). The characteristic peaks of SF(LiBr) and PVA were observed

in all blended nanofibrous scaffolds (75:25, 50:50, and 25:75), which confirm the presence of both SF(LiBr) and PVA. The major peaks in the wave number ranges of 1630-1620  $\text{cm}^{-1}$  and 1515-1500  $\text{cm}^{-1}$  in all blends of nanofiber confirmed the structure of  $\beta$ -sheet in the SF. However, the position of the amide I, amide II, and amide III bands shifted after blending with PVA. In addition, the width of the O-H region in the range of 3300–3200  $\text{cm}^{-1}$  was expanded by blending SF and PVA, which can characterize as the increase in the intensity of hydrogen bonding. The FTIR spectral width of OH region at 3500–3200  $\text{cm}^{-1}$  was extended after blending SF with PVA, and increased the intensity of hydrogen bonding. This confirmed the interaction between SF and PVA molecules (Niu et al., 2019). Moreover, the broad peaks at 3300-3100  $\text{cm}^{-1}$  referred to the combination of -OH and -NH formation groups which overlapped between two groups, hydroxyls (-OH) of PVA and amino (-NH) of SF (Ali et al., 2017). Therefore, our results revealed chemical interactions between the amino group of SF and hydroxyl group of PVA. This finding corresponds with previous work that demonstrated SF( $\text{CaCl}_2$ )/PVA nanofibrous scaffold had main characteristic peaks of SF containing confirmation of  $\beta$ -sheet structure: amide I, amide II, and amide III. PVA showed major vibration peaks of O-H, C-H, C=O, and C-O. In addition, the blended nanofibrous scaffold showed the chemical interactions between the hydroxyl group of PVA and the amino group of SF. However, the FTIR peak shift may not be from only such interactions, but it may come from the loss of water from the surface of silk fibroin due to the PVA. The presence of -OH (hydroxyl groups) in PVA causes water adsorption on the SF surface, resulting in the formation of hydrogen bonds between -OH group of PVA and -OH group of water on SF, which leads to the broad peak and shifts to a lower number at  $\sim 3260 \text{ cm}^{-1}$  (Wang et al., 2010). Based on these findings, both SF/PVA nanofibrous scaffolds revealed that when two polymers are blended, physical blends and chemical interactions alter the characteristic peaks of the spectra. These observations demonstrate that PVA and SF are highly miscible. The formation of intermolecular hydrogen bonds between the -OH and -NH groups in SF and the -OH groups in PVA is the most likely explanation.

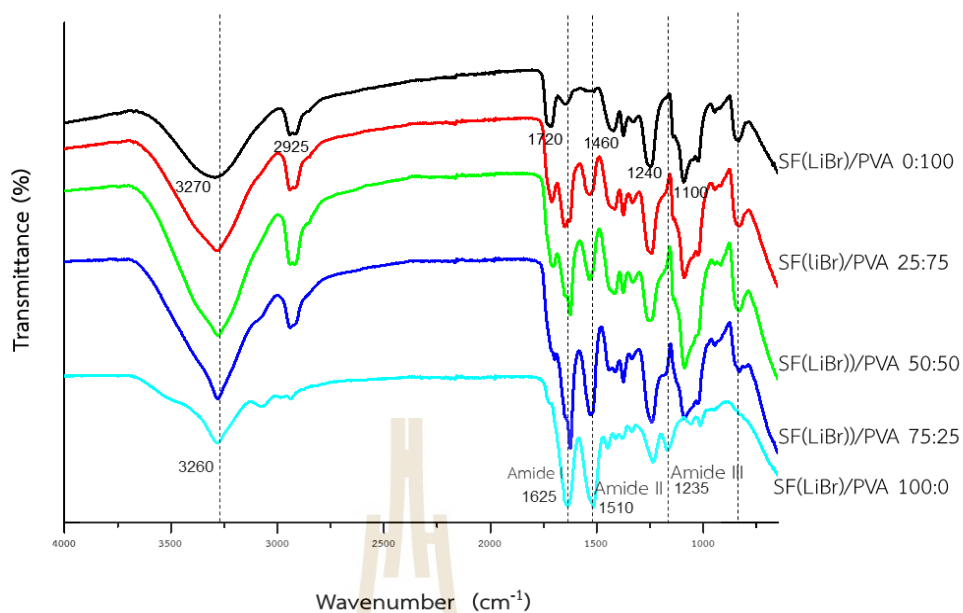


**Figure 4.23** FTIR spectra of SF(LiBr)/PVA nanofiber various ratio.

#### 4.3.3.5 Thermogravimetric analysis

Thermograms from TGA curve for electrospun nanofibrous scaffold were presented in Figure 4.24 SF(LiBr)/PVA nanofibrous scaffold exhibited three decomposition steps. The initial decomposition, due to the loss of water and solvent from the nanofibrous scaffold occurred at 70–150°C with a weight loss of 5%. The second step around 230–370°C is the decomposition of polymer chains, which leads to a major weight loss of about 70%. This was due to the structural degradation followed by fractures of polymer chains in PVA, which is an amorphous polymer and SF with the breakdown of the side-chain group of amino acid remains including the break of peptide bond of SF (Mohd Yusoff et al., 2019). The final step of decomposition occurred above 370°C. This was due to the breakdown of C-C bonds in the polymer backbone, and this is the degradation of the crystalline region in PVA. While the decrease in weight loss and the increase in thermal stability is attributed to the higher thermal stability of silk fibroin. The interaction between SF and PVA played an important role in lowering the rate of degradation of polymer (Sheik et al., 2020). This is similar to data obtained from previous work on SF(CaCl<sub>2</sub>)/PVA nanofibrous scaffold. Therefore, the blending of SF and PVA made the SF/PVA nanofibrous scaffolds possess characteristics of both materials, and all scaffolds were thermally stable during sterilization temperature range (121–134°C). Moreover, SF/PVA nanofibrous scaffold showed a residue amount of less than 30% at 700°C and tended to continue losing mass at higher temperatures. Consequently, it is possible to find a fewer amount of

ash after burning at higher temperatures (1000°C) in high pressure system (Kuchaiyaphum et al., 2020). Normally, sterilization played an important role in scaffold tissue engineering. The heat treatments for sterilization are effective, rapid, easy, and without toxic residues (Dai et al., 2016) whereas sterilization in an autoclave uses steam heat at about 121°C for 15 minutes or 134°C for 3 minutes (Baume et al., 2016). Therefore, the electrospun nanofibers fabricated in this work is suitable for sterilization in steam treatment.

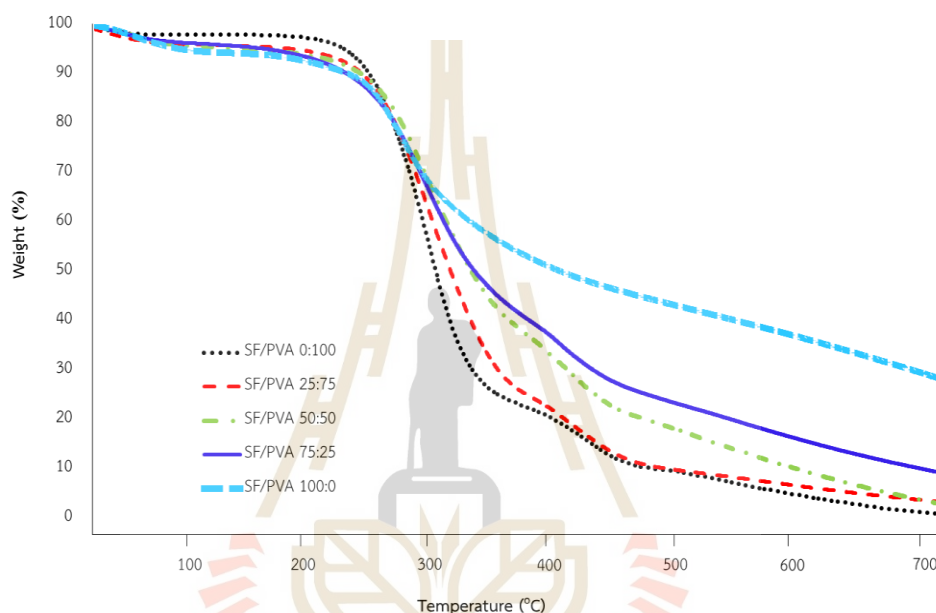


Figure 4.24 TGA thermogram of SF(LiBr)/PVA nanofiber various ratio.

#### 4.4 The development of electrospun SF/PVA for biomimetic scaffold for potential meniscus tissue engineering application

##### 4.4.1 In vitro cell viability and toxicity of SF(CaCl<sub>2</sub>)/PVA nanofibrous scaffold

The cytotoxicity was determined by MTT assay which test on the SF(CaCl<sub>2</sub>)/PVA nanofibrous scaffolds various ratios. As shown in Figure 4.25, it is obvious that of all ratios the nanofibrous scaffolds were non-toxic, supported cell growth, and showed an increase in cell viability with 7 days compared with control. These results followed by international organization for standardization, ISO 10993-5:2009 biological indicated that a decrease of cell viability by 30%, the material is to be considered toxic and hence not biocompatible. This increase in viability is attributed to the initial time taken by cells to adapt to the nature of the nanofibrous scaffold followed by the increase in cellular proliferation (Gopinathan et al., 2017 and Gopinathan et al., 2015). While

the various blended nanofibrous scaffolds prepared of the ratio 50:50 SF(CaCl<sub>2</sub>)/PVA showed the highest viability (115.6±2% at day 7) and ratio of 0:100 SF(CaCl<sub>2</sub>)/PVA showed the lowest viability (49.6±0.3% at day 7). Typically, non-cytotoxicity is defined as a percentage of cell viability greater than 70%. And according to our research, the SF/PVA (50:50) nanofibrous scaffold exhibited no cytotoxicity towards HCPCs. We have therefore selected SF(CaCl<sub>2</sub>)/PVA (50:50) scaffolds for the next phase of gene expression analysis.

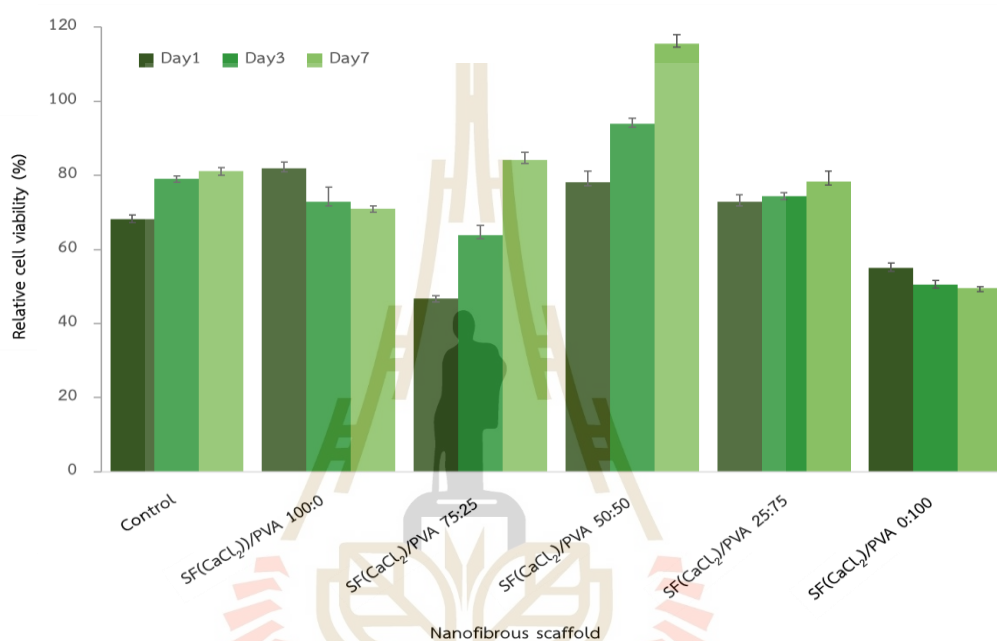


**Figure 4.25** Relative cell viability of SF(CaCl<sub>2</sub>)/PVA nanofibrous scaffold.

#### 4.4.2 Gene expression of SF(CaCl<sub>2</sub>)/PVA nanofibrous scaffold

The qRT-PCR analysis showed that the expression levels of human chondrogenic progenitor cells (HCPCs) were examined to showed cellular phenotype on SF(CaCl<sub>2</sub>)/PVA nanofibrous scaffold of ratio 50:50. Expressions of genes involved in chondrocyte cells, including a collagen type (COL1A1), collagen type II (COL2A1), and aggrecan were analyzed on days 7, 14, and 28 using real-time RT-PCR. The results were shown in Figure 4.26, these studies showed a significant increase in the expression of levels of type COL1A1 and COL2A1 on SF(CaCl<sub>2</sub>)/PVA nanofibrous scaffold on days 14 and 28 was higher than the cell without a scaffold. The expressions of COL1A1 was increased highest in day 28 (9.65±0.3) and the COL2A1 was increased highest in day 14 (2.82±0.7) which slightly higher than day 28 (2.00±0). The expression of ACAN was observed highest on day 7 (8.43±0) while on days 14 (0.00±0) and 28 (0.50±0) was decreased compare with cell without scaffold. The meniscus is composed of a

fibrocartilaginous tissue that displays variations in the distribution of ECM molecules particularly collagens type I and II, aggrecan, and GAGs (Makris et al., 2011; Murphy et al., 2019). The increased expression levels of COL2A1 and ACAN genes in SF(CaCl<sub>2</sub>)/PVA scaffold suggested that a nanofiber might good maintain phenotype of chondrocytes. The expression levels of COL1A1 gene in SF(CaCl<sub>2</sub>)/PVA scaffold is related with dedifferentiation of chondrocytes and osteogenesis. The increased COL1A1 gene expression also suggested that nanofibrous scaffold would benefit to keep the phenotype of seeded chondrocytes.

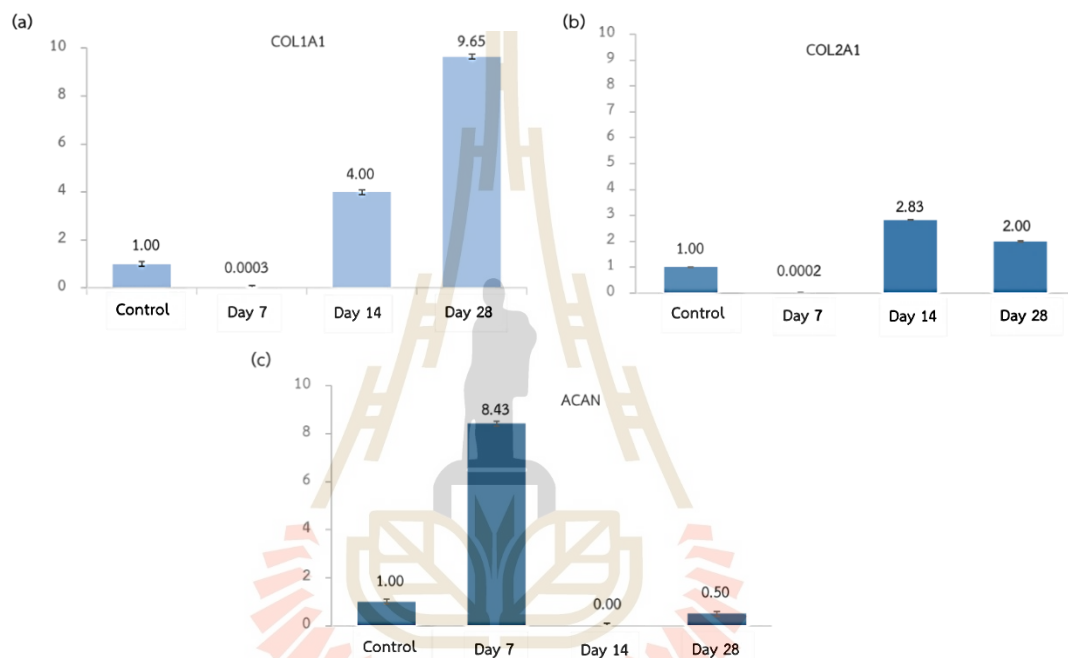


**Figure 4.26** The gene expression of COL1A1, COL2A1, and aggrecan at days 7, 14, and 28 were demonstrated in (a, b, and c), respectively.

#### 4.4.3 In vitro cell viability and toxicity of SF(LiBr)/PVA nanofibrous scaffold

The relative cell viability of HCPCs seeded SF/PVA nanofibrous scaffold in various SF/PVA ratios is demonstrated in Figure 4.27. Generally, SF(CaCl<sub>2</sub>)/PVA scaffolds had higher cell viability compared to SF(LiBr)/PVA nanofibrous scaffolds. The viability of cells on pure SF and PVA scaffolds from both extraction methods declined over time. Compared to the control groups, pure PVA had lower cell viability in every time point viability, 67.80±0.62% of pure SF(LiBr) and 71.00±0.68% of pure SF(CaCl<sub>2</sub>) on day 7 and 44.88±0.83% and 49.64±0.29% of pure PVA on day 7, while SF(LiBr)/PVA scaffold at other ratios enhanced. For 75:25 SF(LiBr)/PVA scaffold, the viability slightly increased from day 1 =71.63±1.42%, day 3=73.65±1.30%, and day 7=75.84±1.40% when SF(CaCl<sub>2</sub>)/PVA nanofibrous scaffold showed that the percentage of cell viability slightly

increased. SF/PVA scaffold of different SF extraction methods at the ratio of 50:50 showed the highest cell viability at an all-time point. On day 7, the value of relative cell viability (%) was  $110.20 \pm 0.54$  (SF(LiBr)/PVA scaffold) and  $115.59 \pm 2.31$  (SF(CaCl<sub>2</sub>)/PVA scaffold). The 25:75 SF(LiBr)/PVA scaffold had the lowest cell viability on day 1 ( $43.43 \pm 0.99\%$ ) and increased on day 3 and day 7 ( $60.15 \pm 0.70\%$ , and  $80.73 \pm 0.92\%$ ), while the 25:75 SF(CaCl<sub>2</sub>)/PVA scaffold showed that the percentage of cell viability increased every time point. Based on these results, LiBr and CaCl<sub>2</sub> solvents on SF extraction when SF was fabricated into a nanofibrous scaffold revealed no cytotoxicity to the cells, and cell viability on both scaffolds after day 7 was more significant than 100%. This finding shows that both nanofibrous scaffolds are biocompatible and non-toxic. Although silk fibroin is a natural polymer that has biocompatibility, the polymer droplets over nanofibers might affect cell adhesion and cell proliferation processes. On the other hand, PVA at higher concentration could interfere cellular environment. For this reason, the appropriate ratio for SF/PVA nanofibrous scaffold according to cell viability is 50:50 (Janarthanan et al., 2019). Generally, percentage of cell viability greater than 70% is considered as non-cytotoxicity (Jiang et al., 2010; Pillai et al., 2016). And from our study, SF/PVA (50:50) nanofibrous scaffold had no cytotoxicity to the HCPCs. Hence, we have chosen SF(LiBr)/PVA (50:50) and SF(CaCl<sub>2</sub>)/PVA (50:50) scaffolds to progress to the next stage of gene expression analysis.

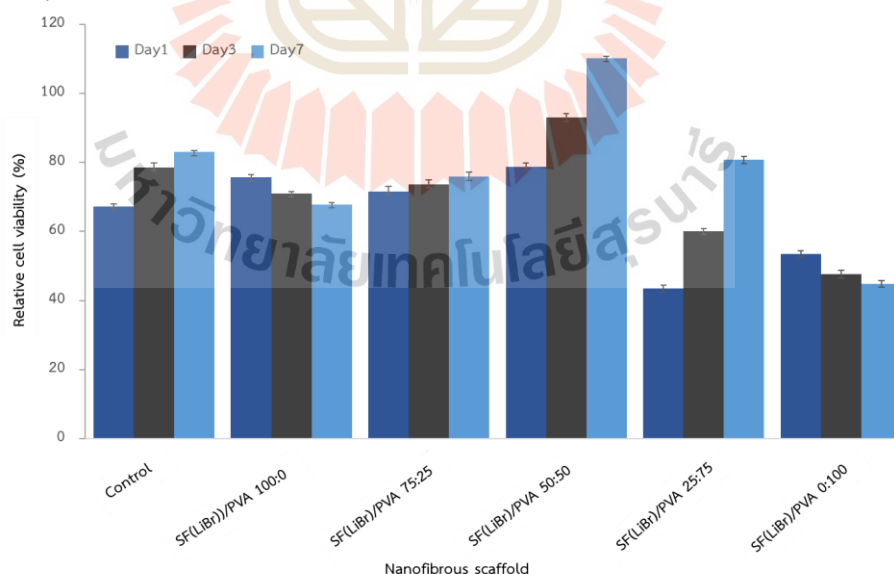


**Figure 4.27** Cell viability of SF(LiBr)/PVA nanofiber various ratio.

#### 4.4.4 Gene expression of SF(LiBr)/PVA nanofibrous scaffold

According to the result on morphological study, tensile strength, and cell viability test, a 50:50 SF(LiBr)/PVA nanofibrous scaffold was carried out on for gene expression analysis. Since collagen I, collagen II, and aggrecan are the major components of the meniscus extracellular matrix, the expression of COL1A1, COL2A1, and ACAN genes were studied. From Figure 4.28, COL1A1 expression slowly increased from  $18.77 \pm 0.014$  on day 7,  $60.97 \pm 0.057$  on day 14, and  $97.68 \pm 0.23$  on day 28. The expression of COL2A1 on day 7 showed  $1.41 \pm 0$  and a slightly increase on day 14 as well as day 28. ACAN showed the highest expression,  $76.90 \pm 0.05$  on day 7 and absent on day 14. This result corresponded to the study by Yang et al. (2014) which reported raising of collagen I gene expression after 21 days of cell seeded nanofibrous scaffold cultured. When compared with SF(CaCl<sub>2</sub>)/PVA (50:50) scaffold, it was found that gene expression of COL1A1 had a lowest of  $0.0003 \pm 0$  on day 7 and increased from day 14 to day 28 ( $4.00 \pm 0$  to  $9.65 \pm 0.30$ ). For COL2A1, it showed  $0.00019 \pm 0$  on day 7 and slight increase on day 14. ACAN was found to have highest expression on day 7 ( $8.43 \pm 0.007$ ), and after that the expression was not observed on day 14. This finding could be from the dedifferentiation of HCPCs. Since our ultimate goal is to apply in clinical practice and growth factors are not allowed to use in human, simple expanded chondrocyte culture medium was used in our study. ACAN is more specific to chondrocytes compared to COL1A1 and COL2A1, without chondrogenic growth factors, dedifferentiation could be found in later passages of the cell culture (Freyman et al., 2012 and Kaps et al., 2006). Anyway, in application of meniscus tissue engineering, the middle and outer zones of the meniscus mostly bear tensile force, which requires collagen I and collagen II for its function. According to the previous research reported, SF was blended into a nanofibrous scaffold, which is expected to facilitate the attachment of cells because SF is dominated by glycine. Glycine is the main amino acid in collagen, which is the main structural protein of connective tissue, such as skin, bone, tendons, meniscus, and cartilage (Giovanni et al., 2019). When SF was blended with PVA and fabricated into a nanofibrous scaffold, it revealed collagen I and collagen II. Therefore, the collagen present in the nanofibrous scaffold gives mechanical strength to the membrane and also helps to mimic the natural ECM of the meniscus, thereby enhancing cell adhesion and proliferation (Pillai et al., 2015; Nanda et al., 2014; Numpaisal et al., 2022).

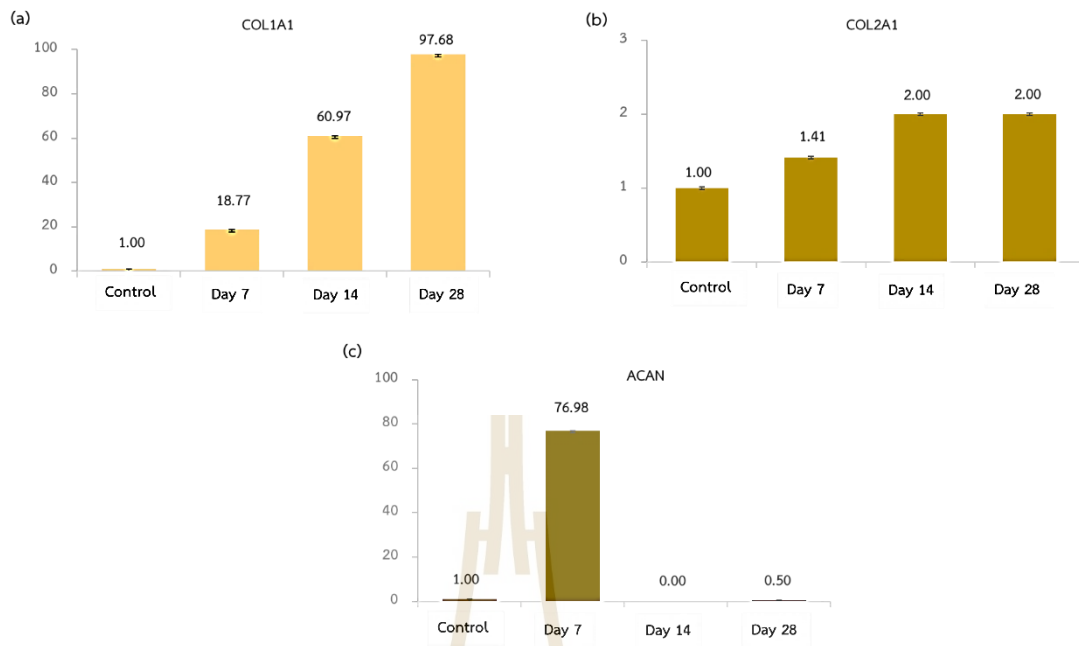
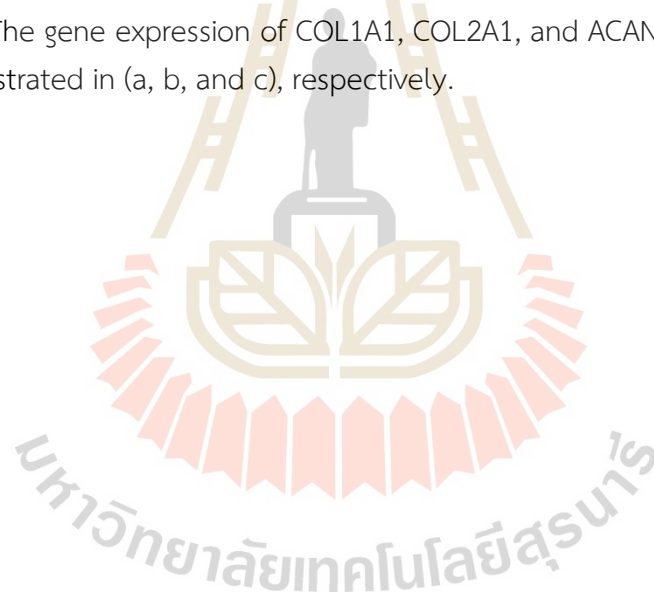


**Figure 4.28** The gene expression of COL1A1, COL2A1, and ACAN at days 7, 14, and 28 were demonstrated in (a, b, and c), respectively.



## CHAPTER V

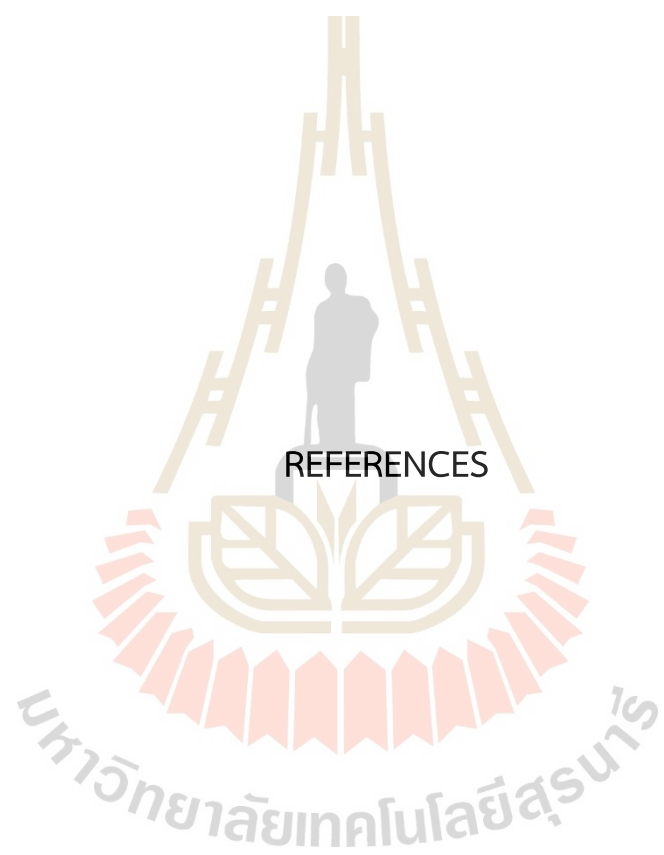
### CONCLUSION AND RECOMMENDATION

In conclusion, this thesis introduces a pioneering methodology in tissue engineering, centered on the development of nanofibrous scaffolds tailored to address meniscus injuries and degeneration. Through a study of the electrospinning fabrication process, a distinctive combination of silk fibroin (SF) and poly(vinylalcohol) (PVA) was utilized. The extraction of SF was meticulously conducted using both  $\text{CaCl}_2$  and LiBr solvents, with LiBr-extracted SF exhibiting commendable yields. The research provided valuable insights into the %crystallinity and molecular weight, confirming the presence of key structural elements, including  $\beta$ -sheet crystalline, random coil, and  $\alpha$ -helix structures, as corroborated by XRD patterns and FTIR spectra. Additionally, the investigations into electrospinning parameters revealed the optimal conditions to be 10% w/v PVA, a relative humidity of 50%, and a high voltage of 20 kV. This optimization resulted in the attainment of desirable average fiber diameter and tensile properties within the electrospun scaffold. Experiments involving various blends of SF( $\text{CaCl}_2$ )/PVA and SF(LiBr)/PVA at varying ratios illuminated the significant enhancements attributed to SF incorporation. This augmentation led to improvements in surface wettability, thermal attributes, tensile strength, and elongation at break, while concurrently diminishing viscosity and average fiber diameter. It was discerned that SF extraction methods, whether employing  $\text{CaCl}_2$  or LiBr solvents, yield subtly differing material characteristics. Biocompatibility assessment involving SF/PVA nanofibrous scaffolds culminated in the identification of the electrospun SF(LiBr)/PVA 50:50 scaffold as the prime candidate for meniscus tissue engineering. This scaffold not only fostered heightened cell viability and exhibited non-toxic traits but also notably facilitated chondrogenic gene expression, notably collagen types I and aggrecan, thus surpassing the capabilities of the SF( $\text{CaCl}_2$ )/PVA scaffold.

Recommendation, In light of these compelling findings, it is recommended that further steps be taken to advance the utilization of the successfully fabricated electrospun nanofibrous scaffold of SF(LiBr)/PVA (50:50). Conducting comprehensive tests through explant models, as well as subsequent validation via animal models, would provide crucial insights into its functional efficacy and safety. Furthermore, the potential for clinical applications merits exploration through rigorous clinical studies.

These efforts should encompass a comprehensive assessment of the scaffold's performance, including its interaction with human tissues and the subsequent implications for meniscus tissue engineering. Given its promising attributes, the SF(LiBr)/PVA (50:50) nanofibrous scaffold presents a compelling avenue for scaffold-augmented sutures, offering a biomimetic solution to meniscus regeneration. By continually refining and expanding upon the knowledge gained from this research, the field of tissue engineering can significantly benefit from this innovative approach, ultimately contributing to enhanced therapeutic interventions and improved patient outcomes.





REFERENCES

## REFERENCES

- Abdel-Fattah, W. I., Atwa, N., and Ali, G. W. (2015). Influence of the protocol of fibroin extraction on the antibiotic activities of the constructed composites. *Progress in Biomaterials*, 4(2-4), 77-88.
- Abdelgaied, A., Stanley, M., Galfe, M., Berry, H., Ingham, E., and Fisher, J. (2015). Comparison of the biomechanical tensile and compressive properties of decellularized and natural porcine meniscus. *Journal of Biomechanics*, 48(8), 1389-1396.
- Abrams, G. D., Frank, R. M., Gupta, A. K., Harris, J. D., McCormick, F. M., and Cole, B. J. (2013). Trends in meniscus repair and meniscectomy in the United States, 2005-2011. *The American Journal of Sports Medicine*, 41(10), 2333-2339.
- Adeli, H., Khorasani, M. T., and Parvazinia, M. (2019). Wound dressing based on electrospun PVA/chitosan/starch nanofibrous mats: Fabrication, antibacterial and cytocompatibility evaluation and in vitro healing assay. *International Journal of Biological Macromolecules*, 122, 238-254.
- Agarwal, S., Wendorff, J. H., and Greiner, A. (2008). Use of electrospinning technique for biomedical applications. *Polymer*, 49, 5603-5621.
- Allardyce, B. J., Rajkhowa, R., Dilley, R. J., Atlas, M. D., Kaur, J., and Wang, X. (2015). The impact of degumming conditions on the properties of silk films for biomedical applications. *Textile Research Journal*, 86(3), 275-287.
- Altman, G. H., Diaz, F., Jakuba, C., Calabro, T., Horan, R. L., Chen, J., Lu, H., Richmond, J., and Kaplan, D. L. (2003). Silk-based biomaterials. *Biomaterials*, 24, 401-416.
- Andiappan, M., Sundaramoorthy, S., Panda, N., Meiyazhaban, G., Winfred, S. B., Venkataraman, G., and Krishna, P. (2013). Electrospun eri silk fibroin scaffold coated with hydroxyapatite for bone tissue engineering applications. *Progress in Biomaterials*, 2(6), 1-11.
- Annabi, N., Nichol, J. W., Zhong X., Ji, C., Koshy, S., Khademhossein, A., and Dehghani, F. (2010). Controlling the porosity and microarchitecture of hydrogels for tissue engineering, *Tissue Engineering Part B, Reviews*, 16(4):371-83.
- Aral, H., and Vecchio-Sadus, A. (2008). Toxicity of lithium to humans and the environment—A literature review. *Ecotoxicology and Environmental Safety*, 70(3), 349-356.

- Aramwit, P. (2014). Bio-response to silk sericin. *In Silk Biomaterials for Tissue Engineering and Regenerative Medicine*, 299-329.
- Aramwit, P., and Sangcakul, A. (2007). The effects of sericin cream on wound healing in rats. *Biosci Biotechnol Biochem*, 71(10), 2473-2477.
- Arnoczky, S. P., and Warren, R. F. (1983). The microvasculature of the meniscus and its response to injury. An experimental study in the dog: An experimental study in the dog. *The American Journal of Sports Medicine*, 11(3), 131-141.
- Aznar-Cervantes, S. D., Vicente-Cervantes, D., Meseguer-Olmo, L., Cenis, J. L., and Lozano-Pérez, A. A. (2013). Influence of the protocol used for fibroin extraction on the mechanical properties and fiber sizes of electrospun silk mats. *Materials Science and Engineering: C*, 33(4), 1945-1950.
- Badami, A. S., Kreke, M. R., Thompson, M. S., Riffle, J. S., and Goldstein, A. S. (2006). Effect of fiber diameter on spreading, proliferation, and differentiation of osteoblastic cells on electrospun poly(lactic acid) substrates. *Biomaterials*, 27(4), 596-606.
- Baek, J., Chen, X., Sovani, S., Jin, S., Grogan, S. P., and D'Lima, D. D. (2015). Meniscus tissue engineering using a novel combination of electrospun scaffolds and human meniscus cells embedded within an extracellular matrix hydrogel. *Journal of Orthopaedic Research*, 33(4), 572-583.
- Baker, B. E., Peckham, A. C., Puppato, F., and Sanborn, J. C. (1985). Review of meniscal injury and associated sports, *Am J Sports Med*, 13, 1-4.
- Baker, B. M., Gee, A. O., Metter, R. B., Nathan, A. S., Marklein, R. A., Burdick, J. A., and Mauck, R. L. (2008). The potential to improve cell infiltration in composite fiber-aligned electrospun scaffolds by the selective removal of sacrificial fibers. *Biomaterials*, 29(15), 2348-2358.
- Baum, E., Deutsch, H., and Herrmann, W. O. (1924). Esters of vinyl alcohol. *DE Patents*, 483, 780.
- Baume, A. S., Boughton, P. C., Coleman, N. V., and Ruys, A. J. (2016). Sterilization of tissue scaffolds, *Characterization and Design of Tissue Scaffolds*, 225-244.
- Bawazeer, T. M., and Alsoufi, M. S. (2017). SURFACE CHARACTERIZATION AND PROPERTIES OF RAW AND DEGUMMED (BOMBYX MORI) SILK FIBROIN FIBER TOWARD HIGH PERFORMANCE APPLICATIONS OF "KISSWA AL-KABBA". *International Journal of Current Research*, 9(03), 48335-48343.
- Beachley, V., and Wen, X. (2009). Effect of electrospinning parameters on the nanofiber diameter and length. *Materials Science and Engineering: C*, 29(3), 663-668.

- Bhattacharjee, P., Kundu, B., Naskar, D., Maiti, T. K., Bhattacharya, D., and Kundu, S. C. (2015). Nanofibrous nonmulberry silk/PVA scaffold for osteoinduction and osseointegration. *Biopolymers*, *103*(5), 271–284.
- Briscoe, B., Luckham, P., and Zhu, S. (2000). The effects of hydrogen bonding upon the viscosity of aqueous poly(vinyl alcohol) solutions. *Polymer*, *41*(10), 3851–3860.
- Buchko, C. J., Chen, L. C., Shen, Y., and Martin, D. C. (1999). Processing and microstructural characterization of porous biocompatible protein polymer thin films. *Polymer*, *40*(26), 7397–7407.
- Bullough, P. G., Munuera, L., Murphy, J., and Weinstein, A. M. (1970). The strength of the menisci of the knee as it relates to their fine structure. *The Journal of Bone and Joint Surgery. British volume*, *52-B*(3), 564–570.
- Buma, P., Ramrattan, N., van Tienen, T., and Veth, R. (2004). Tissue engineering of the meniscus. *Biomaterials*, *25*(9), 1523–1532.
- Bursac, P., Arnoczky, S., and York, A. (2009). Dynamic compressive behavior of human meniscus correlates with its extra-cellular matrix composition. *Biorheology*, *46*(3), 227–237.
- Callone, E., Dire, S., Hu, X., and Motta, A. (2016). Processing Influence on Molecular Assembling and Structural Conformations in Silk Fibroin: Elucidation by Solid-State NMR. *ACS Biomater Sci Eng*, *2*(5), 758–767.
- Campbell, S. E., Sanders, T. G., and Morrison, W. B. (2001). MR Imaging of Meniscal Cysts. *American Journal of Roentgenology*, *177*(2), 409–413.
- Cao, T. T., Wang, Y. J., and Zhang, Y. Q. (2013). Silk reeling of silkworm cocoon in strongly alkaline electrolyzed water as a sericin swelling agent at low temperature. *The Journal of The Textile Institute*, *105*(5), 502–508.
- Caroline R. Uff, Adam D. Scott, Pockley, A. G., and Phillips, a. R. K. S. (1995). Influence of soluble suture factors on in vitro macrophage function. *Biomaterials*, *16*, 355–360.
- Casper, C. L., Stephens, J. S., Tassi, N. G., Chase, D. B., and Rabolt, J. F. (2004). Controlling surface morphology of electrospun polystyrene fibers: Effect of humidity and molecular weight in the electrospinning process. *Macromolecules*, *37*(2), 573–578.
- Chambers, M. C., and El-Amin III, S. F. (2015). Tissue engineering of the meniscus: scaffolds for meniscus repair and replacement. *Musculoskeletal Regeneration*, *2*, 1–9.

- Chan, B. P., and Leong, K. W. (2008). Scaffolding in tissue engineering: general approaches and tissue-specific considerations. *European Spine Journal*, 17(S4), 467–479.
- Chang, A., Moio, K., Chmiel, J.S., Eckstein, F., Guermazi, A., Almagor, O., Cahue, S., Wirth, W., Prasad, P., and Sharma, L. (2011). Subregional effects of meniscal tears on cartilage loss over 2 years in knee osteoarthritis. *Annals of the Rheumatic Disease*, 70(1): 74–79.
- Chen, M., Gao, S., Wang, P., Li, Yan., Guo, W., Zhang, Y., Wang, M., Xiao, T., Zhang, Z., Zhang, X., Jing, X., Li, X., Liu, S., Guo, Q., and Xi, T. (2018). The application of electrospinning used in meniscus tissue engineering. *Journal of Biomaterials Science, Polymer Edition*, 29(5), 461-475.
- Chen, X., Knight, D. P., Shao, Z., and Vollrath, F. (2001). Regenerated Bombyx silk solutions studied with rheometry and FTIR. *Polymer*, 42, 9969-9974.
- Chen, X., Shao, Z., Knight, D. P., and Vollrath, F. (2007). Conformation transition kinetics of Bombyx mori silk protein. *Proteins*, 68(1), 223-231.
- Chen, X., Yin, Z., Chen, J., Liu, H., Shen, W., Fang, Z., and Zou, X. (2014). scleraxis-overexpressed human embryonic stem cell-derived Mesenchymal stem cells for tendon tissue engineering with knitted silk-collagen scaffold. *Tissue Engineering Part A*, 20(11-12), 1583-1592.
- Cheng, G., Wang, X., Tao, S., Xia, J., and Xu, S. (2015). Differences in regenerated silk fibroin prepared with different solvent systems: From structures to conformational changes. *Journal of Applied Polymer Science*, 132(22), 1-9.
- Chiari, C., Koller, U., Dorotka, R., Eder, C., Plasenzotti, R., Lang, S., Ambrosio, L., Tognana, E., Kon, E., Salter, D., and Nehrer, S. (2006). A tissue engineering approach to meniscus regeneration in a sheep model. *Osteoarthritis and Cartilage*, 14(10), 1056–1065.
- Chirila, T. V., Suzuki, S., Bray, L. J., and Barnett, N. L., and Harkin, D. G. (2013). Evaluation of silk sericin as a biomaterial: in vitro growth of human corneal limbal epithelial cells on Bombyx mori sericin membranes. *Progress in Biomaterials*, 2(14), 1-10.
- Cho, H. J., Ki, C. S., Oh, H., Lee, K. H., and Um, I. C. (2012). Molecular weight distribution and solution properties of silk fibroins with different dissolution conditions. *International Journal of Biological Macromolecules*, 51(3), 336-341.
- Chung da, E., Kim, H. H., Kim, M. K., Lee, K. H., Park, Y. H., and Um, I. C. (2015). Effects of different Bombyx mori silkworm varieties on the structural characteristics and properties of silk. *Int J Biol Macromol*, 79, 943-951.

- Coelho, D., Sampaio, A., Silva, C. J., Felgueiras, H. P., Amorim, M. T., and Zille, A. (2017). Antibacterial Electrospun Poly(vinyl alcohol)/Enzymatic synthesized Poly(catechol) Nanofibrous Midlayer membrane for ultrafiltration. *ACS Applied Materials & Interfaces*, 9(38), 33107-33118.
- Cooper, D. E. (1994). Arthroscopic meniscal repair: "Outside-in" technique. *Operative Techniques in Sports Medicine*, 2(3), 190–200.
- Dai, Z., Ronholm, J., Tian, Y., Sethi, B., and Cao, X. (2016). Sterilization techniques for biodegradable scaffolds in tissue engineering applications. *Journal of Tissue Engineering*, 7, 204173141664881.
- Dasic, Z., Bulatovic, N., Kezunovic, M., Bencic, I., and Bokan, V. (2015). Treatment of Medical Meniscus Injury with Partial Meniscectomy. *Acta Clin Croat*, 54, 319-325.
- Dehghan-Manshadi, N., Fattahi, S., Hadizadeh, M., Nikukar, H., Moshtaghioun, S. M., and Aflatoonian, B. (2019). The influence of elastomeric polyurethane type and ratio on the physicochemical properties of electrospun polyurethane/silk fibroin hybrid nanofibers as potential scaffolds for soft and hard tissue engineering. *European Polymer Journal*, 121, 1-8.
- Deitzel, J. M., Kleinmeyer, J., Harris, D., and Beck Tan, N. C. (2001). The effect of processing variables on the morphology of electrospun nanofibers and textiles. *Polymer*, 42(1), 261–272.
- Donnalaja, F., Jacchetti, E., Soncini, M., and Raimondi, M. T. (2020). Natural and Synthetic Polymers for Bone Scaffolds Optimization. *Polymers*, 12(4), 905.
- Doshi, J., and Reneker, D. H. (1995). Electrospinning process and applications of electrospun fibers. *Journal of Electrostatics*, 35(2–3), 151–160.
- Eichhorn, S. J., and Sampson, W. W. (2005). Statistical geometry of pores and statistics of porous nanofibrous assemblies. *Journal of the Royal Society, Interface*, 2(4), 309–318.
- Englund, M., Guermazi, A., Roemer, F. W., Yang, M., Zhang, Y., Nevitt, M. C., and Felson, D. T. (2010). Meniscal pathology on MRI increases the risk for both incident and enlarging subchondral bone marrow lesions of the knee: the MOST Study. *Annals of the Rheumatic Diseases*, 69(10), 1796–1802.
- Esposito, A. R., Moda, M., Cattani, S. M. D. M., de Santana, G. M., Barbieri, J. A., Munhoz, M. M., Cardoso, T. P., Barbo, M. L. P., Russo, T., D'Amora, U., Gloria, A., Ambrosio, L., and Duek, E. A. D. R. (2013). PLDLA/PCL-T Scaffold for Meniscus Tissue Engineering. *BioResearch Open Access*, 2(2), 138–147.

- Eyre, D. R., and Wu, J. (1983). Collagen of fibrocartilage: a distinctive molecular phenotype in bovine meniscus. *FEBS Letters*, 158(2), 265–270.
- Farokhi, M., Mottaghitlab, F., Samani, S., Shokrgozar, M. A., Kundu, S. C., Reis, R. L., Fatahi, Y., and Kaplan, D. L. (2018). Silk fibroin/hydroxyapatite composites for bone tissue engineering. *Biotechnology Advances*, 36(1), 68–91.
- Fathi, A., Khanmohammadi, M., Goodarzi, A., Foroutani, L., Mobarakeh, Z. T., Saremi, J., Arabpour, Z., and Ai, J. (2020). Fabrication of chitosan-polyvinyl alcohol and silk electrospun fiber seeded with differentiated keratinocyte for skin tissue regeneration in animal wound model. *Journal of Biological Engineering*, 14(1), 1–14.
- Feng, Y., Lin, J., Niu, L., Wang, Y., Cheng, Z., Sun, X., and Li, M. (2020). High Molecular Weight Silk Fibroin Prepared by Papain Degumming. *Polymers (Basel)*, 12(9), 1–15.
- Fithian, D. C., Kelly, M. A., and Mow, V. C. (1990). Material Properties and Structure-Function Relationships in the Menisci. *Clinical Orthopaedics and Related Research*, 252, 19-31.
- Fong, H., Chun, I., and Reneker, D. (1999). Beaded nanofibers formed during electrospinning. *Polymer*, 40(16), 4585-4592.
- Freymann, U., Endres, M., Neumann, K., Scholman, H., Morawietz, L., and Kaps, C. (2012). Expanded human meniscus-derived cells in 3-D polymer-hyaluronan scaffolds for meniscus repair. *Acta Biomaterialia*, 8(2), 677-685.
- Fridrikh, S. V., Yu, J. H., Brenner, M. P., and Rutledge, G. C. (2003). Controlling the Fiber Diameter during Electrospinning. *Physical Review Letters*, 90(14), 144501–144504.
- Fukubayashi, T., and Kurosawa, H. (1980). The contact area and pressure distribution pattern of the Knee: A study of normal and Osteoarthrotic knee Joints. *Acta Orthopaedica Scandinavica*, 51(1-6), 871-879.
- Garcia-Fuentes, M., Meinel, A. J., Hilbe, M., Meinel, L., and Merkle, H. P. (2009). Silk fibroin/hyaluronan scaffolds for human mesenchymal stem cell culture in tissue engineering. *Biomaterials*, 30(28), 5068–5076.
- Garg, K., and Bowlin, G. L. (2011). Electrospinning jets and nanofibrous structures. *Biomicrofluidics*, 5(1), 13403.
- Gholipourmalekabadi, M., Mozafari, M., Bandehpour, M., Salehi, M., Sameni, M., Caicedo, H. H., Mehdipour, A., Hamidabadi, H. G., Samadikuchaksaraei, A., and Ghanbarian, H. (2015). Optimization of nanofibrous silk fibroin scaffold as a

- delivery system for bone marrow adherent cells:in vitroandin vivostudies. *Biotechnology and Applied Biochemistry*, 62(6), 785–794.
- Ghosh, P., and Taylor, T. K. F. (1987). The Knee Joint Meniscus. *Clinical Orthopaedics and Related Research*, 224, 52-63.
- Giovanni, R., Wibowo, U. A., Judawisastra, H., and Barlian, A. (2019). Growth of human dermal fibroblasts on polyvinyl alcohol-silk fibroin Nanofiber scaffold. *Journal of Mathematical and Fundamental Sciences*, 51(3), 294-308.
- Gittens, R. A., McLachlan, T., Olivares-Navarrete, R., Cai, Y., Berner, S., Tannenbaum, R., and Boyan, B. D. (2011). The effects of combined micron-/submicron-scale surface roughness and nanoscale features on cell proliferation and differentiation. *Biomaterials*, 32(13), 3395-3403.
- Godbey, W. T., and Atala, A. (2002). In Vitro Systems for Tissue Engineering. *Annals of the New York Academy of Sciences*, 961(1), 10–26.
- Greiner, A., and Wendroff, J. H. (2007). Electrospinning: A Fascinating Method for the Preparation of Ultrathin Fibers. *ChemInform*, 38(42), 5670–5703.
- Greis, P. E., Bardana, D. D., Holmstrom, M. C., and Burks, R. T. (2002). Meniscal Injury: I. Basic Science and Evaluation. *Journal of the American Academy of Orthopaedic Surgeons*, 10(3), 168–176.
- Grogan, S. P., Baek, J., and D’Lima, D. D. (2020). Meniscal tissue repair with nanofibers: future perspectives. *Nanomedicine*, 15(25), 2517–2538.
- Gu, P., Wang, Z., Xie, Q., Sun, H., Huang, Y., Yu, Z., and Lin, M. (2016). Electrospun silk fibroin/poly(lactide-Co-ε-caprolactone) nanofibrous scaffolds for bone regeneration. *International Journal of Nanomedicine*, 1483.
- Gulrajani, M. L. (2008). Degumming of silk. Review of Progress in Coloration and Related Topics, 22(1), 79-89.
- Gunn, J. and Zhang, M. (2010). Polyblend nanofibers for biomedical applications: Perspectives and challenges. *Trends in Biotechnology*, 28(4), 189–197.
- Haider, A., Haider, S., and Kang, I.-K. (2018). A comprehensive review summarizing the effect of electrospinning parameters and potential applications of nanofibers in biomedical and biotechnology. *Arabian Journal of Chemistry*, 11(8), 1165–1188.
- Hajji, S., Chaker, A., Jridi, M., Maalej, H., Jellouli, K., Boufi, S., and Nasri, M. (2016). Structural analysis, and antioxidant and antibacterial properties of chitosan-poly (vinyl alcohol) biodegradable films. *Environmental Science and Pollution Research*, 23(15), 15310–15320.

- Halili, N. A. (2011). Collagen-Based Meniscus Tissue Engineering: Design and Application. Thesis. Doctor of Philosophy in Department of Biotechnology. Middle East Technical University. Turkey.
- Hede, A., Hempel-Poulsen, S., and Jensen, J. S. (1990). Symptoms and level of sports activity in patients awaiting arthroscopy for meniscal lesions of the knee. *The Journal of Bone & Joint Surgery*, 72(4), 550–552.
- Hede, A., Jensen, D. B., Blyme, P., and Sonne-Holm, S. (1990). Epidemiology of meniscal lesions in the knee. *Acta Orthop Scand*, 61, 435-437.
- Hong, J. K., and Madihally, S. V. (2011). Next Generation of Electrospayed Fibers for Tissue Regeneration. *Tissue Engineering Part B: Reviews*, 17(2), 125–142.
- Hong, Y. (2016). Electrospun fibrous polyurethane scaffolds in tissue engineering. *Advances in Polyurethane Biomaterials*, 543-559.
- Huang W., Ling S., Li C., Omenetto F. G., and Kaplan D. L. (2018). Silkworm silk-based materials and devices generated using bio-nanotechnology. *Chem. Soc. Rev*, 47, 6486–6504.
- Huang, C. Y., Hu, K. H., and Wei, Z. H. (2016). Comparison of cell behavior on pva/pva-gelatin electrospun nanofibers with random and aligned configuration. *Scientific Reports*, 6(1), 1–8.
- Huang, Z. M., Zhang, Y. Z., Kotaki, M., and Ramakrishna, S. (2003). A review on polymer nanofibers by electrospinning and their applications in nanocomposites. *Composites Science and Technology*, 63(15), 2223–2253.
- Inoue, S., Tanaka, K., Arisaka, F., Kimura, S., Ohtomo, K., and Mizuno, S. (2000). Silk fibroin of *Bombyx mori* is secreted, assembling a high molecular mass elementary unit consisting of H-chain, L-chain, and P25, with a 6:6:1 molar ratio. *J Biol Chem*, 275(51), 40517-40528.
- Janarthanan, G., Pillai, M. M., Kulasekaran, S. S., Rajendran, S., and Bhattacharyya, A. (2019). Engineered knee meniscus construct: Understanding the structure and impact of functionalization in 3D environment. *Polymer Bulletin*, 77(5), 2611-2629.
- Jeong, L., Lee, K. Y., and Park, W. H. (2007). Effect of Solvent on the Characteristics of Electrospun Regenerated Silk Fibroin Nanofibers. *Key Engineering Materials*, 813, 342–343.
- Jiang, S., Liu, S., and Feng, W. (2011). PVA hydrogel properties for biomedical application. *Journal of the Mechanical Behavior of Biomedical Materials*, 4(7), 1228-1233.

- Jiang, T., Khan, Y., Nair, L. S., Abdel-Fattah, W. I., and Laurencin, C. T. (2010). Functionalization of chitosan/poly(lactic acid-glycolic acid) sintered microsphere scaffolds via surface heparinization for bone tissue engineering. *Journal of Biomedical Materials Research Part A*, 93(3), 1193-1208.
- Jin, H. J., and Kaplan, D. L. (2003). Mechanism of silk processing in insects and spiders. *Nature*, 424(6952), 1057–1061.
- Kamoun, E. A., Chen, X., Mohy Eldin, M. S., and Kenawy, E. S. (2015). Crosslinked poly(vinyl alcohol) hydrogels for wound dressing applications: A review of remarkably blended polymers. *Arabian Journal of Chemistry*, 8(1), 1-14.
- Kang, S. W., Sun-Mi, S., Jae-Sun, L., Eung-Seok, L., Kwon-Yong, L., Sang-Guk, P., Jung-Ho, P., and Byung-Soo, K. (2006). Regeneration of whole meniscus using meniscal cells and polymer scaffolds in a rabbit total meniscectomy model. *Journal of Biomedical Materials Research Part A*, 77A(4), 659–671.
- Kaps, C., Frauenschuh, S., Endres, M., Ringe, J., Haisch, A., Lauber, J., and Burmester, G. (2006). Gene expression profiling of human articular cartilage grafts generated by tissue engineering. *Biomaterials*, 27(19), 3617–3630.
- Kasai, D., Chougale, R., Masti, S., Chalannavar, R., Malabadi, R. B., and Gani, R. (2018). Influence of *Syzygium cumini* leaves extract on morphological, thermal, mechanical, and antimicrobial properties of PVA and PVA/chitosan blend films. *Journal of Applied Polymer Science*, 135(17), 46188.
- Ki, C. S., Kim, J. W., Oh, H. J., Lee, K. H., and Park, Y. H. (2007). The effect of residual silk sericin on the structure and mechanical property of regenerated silk filament. *Int J Biol Macromol*, 41(3), 346-353.
- Kim, H., Song, D., Kim, M., Ryu, S., Um, I., Ki, C., and Park, Y. (2016). Effect of silk fibroin molecular weight on physical property of silk hydrogel. *Polymer*, 90, 26-33.
- Kim, K. H., Jeong, L., Park, H. N., Shin, S. Y., Park, W. H., Lee, S. C., Kim, T. I., Park, Y. J., Seol, Y. J., Lee, Y. M., Ku, Y., Rhyu, I. C., Han, S. B., and Chung, C. P. (2005). Biological efficacy of silk fibroin nanofiber membranes for guided bone regeneration. *Journal of Biotechnology*, 120(3), 327–339.
- Kim, K. O., Akada, Y., Kai, W., Kim, B. S., and Kim, I. S. (2011). Cells Attachment Property of PVA Hydrogel Nanofibers Incorporating Hyaluronic Acid for Tissue Engineering. *Journal of Biomaterials and Nanobiotechnology*, 02(04), 353–360.
- Kim, S. H., Nam, Y. S., Lee, T. S., and Park, W. H. (2003). Silk Fibroin Nanofiber. Electrospinning, Properties, and Structure. *Polymer Journal*, 35(2), 185–190.

- Kirecci, A., Özkoç, M., and İçOğlu, H. B. (2011). Determination of optimal production parameters for polyacrylonitrile nanofibers. *Journal of Applied Polymer Science*, 124(6), 4961–4968.
- Kon, E., Chiari, C., Marcacci, M., Delcogliano, M., Salter, D. M., Martin, I., Ambrosio, L., Fini, M., Tschon, M., Tognana, E., Plasenzotti, R., and Nehrer, S. (2008). Tissue Engineering for Total Meniscal Substitution: Animal Study in Sheep Model. *Tissue Engineering Part A*, 14(6), 1067–1080.
- Kopp, A., Smeets, R., Gosau, M., Kröger, N., Fuest, S., Köpf, M., and Burg, S. (2020). Effect of process parameters on additive-free electrospinning of regenerated silk fibroin nonwovens. *Bioactive Materials*, 5(2), 241–252.
- Kuchaiyaphum, P., Chotichayapong, C., Butwong, N., and Bua-ngern, W. (2020). Silk fibroin/Poly (vinyl alcohol) Hydrogel cross-linked with Dialdehyde starch for wound dressing applications. *Macromolecular Research*, 28(9), 844-850.
- Kudug, E. (2004). Use of fibroin/hyaluronic acid matrices as a drug reservoir in iontophoretic transdermal delivery, Izmir institute of technology, Izmir, Turkey.
- Kumar, A., and Han, S. S. (2016). PVA-based hydrogels for tissue engineering: A review. *International Journal of Polymeric Materials and Polymeric Biomaterials*, 66(4), 159-182.
- Kumar, G., Tison, C. K., Chatterjee, K., Pine, P. S., McDaniel, J. H., Salit, M. L., Young, M. F., and Simon, C. G. (2011). The determination of stem cell fate by 3D scaffold structures through the control of cell shape. *Biomaterials*, 32(35), 9188–9196.
- Kumbar, S. G., James, R., Nukavarapu, S. P., and Laurencin, C. T. (2008). Electrospun nanofiber scaffolds: Engineering soft tissues. *Biomed Mater*, 3(3), 034002.
- Kumkun, P., Tuancharoensri, N., Ross, G., Mahasaranon, S., Jongjitwimol, J., Topham, P. D. and Ross, S. (2019). Green fabrication route of robust, biodegradable silk sericin and poly (vinyl alcohol) nanofibrous scaffolds. *Polymer International*, 68(11), 1903-1913.
- Kunz, R. I., Brancalhão, R. M., Ribeiro, L. F., and Natali, M. R. (2016). Silkworm Sericin: Properties and Biomedical Applications. *Biomed Res Int*, 8175701.
- Lamminmäki, T. T., Kettle, J. P., Puukko, P. J. T., and Gane, P. A. C. (2011). Absorption Capability and Inkjet Ink Colorant Penetration into Binders Commonly Used in Pigmented Paper Coatings. *Industrial & Engineering Chemistry Research*, 50(6), 3287–3294.
- Lanza, R., Langer, R., and Vacanti, J. P. (2000). Principles of Tissue Engineering, Second Edition (2nd ed.). Academic Press.

- Lee, J. S., Choi, K. H., Ghim, H. D., Kim, S. S., Chun, D. H., Kim, H. Y., and Lyoo, W. S. (2004). Role of molecular weight of atactic poly(vinyl alcohol) (PVA) in the structure and properties of PVA nanofabric prepared by electrospinning. *Journal of Applied Polymer Science*, 93(4), 1638–1646.
- Lee, J., Sultan, M., Kim, S., Kumar, V., Yeon, Y., Lee, O., and Park, C. (2017). Artificial Auricular Cartilage Using Silk Fibroin and Polyvinyl Alcohol Hydrogel. *International Journal of Molecular Sciences*, 18(8), 1–15.
- Lee, S. J., Aadalen, K. J., Malaviya, P., Lorenz, E. P., Hayden, J. K., Farr, J., and Cole, B. J. (2006). Tibiofemoral contact mechanics after serial medial Meniscectomies in the human cadaveric knee. *The American Journal of Sports Medicine*, 34(8), 1334-1344.
- Li, C., Vepari, C., Jin, H. J., Kim, H. J., and Kaplan, D. L. (2006). Electrospun silk-BMP-2 scaffolds for bone tissue engineering. *Biomaterials*, 27(16), 3115–3124.
- Li, G., Zhou, P., Shao, Z., Xie, X., Chen, X. Wang, H., Chunyu, L., and Yu, T. (2001). The natural silk spinning process A nucleation-dependent aggregation mechanism. *Eur. J. Biochem*, 268, 6600–6606.
- Li, Z., Kupcsik, L., Yao, S. J., Alini, M., and Stoddart, M. J. (2009). Mechanical load modulates chondrogenesis of human mesenchymal stem cells through the TGF- $\beta$  pathway. *Journal of Cellular and Molecular Medicine*, 14(6a), 1338–1346.
- Liang, J. I., Hsu, H. C., Nien, Y. H., Su, F. C., Wu, H. W., Chen, J. P., and Yeh, M. L. (2009). Cell response to Electrospun PVA and PVA/Chitosan nanofibers. IEEE 35th Annual Northeast Bioengineering Conference.
- Ling, S., Qi, Z., Knight, D. P., Shaoa, Z., and Chen, X. (2013). FTIR imaging, a useful method for studying the compatibility of silk fibroin-based polymer blends. *Polym Chem*, 4, 5401-5406.
- Liu, H., Wei, J., Zheng, L. J., and Zhao, Y. P. (2013). Extraction and Characterization of Silk Fibroin from Waste Silk. *Advanced Materials Research*, 788, 174–177.
- Liu, W., Lipner, J., Moran, C. H., Feng, L., Li, X., Thomopoulos, S., and Xia, Y. (2015). Generation of Electrospun nanofibers with controllable degrees of crimping through a simple, plasticizer-based treatment. *Advanced Materials*, 27(16), 2583-2588.
- Liu, Z., Ju, K., Wang, Z., Li, W., Ke, H., and He, J. (2019). Electrospun jets number and nanofiber morphology effected by voltage value: Numerical simulation and experimental verification. *Nanoscale Research Letters*, 14(1), 310.

- Lü, L., Wang, Y., Mao, X., Xiao, Z., and Huang, N. (2012). The effects of PHBV electrospun fibers with different diameters and orientations on growth behavior of bone-marrow-derived mesenchymal stem cells. *Biomedical Materials*, 7(1), 1-10.
- Lu, Q., Huang, Y., Li, M., Zuo, B., Lu, S., Wang, J., Zhud, H., and Kaplan, D. L. (2011). Silk fibroin electrogelation mechanisms. *Acta Biomater*, 7(6), 2394-2400.
- Luetchford, K. A., Chaudhuri, J. B., and de Bank, P. A. (2020). Silk fibroin/gelatin microcarriers as scaffolds for bone tissue engineering. *Materials Science and Engineering: C*, 106, 110-116.
- Lujerdean, C., Baci, G. M., Cucu, A. A., and Dezmirean, D. S. (2022). The Contribution of Silk Fibroin in Biomedical Engineering. *Insects*, 13(3).
- Makris, E. A., Hadidi, P., and Athanasiou, K. A. (2011). The knee meniscus: Structure–function, pathophysiology, current repair techniques, and prospects for regeneration. *Biomaterials*, 32(30), 7411–7431.
- Mandal, B. B., and Kundu, S. C. (2009). Cell proliferation and migration in silk fibroin 3D scaffolds. *Biomaterials*, 30(15), 2956-2965.
- Mandal, B. B., Park, S. H., Gil, E. S., and Kaplan, D. L. (2011). Multilayered silk scaffolds for meniscus tissue engineering. *Biomaterials*, 32(2), 639–651.
- Martinek, V., Ueblacker, P., Bräun, K., Nitschke, S., Mannhardt, R., Specht, K., Gansbacher, B., and Imhoff, A. B. (2005). Second generation of meniscus transplantation: in-vivo study with tissue engineered meniscus replacement. *Archives of Orthopaedic and Trauma Surgery*, 126(4), 228–234.
- Mcdevitt, C. A., and Webber, R. J. (1990). The Ultrastructure and Biochemistry of Meniscal Cartilage. *Clinical Orthopaedics and Related Research*, 252, 818.
- Mcdevitt, C. A., Mukherjee, S., Kambic, H., and Parker, R. (2002). Emerging concepts of the cell biology of the meniscus. *Current Opinion in Orthopaedics*, 13(5), 345–350.
- Megelski, S., Stephens, J. S., Chase, D. B., and Rabolt, J. F. (2002). Micro- and nanostructured surface morphology on electrospun polymer fibers. *Macromolecules*, 35(22), 8456–8466.
- Milan, P. B., Lotfibakhshaiesh, N., Joghataie, M., Ai, J., Pazouki, A., Kaplan, D., Kargozar, S., Amini, N., Hamblin, M., Mozafari, M., and Samadikuchaksaraei, A. (2016). Accelerated wound healing in a diabetic rat model using decellularized dermal matrix and human umbilical cord perivascular cells. *Acta Biomaterialia*, 45, 234–246.
- Min, B. M., Lee, G., Kim, S. H., Nam, Y. S., Lee, T. S., and Park, W. H. (2004). Electrospinning of silk fibroin nanofibers and its effect on the adhesion and

- spreading of normal human keratinocytes and fibroblasts in vitro. *Biomaterials*, 25(7–8), 1289–1297.
- Mit-uppatham, C., Nithitanakul, M., and Supaphol, P. (2004). Ultrafine Electrospun polyamide-6 fibers: Effect of solution conditions on morphology and average fiber diameter. *Macromolecular Chemistry and Physics*, 205(17), 2327–2338.
- Mohammad Ali Zadeh, M., Keyanpour-Rad, M., and Ebadzadeh, T. (2014). Effect of viscosity of polyvinyl alcohol solution on morphology of the electrospun mullite nanofibres. *Ceramics International*, 40(4), 5461–5466.
- Mohammadzadehmoghadam, S., and Dong, Y. (2019). Fabrication and Characterization of Electrospun Silk Fibroin/Gelatin Scaffolds Crosslinked with Glutaraldehyde Vapor. *Frontiers in Materials*, 6, 1–12.
- Mohd Yusoff, N. I., Wahit, M. U., Jaafar, J., and Wong, T. (2019). Structural and characterization studies of insoluble Thai bombyx Mori silk fibroin films. *Malaysian Journal of Fundamental and Applied Sciences*, 15(1), 18–22.
- Moncada-Saucedo, N., Camacho-Morales, A., and Fuentes-Mera, L. (2019). Scaffolds Based on Silk Fibroin for Osteochondral Tissue Engineering. *Research & Development in Material Science*, 10(3).
- More, S. V., Chavan, S., and Prabhune, A. A. (2017). Silk Degumming and Utilization of Silk Sericin by Hydrolysis Using Alkaline Protease from *Beauveria* Sp. (MTCC 5184): A Green Approach. *Journal of Natural Fibers*, 15(3), 373–383.
- Mow, V. C., Arnoczky, S. P., and Jackson, D. W., MD. (1992). Knee Meniscus: Basic and Clinical Foundations. 52(556).
- Mozafari, M., Moztarzadeh, Jalali, Alhosseini, N., Asgari, Dodel, Samadikuchaksaraei, and Kargozar. (2012). Synthesis and characterization of electrospun polyvinyl alcohol nanofibrous scaffolds modified by blending with chitosan for neural tissue engineering. *International Journal of Nanomedicine*, 25–34.
- Mwiiri, F. K., Brandner, J. M., and Daniels, R. (2020). Electrospun Bioactive Wound Dressing Containing Colloidal Dispersions of Birch Bark Dry Extract. *Pharmaceutics*, 12(8), 1–20.
- Nanda, H. S., Nakamoto, T., Chen, S., Cai, R., Kawazoe, N., and Chen, G. (2014). Collagen microgel-assisted dexamethasone release from PLLA-collagen hybrid scaffolds of controlled pore structure for osteogenic differentiation of mesenchymal stem cells. *Journal of Biomaterials Science, Polymer Edition*, 25(13), 1374–1386.
- Natsu-ume, T., Majima, T., Reno, C., Shrive, N. G., Frank, C. B., and Hart, D. A. (2005). Menisci of the rabbit knee require mechanical loading to maintain homeostasis:

- cyclic hydrostatic compression in vitro prevents derepression of catabolic genes. *Journal of Orthopedic Science*, 10(4), 396–405.
- Neves, N. M., Campos, R., Pedro, A., Cunha, J., Macedo, F., and Reis, R. L. (2007). Patterning of polymer nanofiber meshes by electrospinning for biomedical applications. *International Journal of Nanomedicine*, 2(3), 433–448.
- Ngadiman, N. H. A., Noordin, M., Idris, A., Shakir, A. S. A., and Kurniawan, D. (2015). Influence of Polyvinyl Alcohol Molecular Weight on the Electrospun Nanofiber Mechanical Properties. *Procedia Manufacturing*, 2, 568–572.
- Nguyen, T. P., Nguyen, Q. V., Nguyen, V. H., Le, T. H., Huynh, V. Q. N., Vo, D. V. N., Trinh, Q. T., Kim, S. Y., and Le, Q. V. (2019). Silk Fibroin-Based Biomaterials for Biomedical Applications: A Review. *Polymers*, 11(12), 1933.
- Nguyen, T. H., and Lee, B. T. (2010). Fabrication and characterization of cross-linked gelatin electro-spun nano-fibers. *Journal of Biomedical Science and Engineering*, 03(12), 1117–1124.
- Nielsen, A. B., and Yde, J. (1991). Epidemiology of Acute Knee Injuries: A Prospective Hospital Investigation. *The Journal of Trauma: Injury, Infection, and Critical Care*, 31(12), 1644–1648.
- Niu, C., Li, X., Wang, Y., Liu, X., Shi, J., and Wang, X. (2019). Design and performance of a poly(vinyl alcohol)/silk fibroin enzymatically crosslinked semi-interpenetrating hydrogel for a potential hydrophobic drug delivery. *RSC Advances*, 9(70), 41074–41082.
- Niu, W., Guo, W., Han, S., Zhu, Y., Liu, S., and Guo, Q. (2016). Cell-Based Strategies for Meniscus Tissue Engineering. *Stem Cells International*, 1–10.
- Numpaisal, P., Jiang, C., Hsieh, C., Chiang, H., and Chien, C. (2022). Prospective application of partially digested autologous Chondrocyte for meniscus tissue engineering. *Pharmaceutics*, 14(3), 1–14.
- Numpaisal, P., Rothrauff, B. B., Gottardi, R., Chien, C., and Tuan, R. S. (2016). Rapidly dissociated autologous meniscus tissue enhances meniscus healing: An in vitro study. *Connective Tissue Research*, 58(3-4), 355–365.
- Oruch, R., Elderbi, M. A., Khattab, H. A., Pryme, I. F., and Lund, A. (2014). Lithium: A review of pharmacology, clinical uses, and toxicity. *European Journal of Pharmacology*, 740, 464–473.
- Ou, K., Dong, X., Qin, C., Ji, X., and He, J. (2017). Properties and toughening mechanisms of PVA/PAM double-network hydrogels prepared by freeze-thawing and anneal-swelling. *Materials Science and Engineering: C*, 77, 1017–1026.

- Pain, R. H. (1983). Protein folding, denaturation and stability. *Biochem Soc Trans*, 11(1), 15-16.
- Pandey, S., Rathore, K., Johnson, J., and Cekanova, M. (2018). Aligned nanofiber material supports cell growth and increases osteogenesis in canine adipose-derived mesenchymal stem cells in vitro. *Journal of Biomedical Materials Research Part A*, 106(7), 1780-1788.
- Panilaitis, B., Altman, G. H., Chen, J., Jin, H. J., Karageorgiou, V., and Kaplan, D. L. (2003). Macrophage responses to silk. *Biomaterials*, 24(18), 3079-3085.
- Pelipenko, J., Kristl, J., Janković, B., Baumgartner, S., and Kocbek, P. (2013). The impact of relative humidity during electrospinning on the morphology and mechanical properties of nanofibers. *International Journal of Pharmaceutics*, 456(1), 125-134.
- Pereira, H., Frias, A. M., Oliveira, J. M., Espregueira-Mendes, J., and Reis, R. L. (2011). Tissue engineering and regenerative medicine strategies in meniscus lesions. *Arthroscopy: The Journal of Arthroscopic & Related Surgery: Official Publication of the Arthroscopy Association of North America and the International Arthroscopy Association*, 27(12), 1706-1719.
- Pérez-Rigueiro, J., Elices, M., Llorca, J., and Viney, C. (2001). Tensile properties of silkworm silk obtained by forced silking. *Journal of Applied Polymer Science*, 82(8), 1928-1935.
- Petersen, W., and Tillmann, B. (1998). Collagenous fibril texture of the human knee joint menisci. *Anatomy and Embryology*, 197(4), 317-324.
- Pham, Q. P., Sharma, U., and Mikos, A. G. (2006). Electrospun poly(epsilon-caprolactone) microfiber and multilayer nanofiber/microfiber scaffolds: characterization of scaffolds and measurement of cellular infiltration. *Biomacromolecules*, 7(10), 2796-2805.
- Pillai, M. M., Akshaya, T. R., Elakkiya, V., Gopinathan, J., Sahanand, K. S., Rai, B. K., and Selvakumar, R. (2015). Egg shell membrane – a potential natural scaffold for human meniscal tissue engineering: An in vitro study. *RSC Advances*, 5(93), 76019-76025.
- Pillai, M. M., Gopinathan, J., Indumathi, B., Manjoosha, Y. R., Santosh Sahanand, K., Dinakar Rai, B. K., Selvakumar, R., and Bhattacharyya, A. (2016). Silk-PVA Hybrid Nanofibrous Scaffolds for Enhanced Primary Human Meniscal Cell Proliferation. *The Journal of Membrane Biology*, 249(6), 813-822.
- Pillai, M. M., Gopinathan, J., Senthil Kumar, R., Sathish Kumar, G., Shanthakumari, S., Sahanand, K. S., Bhattacharyya, A., and Selvakumar, R. (2018). Tissue engineering

- of human knee meniscus using functionalized and reinforced silk-polyvinyl alcohol composite three-dimensional scaffolds: Understanding their vitroandin vivobehavior. *Journal of Biomedical Materials Research Part A*, 106(6), 1722–1731.
- Platt, M. A. (2005). Tendon Repair and Healing. *Clinics in Podiatric Medicine and Surgery*, 22(4), 553–560.
- Qi, Y., Wang, H., Wei, K., Yang, Y., Zheng, R. Y., Kim, S., and Zhang, K. Q. (2017). A Review of Structure Construction of Silk Fibroin Biomaterials from Single Structures to Multi-Level Structures. *J. Mol. Sci*, 18(3), 237.
- Rahmati, M., Mills, D. K., Urbanska, A. M., Saeb, M. R., Venugopal, J. R., Ramakrishna, S., and Mozafari, M. (2021). Electrospinning for tissue engineering applications. *Progress in Materials Science*, 117, 1–102.
- Raksa, A., Numpaisal, P., Utke, R., Ruksakulpiwat, C., and Ruksakulpiwat, Y. (2022). NANOFIBROUS SCAFFOLDS OF ELECTROSPUN SILK FIBROIN/POLY(VINYL ALCOHOL) BLENDS FOR TISSUE ENGINEERING. *Suranaree J. Sci. Technol*, 29(3), 010132(010131-010137).
- Raksa, A., Utke, R., Ruksakulpiwat, C., Numpaisal, P., and Ruksakulpiwat, Y. (2020). Morphological and chemical characterization of electrospun silk fibroin/polyvinyl alcohol nanofibers, *AIP Conference Proceeding*, 2279:080004-1.
- Ramakrishna, S., Fujihara, K., Teo, W. E., Lim, T. C., and Ma, Z. (2005). An introduction to electrospinning and nanofibers. *World scientific publishing Co. Pte. Ltd*, 90-105.
- Reneker, D. H., and Yarin, A. L. (2008). Electrospinning jets and polymer nanofibers. *Polymer*, 49(10), 2387–2425.
- Rnjak-Kovacina, J., and Weiss, A. S. (2011). Increasing the pore size of electrospun scaffolds. *Tissue Engineering. Part B, Reviews*, 17(5), 365–372.
- Rockwood, D. N., Preda, R. C., Yücel, T., Wang, X., Lovett, M. L., and Kaplan, D. L. (2011). Materials fabrication from bombyx Mori silk fibroin. *Nature Protocols*, 6(10), 1612-1631.
- Rodeo, S. A. (2000). Arthroscopic Meniscal Repair with Use of the Outside-in Technique. *The Journal of Bone and Joint Surgery-American Volume*, 82(1), 127–141.
- Rodoplu, D., and Mutlu, M. (2012). Effects of Electrospinning Setup and Process Parameters on Nanofiber Morphology Intended for the Modification of Quartz Crystal Microbalance Surfaces. *Journal of Engineered Fibers and Fabrics*, 7(2), 118–123.

- Roos, H., Lauren, M., Adalberth, T., Roos, E. M., Jonsson, K., and Lohmander, L. S. (1998). Knee osteoarthritis after meniscectomy: Prevalence of radiographic changes after twenty-one years, compared with matched controls. *Arthritis and Rheumatism*, 41(4), 687-93.
- Ross, S., Yooyod, M., Limpeanchob, N., Mahasaranon, S., Suphrom, N., and Ross, G. M. (2017). Novel 3D porous semi-IPN hydrogel scaffolds of silk sericin and poly(N-hydroxyethyl acrylamide) for dermal reconstruction. *Express Polymer Letters*, 11(9), 719-730.
- Rothrauff, B. B., Numpaisal, P. O., Lauro, B. B., Alexander, P. G., Debski, R. E., Musahl, V., and Tuan, R. S. (2016). Augmented repair of radial meniscus tear with biomimetic electrospun scaffold: an in vitro mechanical analysis. *Journal of Experimental Orthopaedics*, 3(1), 1–10.
- Ruprecht, J. C., Waanders, T. D., Rowland, C. R., Nishimuta, J. F., Glass, K. A., Stencel, J., DeFrate, L. E., Guilak, F., Weinberg, J. B., and McNulty, A. L. (2019). Meniscus-Derived Matrix Scaffolds Promote the Integrative Repair of Meniscal Defects. *Scientific Reports*, 9(1), 1–13.
- Sakunphanitphan, S., Jantarat, J., Sritanaudomchai, H., Oonkhanond, B. and Hargreaves, K.M. (2019). The effect of silk fibroin hydrogel on proliferation of human stem cells from the apical papilla. *M Dent J*, 39(1), 35-40.
- Sambudi, N. S., Sathyamurthy, M., Lee, G. M., and Park, S. B. (2015). Electrospun chitosan/poly(vinyl alcohol) reinforced with  $\text{CaCO}_3$  nanoparticles with enhanced mechanical properties and biocompatibility for cartilage tissue engineering. *Composites Science and Technology*, 106, 76–84.
- Sayed, M. M., Mousa, H. M., El-Aassar, M., El-Deeb, N. M., Ghazaly, N. M., Dewidar, M. M., and Abdal-hay, A. (2019). Enhancing mechanical and biodegradation properties of polyvinyl alcohol/silk fibroin nanofibers composite patches for cardiac tissue engineering. *Materials Letters*, 255, 126510.
- Selvakumar, R., Varkey, A., Elakkiya, V., PonJanani, S., Gopinathan, J., Bhattacharyya, A., and Pillai, M. M. (2015). Impact of silk fibroin-based scaffold structures on human osteoblast MG63 cell attachment and proliferation. *International Journal of Nanomedicine*, 43–51.
- Setton, L. A., Elliott, D. M., and Mow, V. C. (1999). Altered mechanics of cartilage with osteoarthritis: human osteoarthritis and an experimental model of joint degeneration. *Osteoarthritis and Cartilage*, 7(1), 2–14.

- Sharifi, F., Bai, Z., Montazami, R., and Hashemi, N. (2016). Mechanical and physical properties of poly(vinyl alcohol) microfibers fabricated by a microfluidic approach. *RSC Advances*, 6(60), 55343–55353.
- Sheik, S., and Karikannar Nagaraja, G. (2020). Development, characterization and properties of silk fibre and grafted silk fibre reinforced polymer composite films. *Generation, Development and Modifications of Natural Fibers*, 1-22.
- Shimomura, K., Bean, A. C., Lin, H., Nakamura, N., and Tuan, R. S. (2015). In Vitro Repair of Meniscal Radial Tear Using Aligned Electrospun Nanofibrous Scaffold. *Tissue Engineering Part A*, 21(13–14), 2066–2075.
- Sill, T. J., and von Recum, H. A. (2008). Electrospinning: Applications in drug delivery and tissue engineering. *Biomaterials*, 29(13), 1989–2006.
- Sirc, J., Hobzov, R., Kostina, N., Munzarov, M., Juklickov, M., Lhotka, M., Kubinov, S., Zajicov, A., and Michalek, J. (2012). Morphological Characterization of Nanofibers: Methods and Application in Practice. *J. of Nanomat*, 1-14.
- Sofia, S., McCarthy, M. B., Gronowicz, G., and Kaplan, D. L. (2000). Functionalized silk-based biomaterials for bone formation. *Journal of Biomedical Materials Research*, 54(1), 139-148.
- Sukigara, S., Gandhi, M., Ayutsede, J., Micklus, M., and Ko, F. (2003). Regeneration of Bombyx mori silk by electrospinning—part 1: processing parameters and geometric properties. *Polymer*, 44(19), 5721–5727.
- Sun, A. X., Numpaisal, P. O., Gottardi, R., Shen, H., Yang, G., and Tuan, R. S. (2016). Cell and Biomimetic Scaffold-Based Approaches for Cartilage Regeneration. *Operative Techniques in Orthopaedics*, 26(3), 135–146.
- Supaphol, P., and Chuangchote, S. (2008). On the electrospinning of poly(vinyl alcohol) nanofiber mats: A revisit. *Journal of Applied Polymer Science*, 108(2), 969-978.
- Sweigart, M. A., Zhu, C. F., Burt, D. M., deHoll, P. D., Agrawal, C. M., Clanton, T. O., and Athanasiou, K. A. (2004). Intraspecies and Interspecies Comparison of the Compressive Properties of the Medial Meniscus. *Annals of Biomedical Engineering*, 32(11), 1569–1579.
- Talebian, S., Mehrali, M., Mohan, S., Balaji Raghavendran, H. R., Mehrali, M., Khanlou, H. M., Kamarul, T., Afifi, A. M., and Abass, A. A. (2014). Chitosan (PEO)/bioactive glass hybrid nanofibers for bone tissue engineering. *RSC Adv*, 4(90), 49144–49152.
- Tanaka, K., Inoue, S., and Mizuno, S. (1999). Hydrophobic interaction of P25, containing asn-linked oligosaccharide chains, with the H-L complex of silk fibroin produced by bombyx Mori. *Insect Biochemistry and Molecular Biology*, 29(3), 269-276.

- Tang, Z., Qiu, C., McCutcheon, J. R., Yoon, K., Ma, H., Fang, D., and Chu, B. (2009). Design and fabrication of electrospun polyethersulfone nanofibrous scaffold for high-flux nanofiltration membranes: PES Electrospun Nanofibrous Scaffold for TFNC NF. *Journal of Polymer Science. Part B, Polymer Physics*, 47(22), 2288–2300.
- Tarun, G., Ajay, B., Bhawna, K., Sunil, K., and Ravi, J. (2011). Scaffold: Tissue Engineering and Regenerative Medicine. *International Reserch Journal of Pharmacy*, 2(12), 37-42.
- Tarus, B., Fadel, N., Al-Oufy, A., and El-Messiry, M. (2016). Effect of polymer concentration on the morphology and mechanical characteristics of electrospun cellulose acetate and poly (vinyl chloride) nanofiber mats. *Alexandria Engineering Journal*, 55(3), 2975–2984.
- Tarus, B. K., Mwasiagi, J. I., Fadel, N., Al-Oufy, A., and Elmessiry, M. (2019). Electrospun cellulose acetate and poly(vinyl chloride) nanofiber mats containing silver nanoparticles for antifungi packaging. *SN Applied Sciences*, 1(3).
- Teixeira, M. A., Amorim, M. T. P., and Felgueiras, H. P. (2019). Poly(Vinyl Alcohol)-Based Nanofibrous Electrospun Scaffolds for Tissue Engineering Applications. *Polymers*, 12(1), 7.
- Teuschl, A. H., van Griensven, M., and Redl, H. (2014). Sericin removal from raw Bombyx mori silk scaffolds of high hierarchical order. *Tissue Eng Part C Methods*, 20(5), 431-439.
- Thomas, D., and Cebe, P. (2016). Self-nucleation and crystallization of polyvinyl alcohol. *Journal of Thermal Analysis and Calorimetry*, 127(1), 885-894.
- Thompson, C., Chase, G., Yarin, A., and Reneker, D. (2007). Effects of parameters on nanofiber diameter determined from electrospinning model. *Polymer*, 48(23), 6913–6922.
- Tissakht, M., and Ahmed, A. (1995). Tensile stress-strain characteristics of the human meniscal material. *Journal of Biomechanics*, 28(4), 411-422.
- Tripatanasuwan, S., Zhong, Z., and Reneker, D. H. (2007). Effect of evaporation and solidification of the charged jet in electrospinning of poly(ethylene oxide) aqueous solution. *Polymer*, 48(19), 5742–5746.
- Valluzzi, R., Gido, S. P., Muller, W., and Kaplan, D. L. (1999). Orientation of silk III at the air-water interface. *International Journal of Biological Macromolecules*, 24(2–3), 237–242.
- Vashisth, P., Nikhil, K., Roy, P., Pruthi, P. A., Singh, R. P., and Pruthi, V. (2016). A novel gellan–PVA nanofibrous scaffold for skin tissue regeneration: Fabrication and characterization. *Carbohydrate Polymers*, 136, 851–859.

- Venkatachalam, S., Godsiff, S., and Harding, M. (2001). Review of the clinical results of arthroscopic meniscal repair. *The Knee*, 8(2), 129–133.
- Wadhwa, V., Omar, H., Coyner, K., Khazzam, M., Robertson, W., and Chhabra, A. (2016). ISAKOS classification of meniscal tears—illustration on 2D and 3D isotropic spin echo MR imaging. *European Journal of Radiology*, 85(1), 15–24.
- Wang, C., and Wang, M. (2012). Dual-source dual-power electrospinning and characteristics of multifunctional scaffolds for bone tissue engineering. *Journal of Materials Science: Materials in Medicine*, 23(10), 2381-2397.
- Wang, F., and Zhang, Y. Q. (2015). Bioconjugation of silk fibroin nanoparticles with enzyme and Peptide and their characterization. *Adv Protein Chem Struct Biol*, 98, 263-291.
- Wang, F., Wu, H., Venkataraman, V., and Hu, X. (2019). Silk fibroin-poly(lactic acid) biocomposites: Effect of protein-synthetic polymer interactions and miscibility on material properties and biological responses. *Materials Science and Engineering: C*, 104, 109890.
- Wang, H. Y., Zhang, Y. Q., and Wei, Z. G. (2021). Dissolution and processing of silk fibroin for materials science. *Crit Rev Biotechnol*, 41(3), 406-424.
- Wang, H., Zhang, Y., and Wei, Z. (2021). Dissolution and processing of silk fibroin for materials science. *Critical Reviews in Biotechnology*, 41(3), 406-424.
- Wang, M., Jin, H. J., Kaplan, D. L., and Rutledge, G. C. (2004). Mechanical Properties of Electrospun Silk Fibers. *Macromolecules*, 37(18), 6856–6864.
- Wang, Q., Chen, Q., Yang, Y., and Shao, Z. (2012). Effect of various dissolution systems on the molecular weight of regenerated silk fibroin. *Biomacromolecules*, 14(1), 285-289.
- Wang, Y., Blasioli, D., Kim, H., Kim, H., and Kaplan, D. (2006). Cartilage tissue engineering with silk scaffolds and human articular chondrocytes. *Biomaterials*, 27(25), 4434-4442.
- Wei, X., Xia, Z., Wong, S. C., and Baji, A. (2009). Modelling of mechanical properties of electrospun nanofibre network. *International Journal of Experimental and Computational Biomechanics*, 1(1), 45.
- Wei, Z., Gua, J., Yea, Y., Fanga, M., Langa, J., Yanga, D., and Pan, Z. (2020). Biodegradable poly(butylene succinate) nanofibrous membrane treated with oxygen plasma for superhydrophilicity. *Surf. Coat. Technol*, 381, 1-7.
- Wise, J. K., Yarin, A. L., Megaridis, C. M., and Cho, M. (2009). Chondrogenic Differentiation of Human Mesenchymal Stem Cells on Oriented Nanofibrous Scaffolds:

- Engineering the Superficial Zone of Articular Cartilage. *Tissue Engineering Part A*, 15(4), 913–921.
- Wöltje, M., Kölbl, A., Aibibu, D., and Cherif, C. (2021). A fast and reliable process to fabricate regenerated silk fibroin solution from degummed silk in 4 hours. *International Journal of Molecular Sciences*, 22(19), 10565.
- Wu, J., and Hong, Y. (2016). Enhancing cell infiltration of electrospun fibrous scaffolds in tissue regeneration. *Bioactive Materials*, 1(1), 56–64.
- Xavier, M., Macedo, M., Benatti, A., Jardini, A., Rodrigues, A., Lopes, M., and Kharmandayan, P. (2016). PLLA synthesis and nanofibers production: Viability by human Mesenchymal stem cell from adipose tissue. *Procedia CIRP*, 49, 213–221.
- Xu, C., Inai, R., Kotaki, M., and Ramakrishna, S. (2004). Electrospun Nanofiber fabrication as synthetic Extracellular matrix and its potential for vascular tissue engineering. *Tissue Engineering*, 10(7-8), 1160–1168.
- Xue, J., Feng, B., Zheng, R., Lu, Y., Zhou, G., Liu, W., Cao, Y., Zhang, Y., and Zhang, W. J. (2013). Engineering ear-shaped cartilage using electrospun fibrous membranes of gelatin/polycaprolactone. *Biomaterials*, 34(11), 2624–2631.
- Yamada, H., Nakao, H., Takasu, Y., and Tsubouchi, K. (2001). Preparation of undegraded native molecular fibroin solution from silkworm cocoons. *Materials Science and Engineering: C*, 14(1-2), 41–46.
- Yan, L. P., Oliveira, J. M., Oliveira, A. L., Caridade, S. G., Mano, J. F., and Reis, R. L. (2012). Macro/microporous silk fibroin scaffolds with potential for articular cartilage and meniscus tissue engineering applications. *Acta Biomaterialia*, 8(1), 289–301.
- Yan, R., Chen, Y., Gu, Y., Tang, C., Huang, J., Hu, Y., Zheng, Z., Ran, J., Heng, B., Chen, X., Yin, Z., Chen, W., Shen, W., and Ouyang, H. (2019b). A collagen-coated sponge silk scaffold for functional meniscus regeneration. *Journal of Tissue Engineering and Regenerative Medicine*, 13(2), 156–173.
- Yang, W., Both, S., Van Osch, G., Wang, Y., Jansen, J., and Yang, F. (2014). Performance of different three-dimensional scaffolds for in vivo endochondral bone generation. *European Cells and Materials*, 27, 350–364.
- Yang, Y., Jia, Z., Liu, J., Li, Q., Hou, L., Wang, L., and Guan, Z. (2008). Effect of electric field distribution uniformity on electrospinning. *Journal of Applied Physics*, 103(10), 104307–104311.
- Yazdanpanah, A., Tahmasbi, M., Amoabediny, G., Nourmohammadi, J., Moztafzadeh, F., and Mozafari, M. (2015). Fabrication and characterization of electrospun poly-L -lactide/gelatin graded tubular scaffolds: Toward a new design for

- performance enhancement in vascular tissue engineering. *Progress in Natural Science: Materials International*, 25(5), 405–413.
- Yin, Y., Pu, D., and Xiong, J. (2017). Analysis of the comprehensive tensile relationship in Electrospun silk fibroin/Polycaprolactone Nanofiber membranes. *Membranes*, 7(4), 67.
- Yooyod, M., Ross, G., Limpeanchob, N., Suphrom, N., Mahasaranon, S., and Ross, S. (2016). Investigation of silk sericin conformational structure for fabrication into porous scaffolds with poly(vinyl alcohol) for skin tissue reconstruction. *European Polymer Journal*, 81, 43-52.
- You, Y., Won Lee, S., Jin Lee, S., and Park, W. H. (2006). Thermal interfiber bonding of electrospun poly(L-lactic acid) nanofibers. *Materials Letters*, 60(11), 1331–1333.
- Yuan, X., Zhang, Y., Dong, C., and Sheng, J. (2004). Morphology of ultrafine polysulfone fibers prepared by electrospinning. *Polymer International*, 53(11), 1704–1710.
- Zaarour, B., Zhu, L., Huang, C., and Jin, X. (2018). Fabrication of a polyvinylidene fluoride cactus-like nanofiber through one-step electrospinning. *RSC Advances*, 8(74), 42353–42360.
- Zaoming, W., Codina, R., Fernandez-Caldas, E., and Lockey, R. F. (1996). Partial Characterization of the silk allergens in mulberry silk extract. *The journal of allergy and clinical immunology*, 6(4), 237-241.
- Zhang, F., Lu, Q., Ming, J., Dou, H., Liu, Z., Zuo, B., and Zhang, X. (2014). Silk dissolution and regeneration at the nanofibril scale. *Journal of Materials Chemistry B*, 2(24), 3879.
- Zhang, F., Zuo, B. Q., and Bai, L. (2009). Study on the structure of SF fiber mats electrospun with HFIP and FA and cells behavior. *Journal of Materials Science*, 44(20), 5682-5687.
- Zhou, C., Confalonieri, F., Jacquet, M., Perasso, R., Li, Z., and Janin, A. J. (2001). Silk Fibroin: Structural Implications of a Remarkable Amino Acid Sequence. *PROTEINS: Structure, Function, and Genetics*, 44, 119–122.
- Zhou, Y., Yang, H., Liu, X., Mao, J., Gu, S., and Xu, W. (2013). Electrospinning of carboxyethyl chitosan/poly(vinyl alcohol)/silk fibroin nanoparticles for wound dressings. *International Journal of Biological Macromolecules*, 53, 88–92.
- Zong, X., Kim, K., Fang, D., Ran, S., Hsiao, B. S., and Chu, B. (2002). Structure and process relationship of electrospun bioabsorbable nanofiber membranes. *Polymer*, 43(16), 4403–4412.



APPENDIX

## APPENDIX

21<sup>st</sup> INTERNATIONAL UNION OF MATERIALS RESEARCH SOCIETIES-INTERNATIONAL CONFERENCE IN ASIA (IUMRS-ICA 2020) TO BE HELD DURING FEBRUARY 23-26, 2021 AT FACULTY OF SCIENCE, CHIANGMAI UNIVERSITY, CHIANG MAI, THAILAND.

### NANOFIBROUS SCAFFOLDS OF ELECTROSPUN SILK FIBROIN/POLY(VINYL ALCOHOL) BLENDS FOR TISSUE ENGINEERING

Apinya Raksa<sup>1,4</sup>, Piya-on Numpaisal<sup>2,4</sup>, Rapee Utke<sup>1</sup>, Chaiwat Ruksakulpiwat<sup>3,4,\*</sup>, and Yupaporn Ruksakulpiwat<sup>3,4,\*</sup>

Received: March 13, 2021; Revised: June 14, 2021; Accepted: June 22, 2021

#### Abstract

Electrospinning is a beneficial polymer fabrication process. It is applicable for electrospun nanofibrous scaffold which can mimic nano-scale fibrous component in the extracellular matrix of many tissues. Silk fibroin (SF) is a fibrous protein, mainly produced by silkworms. SF is composed of beta-sheet crystalline and amorphous matrix. It possesses excellent biocompatibility, biodegradability, and cell induction property. Therefore, SF is a promising resource for biomedical materials. Polyvinyl alcohol (PVA) is a semicrystalline hydrophilic polymer. According to their mechanical properties and non-toxicity, PVA is good candidate to use in a high scaffold that required high mechanical strength. In our research, the SF/PVA composite scaffold was fabricated using electrospinning technique, aimed to developed biomimetic scaffold of the meniscus, a fibrocartilage in the knee joint, which provided good biological and mechanical properties. This study focused on the effect of PVA contents in SF/ PVA nanofibrous scaffold. The processability, morphology and hydrophilicity of SF/PVA nanofibers were determined. The results showed a decrease in water contact angle with increasing PVA content in the SF/PVA nanofibers. The results also suggest that a high PVA content in the SF/PVA nanofibers can enhance the cell attachment capability of the scaffold.

**Keywords:** Nanofibrous, electrospinning, scaffold, tissue engineering, meniscus

#### Introduction

Meniscus is the fibrocartilage tissue in the knee joint. There area the medial and the lateral meniscus in the knee joint. They play an important role in distributing mechanical stress, enhances the stability of the knee joint and protects articular cartilage

(Chen *et al.*, 2018). Meniscus has complex extracellular matrix, the major component is collagen fibers, which align in different directions. The blood supply of the meniscus is limited to the outer 1/3 that has a high potential to heal. (Abrams

<sup>1</sup> School of Chemistry, Institute of Science, Suranaree University of Technology, Nakhon Ratchasima, 30000, Thailand.

<sup>2</sup> School of Orthopaedics, Institute of Medicine, Suranaree University of Technology, Nakhon Ratchasima, 30000, Thailand.

<sup>3</sup> School of Polymer Engineering, Institute of Engineering, Suranaree University of Technology, Nakhon Ratchasima 30000, Thailand.  
E-mail: yupa@sut.ac.th

<sup>4</sup> Research Center for Biocomposite Materials for Medical Industry and Agricultural and Food Industry, Nakhon Ratchasima 30000, Thailand.

\* Corresponding author

*et al.*, 2013). Meniscus tear is a common injury among injury in the knee joint. It can be a result from sports or degeneration. However, meniscal injury in the medial meniscus takes place more frequently than in the lateral meniscus (Baker *et al.*, 1985; Hede *et al.*, 1990; Campbell *et al.*, 2001). Irreparable injured meniscus can cause knee pain and disability. Nevertheless, many techniques have been developed for meniscus repair, such as sutures and implant fixation (Roos *et al.*, 1998; Englund *et al.*, 2010; Chang *et al.*, 2011). However, due to the drawback of surgical treatment, there is a need to eliminate this limitation. For this reason, tissue engineering has become an alternative treatment option for meniscus injury. Tissue Engineering (TE) is the creation of a new tissue to replace, restore and maintain the functions of any part of the body. TE has three major components; cells, bioactive molecules, and scaffolds. Generally, the scaffold requires these basic properties; biodegradability, biocompatibility, non-toxicity, and cell conductivity. Currently, scaffolds have been extensively used in the field of biomedical applications (Ross *et al.*, 2017). Scaffold in tissue engineering for musculoskeletal system, such as skin, nerve tissue, tendon, cartilage, and meniscus (Halili, 2011) are from various polymers. Polymers can be derived into natural polymers (i.e. collagen, chitosan, silk fibroin, alginate, albumin, starch) and synthetic polymers (i.e. poly (vinyl alcohol), polylactide, polycaprolactone, poly (lactic acid), polyethylene glycol) (Panilaitis *et al.*, 2003; Tarun *et al.*, 2011; Ross *et al.*, 2017). The advantage of natural polymers are biocompatibility, biodegradability, nontoxicity to the human body. Additionally, it is similar to extracellular matrix component of human tissues. Anyway, natural polymers have limited availability, expensive, natural variety and susceptible to cross-contamination. The advantage of synthetic polymers is they are easier to control physicochemical properties (Agarwal *et al.*, 2008; Sill *et al.*, 2008; Gunn and Zhang, 2010; Ross *et al.*, 2017) but poor cell adhesion. In order to obtain the scaffold with good biological support and mechanical properties, silk fibroin and poly(vinyl alcohol) were used to fabricate into a biocomposite electrospun nanofibers.

Silk fibers from silk cocoon (*Bombyx mori*) comprises two structural proteins: silk fibroin (72-81 wt%) and sericin (19-28 wt%). Silk fibroin (SF) is a major structural protein, contained polypeptide chains with a molecular weight in the range of 25-350 kDa (Su *et al.*, 2019). The main structure of SF consists of repetitive blocks of hydrophobic heavy chains (H-fibroin) and hydrophilic light chains (L-chain) (Nguyen *et al.*, 2019; Sakunphanitphan *et al.*, 2019). In H-fibroin, there are 45.9% of Gly, 30.3% of Ala, 12.1% of Ser, 5.3%

of tyrosine (Tyr), and 1.8% of valine (Val). H-fibroin folds and bonds together via Van der Waals forces, hydrogen bonds, and hydrophobic interactions to form anti-parallel  $\beta$ -sheet crystalline structures (Huang *et al.*, 2018). On the other hand, L-chain comprises of amino acid sequences that contain 14% alanine (Ala), 10% serine (Ser), 9% glycine (Gly) (Nguyen *et al.*, 2019). SF is a good candidate for bioscaffold. It has good biocompatibility and biodegradability. The limitation of SF is low mechanical strength. From this reason, SF generally needs to be blended with other to material which provided better mechanical property. PVA has been widely used in biomedical application. It possess excellent mechanical strength, low cost and non-toxic (Kumkun *et al.*, 2019).

In our study, electrospinning was used to fabricate SF/PVA based nanofibers. Electrospinning, also known as electrostatic spinning. It is a process of polymer fiber fabrication, utilized a strong electric field generated by a high voltage power supply between a polymer containing fluid and a grounded conducting collector (Thompson *et al.*, 2007). The high voltage generates an electrically charged jet which ejects from a needle and undergoes very large stretching. During injection and at the arrival of the conducting collector, the solvent evaporates from the polymer solution, creating polymeric fiber. The creation of a scaffold from electrospinning can produce a porous fiber structure with good mechanical properties. This technique can produce a fibrous scaffold that similar to collagen fibers in the extracellular matrix of the meniscus (Platt, 2005). The high surface to volume ratio and porosity generated by electrospun nanofibers facilitate cell attachment and cell proliferation scaffolds (Kumbar *et al.*, 2008). Additionally, a high tensile strength scaffold can be obtained from this method. Unlike an articular cartilage, when compressive force passes through the meniscus in vertical direction, the meniscus transforms this load into a hoop stress. Circumferential fibers of collagen therefore withstand the tensile stress (Rothrauff *et al.*, 2016). As aforementioned, our research aims to develop a good cell adhesive and high tensile strength scaffold. The effect of SF/PVA ratios on the nanofiber characteristic (morphology, wettability and mechanical properties) was determined.

## Materials and Methods

### Materials

Silk cocoon (*Bombyx mori*) was obtained from Queen Sirikit Sericulture Center, Nakhon Ratchasima, Thailand. The chemical, sodium carbonate ( $\text{Na}_2\text{CO}_3$ ), calcium chloride ( $\text{CaCl}_2 \cdot 6\text{H}_2\text{O}$ ) and 99% formic

acid were purchased from Erba Carlo, Italy. Poly (vinyl alcohol) (PVA) (Mw 146,000-186,000, 87-89% hydrolyzed) was purchased from Sigma Aldrich, Australia.

#### Preparation of Regenerated SF

Silk Fibroin (SF) was extracted by boiling in 1%w/v  $\text{Na}_2\text{CO}_3$  for 20 min and washed with deionized water in order to remove sericin. The degummed silk was dried at 105°C for 3 h. Then, SF was dissolved in 46% w/v  $\text{CaCl}_2 \cdot 6\text{H}_2\text{O}$  and heated at 100±2°C for 1 h. Then, the solution was dialyzed with deionized water. After dialysis, SF solution was freeze dried at -40°C.

#### Electrospinning of Blended SF/PVA

Spinning solution was prepared by dissolving 12% w/v SF in formic acid and 10% w/v PVA in deionized water. The PVA solution was stirred at 80°C until the solution was clear. Next, SF solution mixed with PVA solution and stirred for 2 h to obtain a homogeneous solution. The ratio between SF/PVA solution was varied as shown in Table 1. The blended solution was loaded into a 10 mL syringe with 20 gauge blunt tip needle. The electrospinning was conducted at the voltage setting at 20 kV and flow rate of 0.5 mL/h with a tip to accumulator distance of 10 cm.

**Table 1. Composition of SF blend with PVA (SF/PVA)**

Sample	SF (mL)	PVA (mL)	Ratio
a	100	0	SF/PVA 100:0
b	75	25	SF/PVA 75:25
c	50	50	SF/PVA 50:50
d	25	75	SF/PVA 25:75
e	0	100	SF/PVA 0:100

#### Characterization of Blended Electrospun Nanofiber

##### Morphology

Fiber diameter of the nanofiber sheath were observed by Field Emission Scanning Electron Microscope (FE-SEM) (Zeiss AURIGA FE-SEM/FIB/EDX). The nanofiber was selectively measured in different surface area were investigated.

##### Contact Angle Test

The electrospun nanofiber was observed using contact angle. The water was dropped onto the surface of the nanofiber with a needle syringe. Images of the drop was captured after the drop set onto the nanofiber. The contact angle was calculated by the software image J for analyzing the shape of the drop.

#### Fourier Transform Infrared Spectroscopy

Fourier transform infrared spectroscopy (FT-IR) (Bruker Tensor27) was used to identify the functional groups of SF/PVA nanofibrous scaffold. The spectra were recorded over a wave number range of 4,000-400  $\text{cm}^{-1}$  at resolution of 4  $\text{cm}^{-1}$ .

#### Thermogravimetric Analysis

SF/PVA nanofiber was characterized by the TGA instrument (model STA 6000, Perkin-Elmer) in non-isothermal mode. The heating rate was 10°C/min under an inert nitrogen atmosphere over the temperature range of 50-700°C.

#### Tensile properties

The nanofibrous scaffold was cut into 1.5 cm in width, 10 cm in length and 0.02 mm in thickness tensile test was done according to ASTM D882 by using a universal testing machine (Model 4502, Instron, Norwood, MA) with a load cell of 5 kN.

## Results and Discussion

#### Nanofiber Morphology

Figure 1 shows the field emission scanning electron microscope images of SF/PVA blended nanofiber at various ratio between SF to PVA including 100:0, 75:25, 50:50, 25:75, and 0:100. Each nanofiber shows a different shape and diameter size. The blended SF/PVA of 100:0 with diameter size in range of 34±11 nm, contained beaded formation on nanofiber. The beads formation may be caused by low molecular weight, charge density, or high surface tension. The morphology of SF/PVA at ratio of 75:25, 50:50, and 25:75 showed an interconnecting network structure on the fiber surface and bead free, which their mean diameter were 54±17, 62±21, and 74±18 nm, respectively. Whereas, blended SF/PVA of 0:100 showed random and bead free nanofiber with smooth surface, and diameter size in range of 183±31 nm. However, on blending SF and PVA, the nanofiber diameter was increased when SF content was decreased. The small diameter of SF/PVA nanofiber led to an increase in surface area. This interconnecting network structure on fiber surface of the scaffold nanofiber will play an important role in tissue engineering. In terms of a place for good cell attachment, cell proliferation, and better nutrient diffusion (Pillai *et al.*, 2016). In this study, the morphology of nanofiber from FE-SEM shows the appearance of heterogeneities in the structure that may have significant impact on behaviour of nanofibrous material in medicinal applications, for example cell culture or drug release (Sirc *et al.*, 2012).

### Contact Angle

Hydrophilicity is an important role for biocompatibility of scaffold for tissue engineering. The hydrophilicity of the different blended nanofiber was shown in Figure 2 and Table 2.

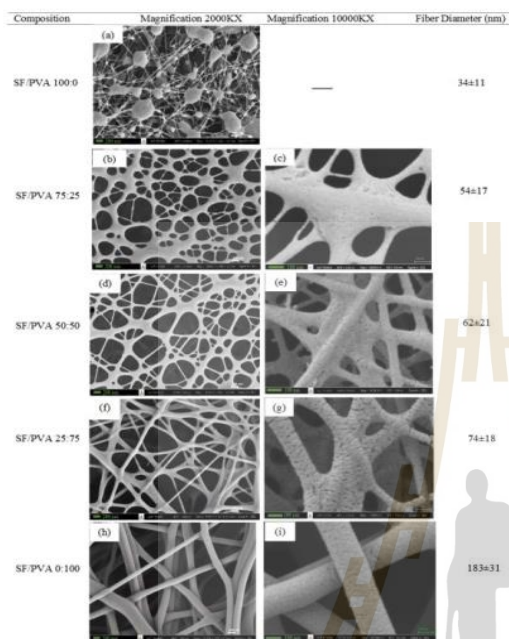


**Figure 1.** FE-SEM image of SF/PVA nanofiber various ratio and different magnification; (a) SF/PVA 100:0, (b) and (c) SF/PVA 75:25, (d) and (e) SF/PVA 50:50, (f) and (g) SF/PVA 25:75, (h) and (i) SF/PVA 0:100

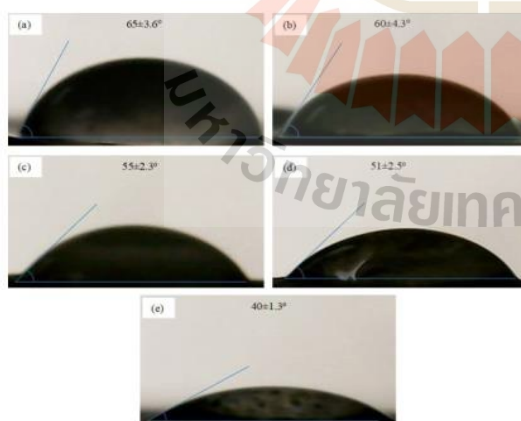


**Figure 2.** Contact angle of SF/PVA nanofiber various ratio; (a) SF/PVA 100:0, (b) SF/PVA 75:25, (c) SF/PVA 50:50, (d) SF/PVA 25:75, and (e) SF/PVA 0:100

Contact angle of the SF/PVA nanofiber showed the value in range of 40°-65°. The increase in contact angle was observed with an increase SF content. This is due to the the hydrophobicity of the SF/PVA nanofiber. Normally, SF is mostly composed of hydrophobic amino acids domains of the H-chain that contains a repetitive hexapeptide sequence of Gly-Ala-Gly-Ala-Gly-Ser and repeat units of Gly-Ala/Ser/Tyr dipeptides. The hydrophobic amino acid domains of H-fibroin fold and bond together via hydrogen bonds, Van der Waals forces, and hydrophobic interactions, to form anti-parallel  $\beta$ -sheet crystalline structures. (Qi *et al.*, 2017; Nguyen *et al.*, 2019). This structural characteristic provides enough hydrophobicity to increase contact angles of the SF/PVA nanofiber. Polymers with an air-water contact angle around 60°-65° leads to cell attachment and cell proliferation (Bhattacharjee *et al.*, 2015). The highest level of cell attachment (NIH 3T3 fibroblasts) at hydrophilic surfaces was obtained from nanofiber with contact angles in the range of 20°-60° (Wei *et al.*, 2020). Therefore, the hydrophilicity of nanofiber prepared from our study was suitable for scaffold tissue engineering application.

### Fourier Transform Infrared (FT-IR) Analysis

FT-IR spectra of the different nanofiber was investigated as shown in Figure 3. The main characteristic peaks of SF contain conformation of  $\beta$ -sheet structure which conformation shows

**Table 2.** Contact angle and Tensile properties of SF/PVA nanofiber various ratio

Composition	Contact angle (°)	Ultimate Tensile Strength (MPa)	Elongation at Break (%)
SF/PVA 100:0	63±3.6	-	-
SF/PVA 75:25	60±4.3	0.94±0.06	10.8±1.1
SF/PVA 50:50	55±2.3	9.45±2.44	39±4.8
SF/PVA 25:75	51±2.5	5.78±0.92	35.3±11
SF/PVA 0:100	40±1.3	3.93±0.64	171±33

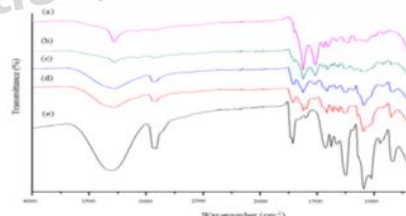


**Figure 3.** FT-IR spectra of SF/PVA nanofiber various ratio (a) SF/PVA 100:0, (b) SF/PVA 75:25, (c) SF/PVA 50:50, (d) SF/PVA 25:75, and (e) SF/PVA 0:100

characteristic peaks; absorption frequencies to  $\beta$ -sheet form at 1,625-1,620  $\text{cm}^{-1}$ , 1,510-1,500  $\text{cm}^{-1}$ , and 1,245-1,240  $\text{cm}^{-1}$ , representing amide I, amide II, and amide III, respectively. The amide I band mainly comes from C=O stretching with minor contributions from N-H in-plane bending while the amide II band is mainly caused by C-N stretching and N-H in-plane bending of the SF backbone (Ling *et al.*, 2013). The spectrum of PVA was obtained at 3,300  $\text{cm}^{-1}$  (-OH stretching), 2,960-2,920  $\text{cm}^{-1}$  (-CH stretching) and 1,750-1,720  $\text{cm}^{-1}$  (-C=O stretching), 1,470-1,450  $\text{cm}^{-1}$  (CHOH bending), 1,250  $\text{cm}^{-1}$  (C-O stretching), and 1,090-1,080  $\text{cm}^{-1}$  (C-O out-of-plane bending), respectively (Bhattacharjee *et al.*, 2015). These bands assigned to PVA became stronger with increasing PVA contents. The characteristic absorption bands of SF/PVA blended nanofiber showing the wave number ranges of amide I, amide II, and amide III were shifted from 1,625-1,620  $\text{cm}^{-1}$  to 1,630-1,627  $\text{cm}^{-1}$ , 1,510-1,500  $\text{cm}^{-1}$  to 1,515-1,512  $\text{cm}^{-1}$ , and 1,245-1,240  $\text{cm}^{-1}$  to 1,250-1,248  $\text{cm}^{-1}$ , respectively. Furthermore, the width of the OH region 3,350-3,300  $\text{cm}^{-1}$  was extended by blending SF and PVA which could characterize the increase of the intensity of hydrogen bonding in FTIR spectra (Niu *et al.*, 2019). This may confirmed the chemical interactions between the amino group of silk fibroin and the hydroxyl group of polyvinyl alcohol. However, it hardly prove the extent of the SF/PVA chemical interactions. This is because the moisture product impurity can also give rise to the broadened IR signal between the 3,350-3,300  $\text{cm}^{-1}$  region.

#### Thermal Stability

Figure 4 shows the thermal stability of SF/PVA at various ratios. The TGA thermogram of all electrospun nanofiber showed the first step of weight loss around 50-180°C caused by the evaporation of water molecules in fiber about 4%. Thermograms of SF/PVA 100:0 and SF/PVA of 0:100 showed the second step decomposition around 200-360°C and 290-350°C, respectively. Decomposition of SF may be related with the breakdown of side-chain groups of amino acid residues as well as the cleavage of peptide bonds of silk fibroin (Raksa *et al.*, 2020) and degradation of PVA that is an amorphous polymer. The third step after 350°C is the degradation of the crystalline region in PVA. The second degradation step of SF/PVA blended nanofiber around 200-380°C may be attributed to the major composition of the silk protein. The third step showed degradation of polymer chain above 390°C. When SF content was increased, it causes an increase in the thermal stability of the blended nanofiber. Usually, sterilization is an important for scaffold and the

suggestion for sterilization in an autoclave use steam heated to 121°C or 134°C. To achieve sterility, a holding time of at least 15 min at 121°C or 3 min at 134°C is required (Baume *et al.*, 2016). The thermal stability of the prepared SF/PVA nanofiber in this study was therefore suitable with sterilization in an autoclave.

#### Tensile Properties

Mechanical properties of SF/PVA nanofiber at different ratio were shown in Table 1 and stress-strain curves of all nanofiber were shown in Figure 5. The result of SF/PVA 0:100 nanofiber exhibited relatively low mechanical strength. The SF/PVA of 50:50 showed higher tensile strength than another nanofiber. Silk fibroin showed an improvement in the tensile strength of the electrospun fibrous scaffold. These improvement in mechanical properties is attributed to well oriented  $\beta$ -sheet crystallite structure and the shear alignment of the fiber chains (Altman *et al.*, 2003). This is essential property for the meniscus scaffold for tissue engineering. However, when SF content was increased to very high ratio (SF/PVA 75:25); the SF/PVA blended nanofiber was more difficult to be processed and nonuniform thickness of the nanofibers were obtained with the lowest tensile strength and elongation at break.

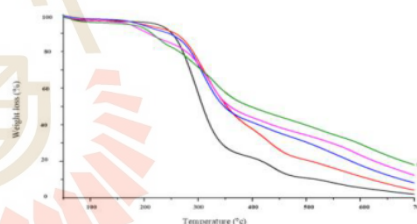


Figure 4. TGA thermogram of SF/PVA nanofiber various ratio; (a) SF/PVA 100:0, (b) SF/PVA 75:25, (c) SF/PVA 50:50, (d) SF/PVA 25:75, and (e) SF/PVA 0:100

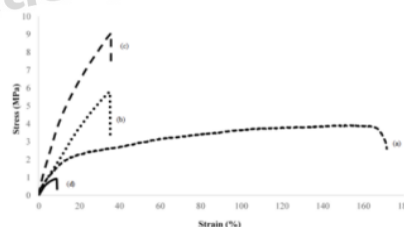


Figure 5. Stress-Strain curve of SF/PVA nanofiber various ratio; (a) SF/PVA 0:100, (b) SF/PVA 25:75, (c) SF/PVA 50:50, and (d) SF/PVA 75:25

## Conclusions

In this study, we have successfully fabricated a nanofibrous scaffold from silk fibroin and polyvinyl alcohol by electrospinning technique. It was found that SF has a direct impact on modifying the fiber morphological properties, wettability, and tensile properties. Specifically, the tensile strength of SF/PVA nanofiber was improved with increasing SF content. The chemical interactions between the amino group of silk fibroin and the hydroxyl group of polyvinyl alcohol were confirmed by FTIR spectra. The thermal stability of the prepared the blended nanofiber was suitable with sterilization.

## Acknowledgement

This work was financially supported by Rajamangala University of Technology Isan, Nakhon Ratchasima, and Suranaree University of Technology, and Science, Research and Innovation Promotion Fund from Thailand Science Research and Innovation (TSRI).

## References

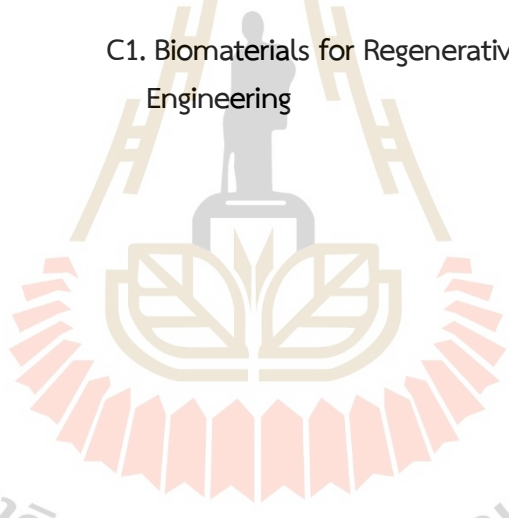
- Abrams, G.D., Frank, R.M., Gupta, A.K., Harris, J.D., McCormick, F.M., and Cole, B.J. (2013). Trends in meniscus repair and meniscectomy in the United States, 2005-2011. *Amer. J. Sport Med.*, 41(10):2,333-2,339.
- Agarwal, S., Wendorff, J.H., and Greiner, A. (2008). Use of electrospinning technique for biomedical applications. *Polymer*, 49:5,603-5,621.
- Altman, G.H., Diaz, F., Jakuba, C., Calabro, T., Horan, R.L., Chen, J., H. Lu, Richmond, J., and Kaplan, D.L. (2003). Silk-based biomaterials. *Biomater.*, 24(3):401-416.
- Baker, B.E., Peckham, A.C., Pupparo, F., and Sanborn, J.C. (1985). Review of meniscal injury and associated sports. *Am. J. Sports Med.*, 13:1-4.
- Baume, A.S., Boughton, P.C., Coleman, N.V., and Ruys, A.J. (2016). Sterilization of tissue scaffolds. *Characterisation and Design of Tissue Scaffolds*. Woodhead Publishing, Sawston, UK, p. 225-244.
- Bhattacharjee, P., Kundu, B., Naskar, D., Maiti, T.K., Bhattacharya, D., and Kundu, S.C. (2015). Nanofibrous nonmulberry Silk/PVA scaffold for osteoinduction and osseointegration. *Biopoly.*, 103(5):271-284.
- Campbell, S.E., Sanders, T.G., and Morrison, W.B. (2001). Mr imaging of meniscal cysts: Incidence, location, and clinical significance. *AJR Am. J. Roentgeno.*, 177:409-413.
- Chang, A., Moio, K., Chmiel, J.S., Eckstein, F., Guermazi, A., Almagor, O., Cahue, S., Wirth, W., Prasad, P., and Sharma, L. (2011). Subregional effects of meniscal tears on cartilage loss over 2 years in knee osteoarthritis. *Annals of the Rheumatic Disease.*, 70(1):74-79.
- Chen, M., Gao, S., Wang, P., Li, Yan., Guo, W., Zhang, Y., Wang, M., Xiao, T., Zhang, Z., Zhang, X., Jing, X., Li, X., Liu, S., Guo, Q., and Xi, T. (2018). The application of electrospinning used in meniscus tissue engineering. *J. Biomater. Sci., Poly. Ed.*, 29(5):461-475.
- Englund, M., Guermazi, A., Roemer, F.W., Yang, M., Zhang, Y., Nevitt, M.C., Lynch, M., J.A., Lewis, C.E., Torner, J., and Felson, D.T. (2010). Meniscal pathology on mri increases the risk for both incident and enlarging subchondral bone marrow lesions of the knee. *Annals of the Rheumatic Diseases*, 69(10):1,796-1,802.
- Gunn, J. and Zhang, M. (2010). Polyblend nanofibers for biomedical applications: Perspectives and challenges. *Trend. Biotech.*, 28(4):189-197.
- Halili, N.A. (2011). Collagen-based meniscus tissue engineering: design and application, Thesis, [Ph.D. thesis, Doctor of Philosophy in Department of Biotechnology]. Middle East Technical University, Turkey.
- Hede, A., Jensen, D.B., Blyme, P., and Sonne-Holm, S. (1990). Epidemiology of meniscal lesions in the knee. *Acta Orthop Scand.*, 61:435-437.
- Huang, W., Ling, S., Li, C., Omenetto, F.G., and Kaplan, D.L. (2018). Silkworm silk-based materials and devices generated using bio-nanotechnology. *Chem. Soc. Rev.*, (47):6,486-6,504.
- Kumbar, S.G., James, R., Nukavarapu, S.P., and Laurencin, C.T. (2008). Electrospun nanofiber scaffolds: Engineering soft tissues. *Biomed. Mater.*, 3(3):034002.
- Kumkun, P., Tuancharoensri, N., Ross, G., Mahasaron, S., Jongjitwimol, J., Topham, P.D., and Ross, S. (2019). Green fabrication route of robust, biodegradable silk sericin and poly (vinyl alcohol) nanofibrous scaffolds. *Poly. Int.*, 68(11):1,903-1,913.
- Ling, S., Qi, Z., Knight, D.P., Shaoa, Z., and Chen, X. (2013). FTIR imaging, a useful method for studying the compatibility of silk fibroin-based polymer blends. *Polym Chem.*, 4:5,401-5,406.
- Nguyen, T.P., Nguyen, Q.V., Nguyen, V-H., Le, T-H, V., Huynh, Q.N., Vo, D.V.N., Trinh, Q.T., Kim, S.Y., and Van Le, Q. (2019). Silk fibroin-based biomaterials for biomedical applications: a review. *Polymers*, 24: 11(12):1933.
- Niu, C., Li, X., Wang, Y., Liu, X., Shi, J., and Wang, X. (2019). Design and performance of a poly(vinyl alcohol)/silk fibroin enzymatically crosslinked semi-interpenetrating hydrogel for a potential hydrophobic drug delivery. *Royal Soc. Chem.*, 9:41074.
- Panilaitis, B., Altman, G.H., Chen, J., Jin, J.H., Karageorgiou, V., and Kaplan, D.L. (2003). Macrophage responses to silk. *Biomater.*, 24(18):3,079-3,085.
- Pillai, M.M., Gopinathan, J., Indumathi, B., and Manjoocha, Y.R. (2016). Silk-pva hybrid nanofibrous scaffold for enhanced primary human meniscus cell proliferation. *J. Membrane Biol.*, 249(6):813-822.
- Platt, M.A. (2005). Tendon repair and healing. *Clin. Podiatr. Med. Surg.*, 22:553.
- Qi, Y., Wang, H., Wei, K., Yang, Y., Zheng, R.Y., Kim, S., and Zhang, K.Q. (2017). A review of structure construction of silk fibroin biomaterials from single structures to multi-level structures. *J. Mol. Sci.*, 18(3):237.
- Raksa, A., Utke, R., Ruksakulpiwat, C., Numpaisal, P., and Ruksakulpiwat, Y. (2020). Morphological and chemical characterization of electrospun silk fibroin/polyvinyl alcohol nanofibers. *AIP Conference Proceeding*, 2279:080004-1.
- Roos, H., Lauren, M., Adalberth, T., Roos, E.M., Jonsson, K., and Lohmander, L.S. (1998). Knee osteoarthritis after meniscectomy: Prevalence of radiographic changes after twenty-one years, compared with matched controls. *Arthritis Rheum.*, 41(4):687-693.
- Ross, S., Yooyod, M., Limpeanchob, N., Mahasaron, S., Suphrom, N., and Ross, G.M. (2017). Novel 3D porous semi-IPN hydrogel scaffolds of silk sericin and poly(N-hydroxyethyl acrylamide) for dermal reconstruction. *Express Poly. Lett.*, 11(9):719-730.

- Rothrauff, B.B., Numpaisal, P., Lauro, B.B., Alexander, P.G., Debski, R.E., Musahl, V., and Tuan, R.S. (2016). Augmented repair of radial meniscus tear with biomimetic electrospun scaffold: an in vitro mechanical analysis. *J. Experim. Orthop.*, 3(23):1-10.
- Sakunphanitphan, S., Jantarat, J., Sritanaudomchai, H., Oonkhanond, B., and Hargreaves, K.M. (2019). The effect of silk fibroin hydrogel on proliferation of human stem cells from the apical papilla. *M. Dent. J.*, 39(1):35-40.
- Sill, T.J. and Von Recum H.A. (2008). Electrospinning: Applications in drug delivery and tissue engineering. *Biomat.*, 29(13):1,989-2,006.
- Sirc, J., Hobzov, R., Kostina, N., Munzarov, M., Juklickov, M., Lhotka, M., Kubinov, S., Zajicov, A., and Michalek, J. (2012). Morphological characterization of nanofibers: methods and application in practice. *J. Nanomat.*, p. 1-14.
- Su, D., Ding, S., Shi, W., Huang, X., and Jiang, L. (2019). Bombyx mori silk-based materials with implication in skin repair: Sericin versus regenerated silk fibroin. *J. Biomat. Appl.*, 34(1):36-46. DOI: <https://doi.org/10.1177/0885328219844978>
- Tarun, G., Ajay, B., Bhawna, K., Sunil, K., and Ravi, J. (2011). Scaffold: tissue engineering and regenerative medicine. *Int. Res. J. Pharm.*, 2(12):37-42.
- Thompson, C.J., Chase, G.G., Yarin, A.L., and Reneker, D.H. (2007). Effects of parameters on nanofiber diameter determined from electrospinning model. *Poly.*, 48(23):6,913-6,922.
- Wei, Z., Gua, J., Yea, Y., Fanga, M., Langa, J., Yanga, D., Pan, Z. (2020). Biodegradable poly(butylene succinate) nanofibrous membrane treated with oxygen plasma for superhydrophilicity. *Surf. Coat. Technol.*, 381:1-7.

Preferred type of talk (Oral, Poster): Oral Presentation

Preferred conference session: C. Bioplastic, Biomaterials and Medical Devices

C1. Biomaterials for Regenerative Medicine and Tissue Engineering



มหาวิทยาลัยเทคโนโลยีสุรนารี

## CURRICULUM VITAE

**Name** Apinya Raksa  
**Place of birth** Khon Kaen, Thailand  
**Education:**  
1998-2002 B.Sc. Chemistry  
Maejo University, Chiang Mai, Thailand  
2007-2010 M.Sc. Applied Chemistry  
Maejo University, Chiang Mai, Thailand  
2017-Present Ph.D. candidate (Chemistry)  
Suranaree University of Technology, Nakhon  
Ratchasima, Thailand

### Publications

- Raksa, A., Numpaisal, P.O., Utke, R., Ruksakulpiwat, C. & Ruksakulpiwat, Y. (2021). Nanofibrous scaffolds of electrospun silk fibroin/poly(vinyl alcohol) blends for tissue engineering. *Suranaree Journal of Science and Technology*, 29(3), 010132(1-7).
- Raksa, A., Numpaisal, P.-O., & Ruksakulpiwat, Y. (2021). The effect of humidity during electrospinning on morphology and mechanical properties of SF/PVA nanofibers. *Materials Today: Proceedings*, 47, 3458–3461.
- Raksa, A., Utke, R., Ruksakulpiwat, C., Numpaisal, P.-O., & Ruksakulpiwat, Y. (2020). Morphological and chemical characterization of electrospun silk fibroin/polyvinyl alcohol nanofibers. *THE SECOND MATERIALS RESEARCH SOCIETY OF THAILAND INTERNATIONAL CONFERENCE*. AIP Publishing.